Studies on the effect of high energy ball milling on the structural, electrical and magnetic properties of some normal spinels in the ultrafine regime

Thesis submitted to

Cochin University of Science & Technology

In partial fulfilment of the requirements for the award of the degree of

Doctor of Philosophy

By

Santhosh D.Shenoy

Department of Physics

Cochin University of Science and Technology

Cochin – 682 022, India.

July 2004

Dr.M.R.Anantharaman
Reader
Department of Physics
Cochin University Of Science and Technology
Cochin – 682 022
India.

CERTIFICATE

Certified that the work presented in this thesis entitled **"Studies on the effect of high energy ball milling on the structural, electrical and magnetic properties of some normal spinels in the ultrafine regime"** is based on the bonafide research work done by Mr. Santhosh D. Shenoy under my guidance, at the Magnetics laboratory of the Physics Department, Cochin University of Science and Technology, Cochin – 682 022, and has not been included in any other thesis submitted previously for the award of any degree.

Cochin - 22
22-07-2004

Dr.M.R.Anantharaman
(Supervising Guide)

Ph. No: 0484-2577404 Extn 30 (Off), 0484-2576200
E Mail: mra@cusat.ac.in mraiyer@yahoo.com

PREFACE

Magnetism and magnetic materials have been a fascinating subject for the mankind ever since the discovery of lodestone. Since then, man has been applying this principle of magnetism to build devices for various applications. It is a historical fact that humankind owes a lot to magnetic compass, which paved the way for the discovery of continents and expeditions. Efforts by scientists and engineers in the 19^{th} and 20^{th} centuries have resulted in the development of a horde of devices for various applications. Nowadays, a piece of magnet is a common component in devices like television sets, transformer cores, loud speakers and telephone receivers. Magnetic materials are employed in audio and video gadgets and also as secondary storage devices in computers. In modern times they are being considered as a potential material for primary storage in computers and thought of as an environmentally friendly material alternative in place of CFC's for refrigeration.

Magnetism can be classified broadly into five categories. They are diamagnetic, paramagnetic, ferromagnetic, antiferromagnetic and ferrimagnetic. Of these, ferro and ferri magnetic materials assume great commercial importance due to their unique properties like appropriate magnetic characteristics, high resistivity and low eddy current losses.

The discovery of ferrites in the early 20^{th} century and the subsequent theory of ferrimagnetism propounded by Louis Neel resulted in a surge of research activities. This made possible to devise/tailor materials for various applications. It must be mentioned here that most of the devices like television sets, transformer cores, loud speakers, telephone receivers, memory devices, magnetic sensors and permanent magnets are based on ferrites.

The emergence of nanoscience and nanotechnology during the last decade had its impact in the field of magnetism and magnetic materials too. Now, it is common knowledge that materials synthesized in the nanoregime exhibit novel and superlative properties with respect to their coarser sized counterparts in the micron regime. Nanomagnetic materials exhibit various phenomenon like quantum magnetisation, quantum tunnelling and spin polarized tunnelling to name a few. So nanomaterials possess bigger challenges to the scientific community. These challenges lead to the proper understanding of the physics of these materials at the nanolevel. For instance, a

ferrite material prepared in the nanoregime will exhibit altogether different magnetic and electrical properties when compared to their coarser sized cousins. The emergence of nanomagnetism has further lead to new synthesis methods like reverse micelle synthesis, coprecipitation, thermal decomposition, solgel, aerogel process and high energy ball milling. Phenomenon like superparamagnetism and single domain characteristics have been a hallmark of nanomagnetic materials. Both classical and quantum mechanical concepts were invoked to explain various phenomenon exhibited by magnetic ultrafine/nano materials. With the advent of nanotechnology and spin offs derived from magneto optical storage devices based on multilayer thin films, new devices called spin valve transistors have started emerging in the horizon of Science & Technology. There is also a new class of rheological fluids, which are commonly called as ferrofluids. The precursors for synthesis of these fluids are ultrafine magnetic materials. They have tremendous applications in engineering and medicine.

Ferrites are ferrimagnetic materials and they can be further classified into three, based on their crystal structure. They are spinels, with cubic crystal structure, garnets, with cubic crystal structure and magnetoplumbites, with hexagonal crystal structure. Spinel ferrites resemble the structure of the naturally occurring mineral $MgAl_2O_4$. They are further categorized into two - normal and inverse spinels. Zinc ferrite belongs to the class of normal spinels. Zinc ferrite when prepared in the micron regime by ceramic methods is antiferromagnetic with $T_N \approx 10K$. Recently many researchers, worldwide, observed anomaly in the magnetic properties of zinc ferrites when they are prepared in the ultrafine regime. Contrary to the earlier beliefs, they exhibited net magnetisation at room temperature. The reason for this anomalous behaviour of nano zinc ferrites is still unknown and many schools of thought exist. One theory is that the cation redistribution on the A and B sites is responsible for the ferrimagnetic ordering found in these nanomaterials. Others believe that the existence of superparamagnetic particles and spin clusters are responsible for the enhanced magnetisation. It is also reasonable to assume that surface spins or surface magnetism play a very vital role in determining the magnetic properties of these type of materials in the ultrafine regime. So zinc ferrite can be a candidate material for checking any of the hypotheses mentioned above. Moreover, finite size effects on the magnetic properties also play a crucial role in deciding the performance characteristics of a magnetic material when employed as a device. So study of various properties, namely,

structural, electrical and magnetic assume significance both from the fundamental and application points of view. With this motivation, a systematic study on ultrafine zinc ferrite is undertaken by synthesizing the zinc ferrite in the fine particle regime by cold coprecipitation methods. The study of the finite size effects on the structural, electrical and magnetic properties was carried out by systematically reducing the size of the as prepared materials by high energy ball milling. Both wet milling and dry milling were employed to fine-tune the size.

Various analytical tools like X-ray diffraction, Transmission electron microscopy, Vibrating sample magnetometer, AC magnetic susceptibility, Mössbauer spectrometer, Keithley source measuring unit and Impedance analyser were employed to characterize and evaluate the properties at various stages of preparation. The results are correlated in order to tailor the properties and to propose a plausible mechanism for the anomaly exhibited by zinc ferrites in the ultrafine regime.

Zinc aluminate ($ZnAl_2O_4$), an isostructural material with $ZnFe_2O_4$, a widely used catalyst, is a nonmagnetic normal spinel and is an ideal template to test the hypothesis of cation redistribution, if any, in the nanoregime. Moreover the finite size effects on the electrical and structural properties are also studied for comparison sake. The thesis is divided into nine chapters.

CHAPTER 1 gives a brief introduction about the history of magnetic materials and their classification. Theoretical aspects relating to the structural, magnetic and electrical properties of spinel ferrites also discussed in this chapter. A brief description about fine particle research and high energy ball milling is also included in this chapter.

CHAPTER 2 describes the synthesis of ultrafine zinc ferrites and zinc aluminates. Various characterisation tools namely X-ray diffraction, Transmission electron microscopy, Vibrating sample magnetometer, AC magnetic susceptibility, Mössbauer spectrometer, Keithley source measuring unit and Impedance analyzer employed for the evaluation of properties at various stages are also discussed in this chapter.

CHAPTER 3 presents a detailed study of the structural properties of both wet milled and dry milled zinc ferrites. Morphological and particle size investigations by transmission electron microscopy (TEM) are also included in this chapter.

Magnetic properties of zinc ferrites were carried out using Vibrating sample magnetometer. Thermomagnetisation curves (including ZFC-FC) were plotted for

representative samples to check the spin glass like properties of ultrafine zinc ferrites. AC magnetic susceptibility studies were also conducted for dry milled samples. All the results are correlated and included in **CHAPTER 4**.

CHAPTER 5 discusses the Mössbauer spectroscopy results for zinc ferrite samples both at room temperature and at low temperatures..

DC conductivity studies on dry milled zinc ferrite samples were carried out by using a Keithley 236 source/measure unit and dielectric studies on both wet and dry milled zinc ferrites were carried out by an impedance analyser (model: HP4285A). The frequency dependence and temperature dependence of dielectric permittivity and ac conductivity were investigated. A plausible mechanism for conduction mechanism in these materials is proposed. The correlated results are cited in **CHAPTER 6**.

Structural properties and particle size evaluation of ultrafine zinc aluminate milled in dry and wet conditions were carried out using X-ray diffraction. Energy dispersion X-ray analysis (EDX) was also employed to check the composition. The results are correlated. This is the major theme of **CHAPTER 7**.

DC conductivity, ac conductivity and dielectric permittivity measurements were performed on ultrafine zinc aluminates. The results are correlated and included in **CHAPTER 8**.

CHAPTER 9 is the concluding chapter of the thesis and in this chapter the salient observations and the inferences drawn out of these investigations are presented in a nutshell. The scope for future investigations based on the present study is also brought out.

CONTENTS

CHAPTER 1
INTRODUCTION

Magnetisation and magnetic materials have been an integral part of human life from time immemorial. The original association of magnetism with human civilization started with the discovery of lodestone sometime around a few centuries before Christ in the modern day Turkey [1-3]. It is needless to emphasize that this only has lead to the discovery of new continents and saw the birth of many civilizations. In modern times, it is anybody's knowledge that magnetism/magnetic material is a significant contributor in everyday life in the form of devices in TV, loudspeaker, transformer cores, and telephone receivers. In information technology, they make their presence felt in the form of hard disk and other primary/secondary memory in computers. Recently people are exploiting the possibility of making a high density Magnetic Random Access Memory (MRAM) and magnetic refrigeration by employing magnetic materials. These are all the results of valiant efforts by various researchers over the centuries. This has culminated in introducing many modern day gadgets based on magnetism.

From the fundamental point of view, electricity and magnetism are closely related as it is with earth and magnetism. If there is flow of current, there is magnetism and if there is magnetism, current can be created. In this context it is important to start with the electrons in atoms and discuss the origin of magnetism. Some fundamental terms regarding magnetism are dealt in a simple manner below.

Substances, which react to a magnetic field, are called magnetic materials. The classification of magnetic materials was made according to their magnetic structure. The two possible atomic origins of magnetism, which lead to the magnetisation of magnetic substances, are the orbital motion and the spin motion of electrons [1-3]. An atom, which has a magnetic moment, caused by spin or by orbital motion of electrons or by both is generally called a magnetic atom.

The magnetic moment produced by the motion of electron is given by

$$M = -g\mu_0 eP/2m \qquad \text{----------} \quad (1.1)$$

Where 'μ_0' is the permeability of free space, 'e' the electronic charge and 'm' the mass of an electron. 'P' is the angular momentum due to the circular motion of electrons.

'g' is called the gyromagnetic ratio or g factor. If g = 1 the motion is purely orbital and if g = 2 the motion is purely spin.

The magnetisation $\vec{M}$ of a magnetic material may be defined as the magnetic moment per unit volume,

$$\vec{M} = \frac{\vec{m}}{V} \quad \text{---------} \quad (1.2)$$

The magnetic properties of a material are characterized not only by the magnitude and sign of $\vec{M}$ but also by the way in which $\vec{M}$ varies with an applied magnetic field H. The ratio of these two quantities is called magnetic susceptibility

$$\chi = \frac{M}{H} \quad \text{---------} \quad (1.3)$$

Although equation (3) is a linear relation, it holds good only at low fields. At higher fields, substances exhibit saturation of magnetisation. This is because at higher fields, all of the atomic magnetic dipoles get aligned parallel to the applied field and further increase in magnetisation is not possible. Hence a saturation of magnetisation occurs. Classical Langevin theory agrees with this [2-3].

1.1 Classification of magnetic materials.

Magnetism can be categorized into diamagnetism, paramagnetism, ferromagnetism, antiferromagnetism and ferrimagnetism. Diamagnetism is a weak magnetism in which a magnetisation is exhibited opposite to the direction of the applied field. The susceptibility is negative and the order of magnitude of χ is usually about 10^{-5}. The origin of this magnetism is the orbital motion of electrons around the nuclei induced electromagnetically by the application of an external field [1]. Copper, silver, gold, bismuth and beryllium are examples of diamagnetic materials.

Paramagnetism is exhibited in substances, which contain magnetic atoms, or ions whose spins are isolated from their magnetic environment and can more or less freely change their directions. At finite temperatures, the spins are thermally agitated and take random orientations. Upon application of a magnetic field, the average orientations of spins are slightly changed so as to produce a weak induced magnetisation parallel to the applied magnetic field. The order of magnitude of χ is 10^{-3} to 10^{-5}. Aluminium, platinum and manganese (above 100 K) are examples of paramagnetic materials.

Ferromagnetism is a cooperative phenomenon resulting out of strong positive interaction between the neighboring spins. Here spins become aligned parallel to one another by this strong exchange interaction. As the temperature increases, the arrangement of spins is disturbed by thermal agitation, thus resulting in a temperature dependence of spontaneous magnetisation. Ferromagnetism is exhibited mostly by metals like iron, cobalt, nickel, gadolinium and alloys like permalloy, supermalloy etc, and by a few exceptional oxides such as CrO_2 and EuO. According to Heisenberg, the exchange force between magnetic atoms is of quantum mechanical nature. The exchange potential energy between two atoms having spins S_i and S_j can be written as follows:

$$E_{ij} = - 2 J S_i.S_j \quad \text{----------} \quad (1.4)$$

where J is the exchange integral [3]. If J is positive, the energy is least when S_i is parallel to S_j; if J is negative, the stable state is that in which S_i is antiparallel to S_j.

Antiferromagnetism is a weak cooperative magnetism, which is similar to paramagnetism and exhibits a small positive susceptibility. The temperature dependence of the susceptibility of this magnetism is characterized by a transition in the χ-T curve at the so-called Neel temperature. The reason for this is that below this temperature an antiparallel spin arrangement is established in which the plus and minus spins completely cancel each other. Since in such an antiferromagnetic arrangement of spins the tendency to be magnetised by the external field is opposed by a strong negative interaction acting between plus and minus spins, the magnetic susceptibility decreases with a decrease in temperature, contrary to the usual paramagnetic behavior. Above the Neel temperature, the spin arrangement becomes random, so that the magnetic susceptibility now decreases with an increase of temperature. MnF_2, α-Fe_2O_3, chromium (below 310K), manganese (below100K), $ZnFe_2O_4$ (Below 10K) are examples of antiferromagnetic materials.

Ferrimagnetism is the term coined by Neel to describe the magnetism of ferrites. In these substances magnetic ions occupy two kinds of lattice sites, A and B. Spins on A sites and spins on B sites point in opposite direction and hence a strong negative interaction exists between these two spin systems. The number of magnetic ions and the magnitude of individual ion spin are different on the A and B sites. Therefore such an ordered arrangement of spins gives rise to a resultant magnetisation. This is called spontaneous magnetisation since the magnetisation produced here is without the action of

any external magnetic field. $NiFe_2O_4$, γ-Fe_2O_3, Fe_3O_4, $BaFe_{12}O_{19}$, $SrFe_{12}O_{19}$ etc are all examples of ferrimagnetic materials.

1.2 Magnetic domains

In spite of the presence of spontaneous magnetisation, a block of ferromagnetic or ferrimagnetic substance is usually not spontaneously magnetised but exists rather in a demagnetised state. This is because the interior of the block is divided into many magnetic domains, each of which is spontaneously magnetised. Since only the direction of domain magnetisation varies from domain to domain, the resultant magnetisation can be changed from zero to the value of spontaneous magnetisation. Actually if an external field is applied, the apparent magnetisation of the block is changed and finally reaches the saturation magnetisation which is equal to the spontaneous magnetisation. If the field is reduced, the magnetisation is again decreased, but does not come back to the original value. Such an irreversible process of magnetisation is called hysteresis. The presence of saturation magnetisation and hysteresis is an important feature of ferro and ferrimagnetism.

A ferro or ferrimagnetic substance consists of many magnetic domains each of which is magnetised in a different direction. The magnetisation inside each domain is made up of many atomic moments, which are lined up, by the action of an exchange force. Weiss first predicted the presence of the ferromagnetic domain structure in 1907 in his famous paper on the hypothesis of his molecular field theory. Barkhaussen made the first experimental verification of the presence of ferromagnetic domains in 1919 by an indirect method. The direct observation of ferromagnetic domain structure was attempted by Bitter in 1931. In 1932, Bloch showed theoretically that the boundary between domains is not sharp on an atomic scale but is spread over a certain thickness wherein the direction of spins changes gradually from one domain to the next. This layer is usually called a domain wall or Bloch wall.

The size and shape of the domain is dependent of the size and shape of the specimen in homogeneous materials. But in inhomogeneous magnetic materials, the size of the domain is determined exclusively by the inhomogeniety of the materials, independent of the shape of the specimen. The kinds of inhomogeneity, which can affect

the domain structure, are voids, inclusions, precipitations, fluctuation in alloy compositions, internal stress, local directional order, crystal boundaries etc.

1.3 Ferrites

Ferrites are weak ferromagnetic or ferrimagnetic materials with iron as one of the components. They are mixed metal oxides with general chemical composition $MO.Fe_2O_3$ where M is a divalent metal such as Fe, Mn. Mg, Ni, Zn, Cd, Co, Cu, Al or a mixture of these. Three different crystal types exist for ferrites and accordingly they are classified into three groups [4]. They are the spinels. garnets and the magnetoplumbites. Spinels crystallize in the cubic crystal structure and the general formula is $M^{2+}Fe_2O_4$ where M = Fe, Mn, Mg, Ni, Zn, Cd, Co, Cu, Al or a mixture of these. Garnets too possess cubic crystal structure and can be represented by formula $Ln_3^{3+}Fe_5O_{12}$ where Ln = Y, Sm, Eu, Gd, Tb, Dy, Ho, Er, Tm, or Lu. Magnetoplumbites form hexagonal structure and the chemical formula can be of the form M^{2+} Fe_{12} O_{19} where M = Ba or Sr.

The structural, magnetic and electrical properties of these compounds are governed critically by their chemical composition. Hence preparation of these ferrites with specific properties has gained much importance. Ferrites can be prepared by conventional solid-state methods and numerous chemical routes, such as reverse micelle synthesis, coprecipitation, thermal decomposition, solgel and aerogel process.

Ferrites and materials derived from ferrites find extensive application in devices like transformers, TV Yokes, loud speakers and in many other devices. They are also one of the largely used material medium for audio/video applications and computer memories and switches. At microwave frequencies, it is used in various polarization rotators, resonance isolators and phase shifters.

The focal theme of this thesis is on the ultrafine spinel ferrites and a brief description of the various properties of these materials in general is discussed below. In this section the structural properties are dealt with.

1.4 Spinel ferrites

Ferrites crystallize in the spinel structure, which is named after the mineral spinel, $MgAl_2O_4$. Primarily the oxygen ions lattice determines the spinel crystal structure. The radii of the oxygen ions are several times larger than the radii of the metallic ions in the compound. Consequently, the crystal structure can be thought of as being made up of the

closest possible packing of layers of oxygen ions, with the metallic ions fit in at the interstices A and B (Figure 1.1) [5].

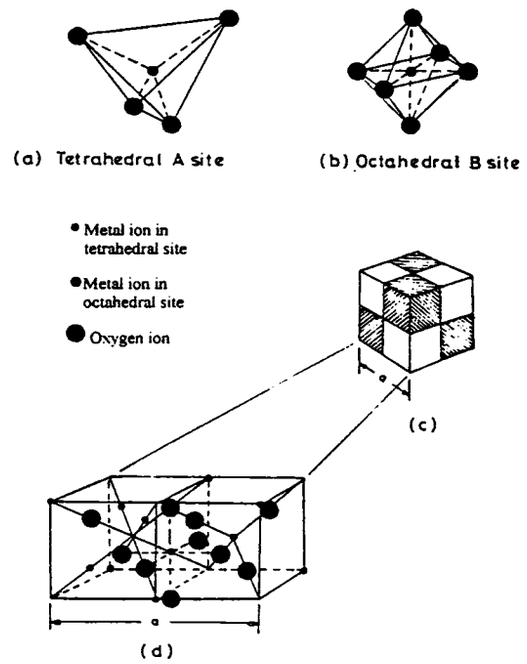

Figure 1.1 Crystal structure of a cubic ferrite.

A metallic ion located at the A site has four nearest oxygen ion neighbours in tetrahedral coordination. The metallic ion, which is situated at site B, has six nearest oxygen ion neighbours and is in the octahedral coordination.

Thus the spinel ferrites have the general formula $\{(M)_{\delta}(Fe)_{1-\delta}\}[(M)_{1-\delta}(Fe)_{1+\delta}]O_4$. The divalent metal ion M (eg:- Zn, Mg, Mn, Fe, Co, Ni or a mixture of them) can occupy either tetrahedral(A) or octahedral(B) sites as depicted by curled and square brackets respectively. In the above formula when $\delta = 1$, it is called normal spinel. $ZnFe_2O_4$ and $CdFe_2O_4$ are examples of normal ferrites. When $\delta = 0$, it is called inverse spinel and examples are $NiFe_2O_4$, $CoFe_2O_4$, $CuFe_2O_4$ etc. When $\delta = 1/3$, it is called a random spinel.

The interesting and useful electrical and magnetic properties of the spinel ferrites are governed by the distribution of the iron (Fe^{2+}/Fe^{3+}) and the divalent metal ions among the octahedral and tetrahedral sites of the spinel lattice. This cation distribution is

determined by a variety of factors like method of preparation, grain size, temperature, madelung energy, cationic size, cation valency, oxygen parameter and site preference energy [4].

1.4.1 Magnetic properties of spinel ferrites

In ferrites three kinds of magnetic interactions are possible, between the magnetic ions, which are occupied in the two crystallographically distinct lattice sites. These interactions are possible through the intermediate O^{2-} ions by superexchange mechanism. The three possible interactions are A-A interaction, B-B interaction and A-B interaction. Strength of these interactions is determined by A-B, B-B, A-A distances and the angle of AOB. This is evident from figure 1.2. Whether the interaction is ferri, ferro or antiferro, is determined by the value of J and is governed by equation 1.4. It has been established experimentally that these interaction energies are negative for ferrites and hence induce an antiparallel orientation. However the magnitudes of the A and B sublattice magnetisations are not equal and this will produce a resultant net magnetisation in ferrites. In general the magnitude of the interaction energy between two magnetic ions depends upon the distance from these ions to the oxygen ion (through which the interaction occurs) and also the angle φ between the magnetic ions (Me^{I} – O - Me^{II}).

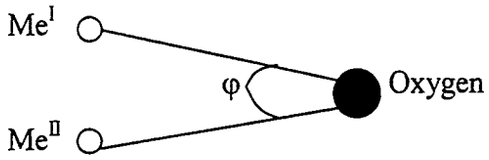

Figure 1.2 Interactions of spinel ferrites.

An angle of 180^0 will give rise to the greatest exchange energy and the energy decreases very rapidly with increasing distance. Based on the values of the distance and the angle φ it may be concluded that, of the three interactions the A-B interaction is of the greatest magnitude. The A–A interaction is the weakest. Thus with only A–B interaction predominating, the spins of the A and B site ions, in ferrite will be oppositely magnetised in the A and B sublattilces, with a resultant magnetic moment equal to the difference between those of A and B site ions. In general the value of saturation magnetic

moment for the B lattice (M_B) is greater than that of the A lattice (M_A) so that the resultant saturation magnetisation (M_S) may be written as $M_S = M_B - M_A$.

1.4.2 Electrical properties of spinel ferrites

Spinel ferrites have a low electrical conductivity when compared to other magnetic materials hence they find wide use at microwave frequencies. Spinel ferrites, in general are semiconductors with their conductivity lying in between 10^2 and 10^{-11} Ohm^{-1} cm^{-1}. The eddy current losses in ferromagnetic materials are inversely proportional to the resistivity [5]. Hence eddy current losses can be minimized by use of magnetic materials of high resistivity. The search for ferromagnetic materials of unusually high resistivity resulted in the emergence of ferrites. Ferrites having a resistivity of upto 10^7 ohm-meter as compared to 10^{-7} ohm-meter for iron, reduce the eddy current losses in them to negligible values, even at microwave frequencies (the eddy current power loss is proportional to the square of the frequencies and hence this high resistivity at microwave frequencies is imperative). The conductivity and dielectric properties of spinel ferrites depend upon several factors namely chemical composition, method of preparation, cation distribution, grain size etc. These materials behave as inhomogeneous dielectric materials in which individual high conducting grains are separated by either air gaps or low conducting grains.

The conductivity is due to the presence of Fe^{2+}, oxygen ion vacancies and the metal ions if it has an oxidation state of 3+ (Me^{3+}). The presence of Fe^{2+} results in n-type behaviour by $Fe^{3+} \leftrightarrows Fe^{2+}$ hopping. $Me^{3+} \leftrightarrows Me^{2+}$ hopping and oxygen ion vacancy conduction results in p–type behaviour. The conductivity arises due to the mobility of the extra electron or the positive hole through the crystal lattice. The movement is described by a hopping mechanism, in which the charge carriers jump from one ionic site to the next. In short, one can say that the electrostatic interaction between conduction electron (or hole) and nearby ions may result in a displacement of the latter and hence in polarization of the surrounding region so that the carrier is situated at the centre of a polarization potential well. The carrier is trapped at a lattice site, if this potential well is deep enough. Its transition to a neighbouring site is determined by thermal activation. This has been described as the hopping mechanism. Expression for conductivity for semi conductors can be represented by

$$\sigma T = \sigma_0 \exp^{-E_a/kT} \quad \text{---------} \quad (1.5)$$

where E_a represents an activation energy which, according to Verwey and DeBoer is the energy needed to release an electron from the ion for a jump to the neighbouring ion, so giving rise to electrical conductivity.

In fine particle systems, which are discussed in the next section, some other conduction phenomenon such as Coulomb blockade and spin polarized tunnelling also contribute to conduction [6].

1.5 Fine particles

Fine particles with size in the nanometric scale have made greatest revolution in materials science research. During the last few decades many efforts have been devoted to the comprehension of the physical phenomenon appearing in magnetic fine particle systems. The new synthesis methods to produce nanoscale materials and the development of new and sophisticated measuring techniques resulted the materials research to follow rigorous activities in these materials throughout the world [7].

One of the main features of nanomaterials is the fact that their microscopic structure—which results from the synthesis method—largely, affects the macroscopic properties, giving rise to a wide variety of new phenomenon. Current research is devoted to tailor the microstructure at the nanometric scale and correlate it to the macroscopic properties. Some of these anomalous or enhanced properties are: giant magnetoresistance (GMR), colossal magnetoresistance (CMR) and extraordinary Hall effect in metallic systems; large tunnelling magnetoresistance (TMR) in insulating materials; remanence, coercivity and magnetocaloric effect enhancements; glassy behaviour and quantum tunneling of magnetisation. These new properties exhibited by nanomaterials have an enormous technological impact, as in the new generation of ultra-high density magnetic information storage devices, and on some industrial technologies (e.g. magnetic sensors, refrigerant materials and permanent magnets). Besides, magnetic particles and clusters of nanometric size possess an increasing importance in quantum computing, and as diagnostic and therapeutic tools in medicine and other life sciences [6]. Consequently, the magnetism of nanomaterials is a good example of how 'guided' research is relevant from both the fundamental and applied points of view, and how they complement each other:

fundamental research leads to the discovery of new phenomenon and the potential applications of the latter attract a larger number of researchers.

The most studied finite-size effect in small particle magnetic systems is superparamagnetism, which is a finite-size effect since the particle anisotropy is generally proportional to its volume and is discussed below.

There are several directions along which the magnetisation takes place easily. These are called directions of easy magnetisation [1]. For instance, (100), (010), and (001) are the directions of easy magnetisation for iron. This means that the internal magnetisation is stable when pointing parallel to one of these directions. Consider an assembly of uniaxial, single domain particles, each with an anisotropy energy,

$$E = KV \sin^2\theta \quad \text{---------- (1.6)}$$

where K is the anisotropy constant, θ the angle between M_s and the easy axis and V is the particle volume [3]. If the volume of each particle is V, then the energy barrier ΔE that must be overcome before a particle can reverse its magnetisation is KV. Now in any material, fluctuations of thermal energy are continually occurring on a microscopic scale. In 1949 Neel pointed out that, if single domain particle become small enough, KV would become so small that energy fluctuations could overcome the anisotropy forces and spontaneously reverse the magnetisation of a particle from one easy direction to the other, even in the absence of an applied field. Each particle has a magnetic moment,

$$\mu = M_s V \quad \text{---------- (1.7)}$$

If a field is applied, the field will tend to align the moments of the particles, whereas the thermal energy will tend to disalign them. This is just like the behaviour of normal paramagnetic, with one notable exception that the magnetic moment per atom or ion is very high in this case. As a result, Bean has coined the very apt term called superparamagnetism to describe the magnetic behaviour of such particles.

In the superparamagnetic state, the magnetic direction is not fixed along any of the easy axes. It fluctuates among the easy axes of magnetisation when there is no external magnetic field. The superparamagnetic relaxation time 'τ' is the average time that it takes the particle magnetisation to jump from one direction to another. The relaxation time 'τ' depends on the size of the particle and the temperature, which is approximated by Neel as

$$\tau = \tau_0 \exp (KV/k_B T) \quad \text{---------- (1.8)}$$

where K is the anisotropy constant of the particle, V the particle volume, k_B the Boltzmann constant and T the temperature [7]. τ_0 is a constant and is usually taken as $\tau_0 \cong 10^{-10}$ s.

Under the application of a magnetic field H, the equation (1.6) becomes,

$$E = KV \sin^2\theta + HM_sV \cos\theta \quad \text{----------} \quad (1.9)$$

Solving for saturation magnetisation (M_s) from the above equation,

$$M_s = \frac{2K}{H_c} [1-(25kT/KV)^{1/2}] \quad \text{----------} \quad (1.10)$$

For particles of constant size there will be a temperature T_B, called the blocking temperature, below which the magnetisation will be stable [3]. For uniaxial particles,

$$T_B = \frac{KV}{25k} \quad \text{----------} \quad (1.11)$$

The superparamagnetic (SPM) limit has important implications in the thermal and time stability of the bits written in recording media.

The magnetic behaviour of the particle surface differs from that corresponding to the core, because of the distinct atomic coordination, compositional gradients and, concentration and nature of the defects present in both regions. Thus, whereas the core usually displays a spin arrangement similar to that of the bulk material, a much higher magnetic disorder is present in the surface, giving rise to magnetic behaviours which cover from that of a dead magnetic layer to that of a spin glass like.

Nanoparticles of many ferrites have been successfully obtained by numerous chemical routes such as reverse micelle synthesis, coprecipitation, thermal decomposition, solgel and aerogel process. High energy ball milling is being extensively employed as an alternate route to obtain novel materials through solid state reactions.

1.6 High energy ball milling

As already mentioned in the last section, high energy ball milling is being extensively employed as an alternate route to obtain novel fine particle systems through solid state reactions. The high energy ball milling is an excellent tool to produce fine particle materials with a wide range of particle sizes. The decrease in particle size with milling occurs which is due to the fact that the kinetic energy generated by the series of

collisions among balls is transferred to the powder taken in the vial. The details about the experimental set up and theory of high energy ball milling is described in chapter 2.

1.7 Fine particle zinc ferrite

Zinc ferrite which is purported to be a normal spinel, is a classic example of an antiferromagnetic material with a Neel temperature of 10K. Ultrafine $ZnFe_2O_4$ have been reported to be exhibiting a net magnetic moment at room temperature in the fine particle regime [8-19]. From the application point of view, zinc ferrites are widely used catalysts [10] and in the nanoregime the modification of surface properties will have a profound bearing in determining the catalytic properties of these materials. Moreover since they exhibit useful magnetisation at room temperature in the nanoregime they can be potential materials for other applications too.

Zinc ferrite if prepared in the nanoregime, exhibits inversion and the percentage of occupancy of Zn^{2+} ions depends on the method of preparation, vis-à-vis cold preparation technique or ball milling etc [8,9,12-13,20-21]. Results by H.H.Hamdeh et al show a relatively high inversion parameter when coprecipitation method is employed [8,9,13]. There are also reports indicating that the ball milling facilitate inversion and changes magnetic ordering [9,13,21]. In inverse spinels like nickel ferrite, redistribution from inverse to mixed spinel type occurs at nanolevel resulting in an enhancement in magnetisation as compared with bulk. Chinnasamy et al. [17,22] reported an 8% increase in the value of M_s for 1 hour milled nickel ferrite. But prolonged milling reduced the M_s value because of spin-glass like surface disorder exhibited by the particles in the ultrafine regime. The theoretical and technological lowest size of magnetically ordered systems are still an open question of major relevance to applications of nanostructured systems in high density magnetic recording devices [11]. Hence research on the fine particle zinc ferrite is of utmost interest in understanding the behaviour at the nanolevel.

1.8 Fine particle zinc aluminate

Zinc aluminate ($ZnAl_2O_4$) is isostructural with zinc ferrite ($ZnFe_2O_4$) in the sense that both are candidate materials belonging to the class of normal spinels. The only exception is that while $ZnFe_2O_4$ is antiferromagnetic, $ZnAl_2O_4$ is totally nonmagnetic. Both $ZnFe_2O_4$ and $ZnAl_2O_4$ have been materials of yore and tremendous amount of literature exist [4,8-22]. Both have been subjected to detailed investigation. Most of the

literatures pertaining to $ZnAl_2O_4$ as a catalyst [23-26] and mostly it is dealt in the micron regime. However with nanostructured/nanosurface chipping in $ZnAl_2O_4$ and $ZnFe_2O_4$ are revisited for studying their various physical properties in the ultrafine regime.

1.9 Motivation and objectives of the present work

It has been pointed in the beginning that both zinc ferrite and zinc aluminate represent a family of materials called spinels. In the coarser regime, they crystallize in the normal spinel structure without any inversion. Zinc ferrite exhibits antiferromagnetic characteristics with a Neel temperature~10K while zinc aluminate is a widely used catalytic material for various reactions. It must be mentioned here that zinc ferrite is also a widely used catalyst for various reactions and both $ZnAl_2O_4$ and $ZnFe_2O_4$ are important commercially.

However, in the nanoregime, zinc ferrite exhibits anomaly and has been found to be displaying ferrimagnetic properties at room temperature. Many reasons have been attributed to the anomalous magnetic behaviour of these materials. Among them are the cation redistribution between the tetrahedral and octahedral sites, existence of superparamagnetic or spin glass clusters with increase in fineness. The contribution of surface spins or surface magnetisation is also thought to be contributing to the observed magnetisation at room temperature. In short, many schools of thought and hypotheses exist and needs to be tested. Moreover, it has been brought out by various researchers that most of the solid state properties exhibited by these materials are preparation specific. Preliminary studies conducted in the magnetics laboratory by Anantharaman et al [15] indicated that zinc ferrite when prepared in the nanoregime using cold precipitation technique exhibited a net magnetisation at room temperature.

The surface composition analysis carried out by Low Energy Ion Scattering (LEIS) reveals preferential exposure of certain crystallographic sites on the surface where zinc was found to be on the octahedral site in the place of iron [15]. This has lead to the belief that there could be cation redistribution, which is mainly responsible for the observed magnetism, while various other researchers attributed this to superparamagnetism, Quantum magnetism, spin glass etc. So, essentially, any study on ultrafine zinc ferrite is a study of finite size effects on the magnetic and electrical properties. In the ultrafine regime nickel ferrite is also is found to be deviating from the

Neels model and exhibits finite size effects. So it is clear that not only normal spinels but also inverse spinels like nickel ferrite display anomaly in the magnetic properties. Since there exist a correlation between the composition and structure with the electric and magnetic properties, any anomaly in magnetic properties should be reflected in the electrical properties too.

Both Mössbauer and ac magnetic susceptibility (χ_{ac}) are valuable experimental tools to deduce the superparamagnetic/single domain nature of magnetic materials. Mössbauer spectroscopy can be a complementary tool to distinguish the nuclear environment and to deduce parameters like Isomer shift, Quadrupole splitting and Hyperfine field.

Zinc aluminate belongs to the class of normal spinels. Any change taking place structurally with fineness should also be reflected on this material and is an ideal nonmagnetic template for comparison. In the case of zinc aluminate, cold precipitation is employed to prepare zinc aluminate and HEBM is employed to further reduce the size. Electrical properties are evaluated with a view to gain an understanding of the conduction mechanism and correlate it to the finite size effects. Finally a comparison between the two – a magnetic normal spinel and a nonmagnetic spinel will be made and inference will be drawn.

If the presence of oxygen vacancies is responsible for the surface magnetism, these are going to profoundly affect the conduction in these materials. So evaluation of electrical properties – dc conductivity, ac conductivity and dielectric permittivity will bring out signatures of quantum magnetic effects taking place in the conduction mechanism in the form of spin polarized tunnelling.

In order to study the finite size effects one has to prepare pure zinc ferrite and adopt an appropriate method to downsize the particles. In our case, HEBM is employed to reduce the particle size. Phase purity or the presence of impurities is to be ascertained and hence is to be characterized thoroughly by XRD. For studying the magnetic properties, VSM is employed and for evaluation the electrical properties, techniques like dc conductivity, ac conductivity and dielectric studies are utilized. Technique like χ_{ac} were carried out at room temperature and low temperature along with ZFC-FC

measurements in order to delve into the thermomagnetic properties of these particles at low temperature.

So in this investigation, it is envisaged to prepare zinc ferrite in the ultrafine regime by cold precipitation and further reduce the particle size by HEBM. Their structural, magnetic and electrical properties are to be evaluated by techniques like X-ray diffraction, Transmission electron microscopy, Vibrating sample magnetometry, AC magnetic susceptibility, Mössbauer spectroscopy, Conductivity measurements using Keithley source measuring unit and dielectric studies using impedance analyzer. Thus the primary objectives of this proposed work is as follows:

- Synthesis of fine particles of $ZnFe_2O_4$ and $ZnAl_2O_4$ by coprecipitation method.
- Further reduction in size and tuning of size using high energy ball milling (both dry and wet milling).
- Structural studies on $ZnFe_2O_4$ and $ZnAl_2O_4$ including the evaluation of grain size, lattice parameter and lattice strain using X-ray diffraction technique.
- Microstructural studies on $ZnFe_2O_4$ by using Transmission Electron Microscopy (TEM) and surface composition study on $ZnAl_2O_4$ by using Energy Dispersion X-ray (EDX) analysis.
- Comparison of basic properties of $ZnFe_2O_4$/$ZnAl_2O_4$ in the ultrafine regime with respect to grain size/surface composition.
- Magnetic studies on $ZnFe_2O_4$ including Vibrating Sample Magnetometric (VSM) studies and ac magnetic susceptibility studies.
- Room temperature and low temperature Mössbauer studies on $ZnFe_2O_4$.
- Correlation of these results and assigning the reasons for the reported anomaly.
- Electrical studies on $ZnFe_2O_4$ and $ZnAl_2O_4$ including dielectric permittivity, dc conductivity and ac conductivity studies.
- Proposing a model for the conduction mechanism in ultrafine spinels and correlation of electrical and magnetic properties of $ZnFe_2O_4$ with the structural and surface composition.

References:

1.Soshin Chikazumi, *Physics of magnetism , John Wiley and sons, Inc., New York.*

2.David Jiles, *Introduction to magnetism and magnetic materials, Chapman and hall,London.*

3.B.D.Cullity, *Introduction to magnetic materials , Addison Wesley publishing Company.*

4.B.Viswanathan and V.R.K.Murthy, *Ferrite materials – Science & Technology, Narosa publishing house, New Delhi.*

5.Ronald F.Soohoo, *Theory and application of ferrites, Prentice hall Inc, New Jersey.*

6.Xavier Battle, Amilcar Laborta 2002 *J.Phys.D.Appl.Phys* **35** R15

7.Qi Chen, Adam.J.Rondinone, Bryan.C.Chakoumakos, Z.John.Zhang 1999 *J.Magn.Magn.Mater* **194** 1

8.J.C.Ho,H.H.Hamdeh, Y.S.Chen, S.H.Lin, Y.D.Yao, R.J.Willey, S.A.Oliver 1995 *Phys.Rev.B* **52** 10122

9.H.Hamdeh, J.C.Ho, S.A.Oliver, R.J.Willey, G.Oliveri, G.Busca 1997 *J.Appl.Phys* **81** 1851

10.H.Ehrhardt, S.J.Campbell, M.Hofmann 2002 J.Alloys *and Compounds* **339** 255

11.G.F.Goya, H.R.Richenberg, M.Chen, W.B.Yelon 2000 *J.Appl.Phys.* **87** 8005

12.T.Kamiyama, K.Haneda, T.Sato, S.Ikeda, H.Asano 1992 *Sol.state.communi.***81** 563

13.H.H.Hamdeh, J.C.Ho, S.A.Oliver, R.J.Willey, J.Kramer, Y.Y.Chen, S.H.Lin, Y.D.Yao, M.Daturi, G.Busca 1995 *IEEE Trans.magn.* **31** 3808

14.T.Sato, K.Haneda, M.Seki, T.Iijima 1990 *Appl.Phys. A* **50** 13

15.M.R.Anantharaman, S.Jagatheesan, K.A.Malini, S.Sindhu, A.Narayanasamy, C.N.Chinnasamy, J.P.Jacobs, S.Reijne, K.Seshan, R.H.H.Smits, H.H.Brongersma 1998 *J.Magn.Magn.Mater* **189** 83

16.G.F.Goya, H.R.Rechenberg 1999 *J.Magn.Magn.Mater* **196-197** 191

17.C.N.Chinnasamy, A.Narayanasamy, N.Ponpandian, K.Chattopadhyay, K.Shinoda, B.Jeyadevan, K.Tohji, K.Nakatsuka, T.Furubayashi, I.Nakatani 2001 *Phy.Rev.B* **63** 184108

18.W.Schiessel, W.Potzel,H.Karzel, M.Steiner, G.M.Kalvius, A.Martin, M.K.Krause, I.Halevy, J.Gal, W.Schafer, G.Will, M.Hillberg, R.Wappling 1996 *Phys.Rev B* **53** 9143

19.Lotgering.F.K 1996 *J.Phy.Chem.Solids* **27** 139

20.B.Jeyadevan, K.Tohji, K.Nakatsuka 1994 *J.Appl.Phys* **76** 6325

21.Vladimir.Sepelak, Peter.Druska, Ursula.Sleinike 1999 *Mater.Structure* **6** 100

22.C.N.Chinnasamy, A.Narayanasamy, N.Ponpandian, R.Justin Joseyphus, B.Jeyadevan, K.Tohji, K.Chattopadhyay 2002 *J.Magn.Magn.mater* **238** 281

23.Alexandra Navrotsky, 1986 *Am.Minerl.* **71** 1160

24.Hugh S_T. C. O'Nell and Alexandra Navrotsky, 1983 *Am.Mineral.* **68** 181

25.S Mathur, M. Hass, N. Lecerf, M. Veith, H. Shen, S. Hufner, R.Haherkorn, H.P. Beck and M. Jillavi 2001 *J.Am.Ceram.Soc.* **84(9)** 1921

26.Sergio Lucchesi, Umberto Russo, Antonio Della Giusta 1991 *Eur. J.Mineral.***11** 501

CHAPTER 2
EXPERIMENTAL TECHNIQUES

This chapter deals with the techniques employed for the synthesis of ultrafine zinc ferrites and ultrafine zinc aluminates. No thesis on material science/solid state physics is complete without sample preparation and characterization. In most of the cases, the preparative techniques are material specific and the conditions are often to be worked out by trial and error methods. This is more so when phase pure ultrafine particles are to be synthesized. A brief description of the principle and theory of the various analytical tools employed for the characterization of these materials are also described in this chapter.

It is well known that nanostructured materials can be synthesized based on two general principles, which have become known as the bottom up approach and the top down method. The chemical reactions with sufficient driving force can build up particles (bottom up approach) of the material from atomic scale to micron level and above. Here constituent atomic clusters are assembled forming the required nanosized materials by various processes like coprecipitation, reverse micelle, sol gel, electrochemical methods, sputtering, gas evaporation, plasma methods, aerogel methods etc. [1]. In another approach, larger sized particles prepared by high temperature sintering methods, are converted into finer particles by ball milling. The High-energy ball milling reduces the particle size from micron level and above to nanoscale (top down approach). In recent years, there is an increased interest in establishing appropriate processing routes by employing both bottom up and top down approaches. The 'bottom up' methods, which are associated with the dispersion and rapid mixing of dissolved reagents on an atomic level, has obvious advantages over 'top down' methods [2]. But the method of ball milling has the advantage that the material properties including the grain sizes and various characteristic properties can be fine tuned. In this work coprecipitation is employed to generate fine particles and high-energy ball milling (HEBM) is used to further reduce the particle size.

The various characterization tools employed are X-ray diffraction studies, Transmission electron microscopy, Energy dispersive x-ray analysis, Vibrating sample

magnetometry, AC magnetic susceptibility measurements, Mössbauer spectroscopy, DC Conductivity, Dielectric permittivity and AC conductivity studies.

2.1 Coprecipitation

Coprecipitation method offers distinct advantages [3] like simple and rapid preparation, easy control of particle size and composition and various possibilities to modify the particle surface state and overall homogeneity over other preparative methods.

Coprecipitation of various salts (nitrates, sulphates, chlorides, perchlorates etc.) under a fine control of pH by using NaOH or NH_4OH solutions yields corresponding spinel oxide nanoparticles. For example, to prepare zinc ferrite, zinc nitrate and ferric nitrate are used as starting precursors. The pH of the medium should be greater than 8 for a better yield. Particle size of the coprecipitated material is strongly dependent on pH of the precipitation medium and molarity of the starting precursors. Consequently particle size control can be easily achieved.

A crystalline phase is achieved even with a pH of around 8 if we use a salt that contains Fe^{2+} ions. The electron mobility between Fe^{2+} and Fe^{3+} acts as the driving force for the spinel phase formation. But when we have to deal with normal spinel ferrites where in only Fe^{3+} species exist, the pH of the medium has to be enhanced by trial. It has been found that an optimum pH of 12 is ideal.

If we increase the molarity of the solution, particle size gets reduced. But this size reduction is achieved at the expense of large amount of chemicals. Hence a compromise between this leads us to prefer a moderate molarity for the starting solutions. In our synthesis, 0.1M and 0.2M solutions were employed to initiate the coprecipitation.

2.1.1 Synthesis of $ZnFe_2O_4$

0.1M aqueous solution of zinc nitrate and 0.2M aqueous solution of ferric nitrate were prepared separately. Both the solutions were mixed together and stirred using a magnetic stirrer keeping the temperature at 373 K. While stirring this mixture, pure ammonium hydroxide solution was added until the pH of the solution becomes 12. The precipitate produced was dried at 373 K and annealed in air at 773 K which yielded crystalline zinc ferrite.

2.1.2 Synthesis of $ZnAl_2O_4$

0.1M aqueous solution of zinc nitrate and 0.2M aqueous solution of aluminium nitrate were prepared separately. Both the solutions were mixed together and stirred using a magnetic stirrer keeping the temperature at 373 K. While stirring this mixture, pure ammonium hydroxide solution was added until the pH of the solution becomes 12. The precipitate produced was dried at 373 K and annealed in air at 773 K which yielded crystalline zinc aluminate.

2.2 High energy ball milling

High-energy ball milling of powder particles as a method for materials synthesis has been developed as an industrial process to successfully produce new alloys and phase mixtures in 1970's [4]. This powder metallurgical process allows the preparation of alloys and composites, which cannot be synthesized via conventional routes. In nanomaterials research, this top down technique is increasingly employed to fine-tune the grain sizes of the materials in nanoscale.

A variety of milling devices has been developed for different purposes including tumbler mills, attrition mills, shaker mills, vibratory mills, planetary mills etc.

In this work, Fritsch planetary micro mill, 'pulverisette 7' was used for milling (figure 2.1). Here grinding bowls rotate on their own axis while simultaneously rotating through an arc around the central axis (figure 2.2). The grinding balls and the material in the grinding bowl are thus acted upon by the centrifugal forces, which constantly change in direction and intensity resulting in efficient, fast grinding process. The grinding bowl and the supporting disc rotate in opposite directions, so that the centrifugal forces alternatively act in the same and opposite directions. This results in, as a frictional effect, the grinding balls running along the inner wall of the grinding bowl, and impact effect, the balls impacting against the opposite wall of the grinding bowl. The energy thus created by impact is many times higher than for traditional mills. This results in excellent grinding performance and considerably shorter grinding times. Atmospheric contamination can be minimized by sealing the vial with a flexible 'O' ring after the powder has been loaded. If a milling medium-a fluid (usually an organic fluid) is used, contamination by the milling tools can be prevented and also it minimizes the wear.

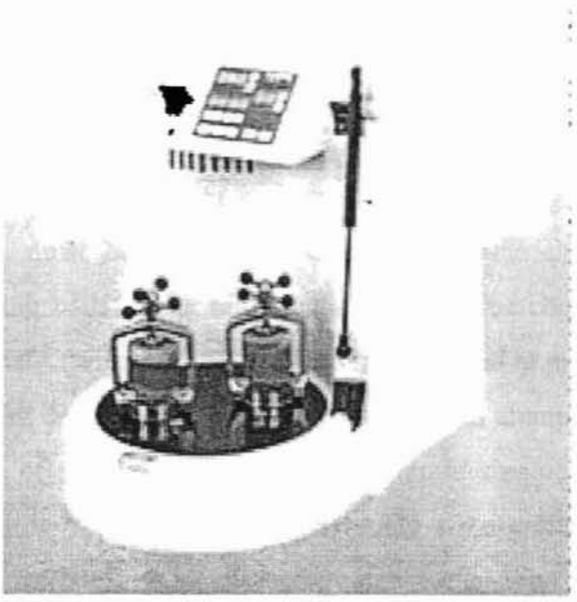

Figure 2.1 Fritsch Planetary micromill 'pulverisette 7'.

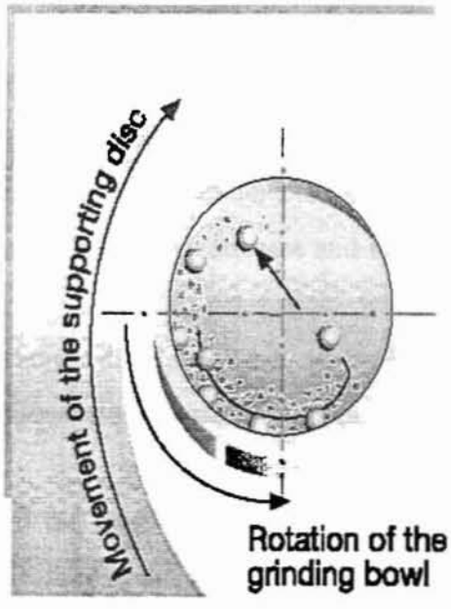

Figure 2.2 Rotation of the bowl and balls around the central axis.

A few parameters exists in high energy ball milling which on changing, we can produce a wide range of fine particles with different sizes and consequently with different physical properties [5]. These parameters are type of mill, milling atmosphere, milling media, intensity of milling, ball to powder weight ratio (BPR), milling time and milling temperature.

The reduction in grain size is accomplished by the kinetic energy transfer from balls to powder. Since the kinetic energy of the balls is a function of their mass and velocity, dense materials are preferred like steel or tungsten carbide. Other materials used as balls are agate, sintered corundum, zirconium dioxide, Teflon, chrome nickel, silicon nitride etc. In order to prevent excessive abrasion, the hardness of the grinding bowl used and of the grinding balls must be higher than that of the materials used. Normally grinding bowls and grinding balls of the same material should be chosen. In this work tungsten carbide vial and balls (with density~14.75 g/cm^3) are used to mill ferrite system and steel vial and balls (with density~7.85 g/cm^3) are used to mill aluminate systems.

In the initial stage of milling, a fast decrease of grain size occurs which slows down after extended milling. Once the minimum steady state grain size is reached, further refinement ceases. Initially the kinetic energy transfer leads to the production of an array of dislocations. This is accompanied by atomic level strains. At a certain strain level, these dislocations annihilate and recombine to form small angle grain boundaries separating the individual grains. Thus subgrains are formed with reduced grain size. During further milling, this process extends throughout the entire sample. To maintain this reduction in size, the material must be subjected to very high stress. But extended milling could not able to maintain the high stresses and hence reduction of grain size is limited in extended milling. The other two parameters, which restrict reduction of grain size, are the local temperature developed due to ball collisions and the overall temperature in the vial [6]. Temperature rise arises from balls to balls, balls to powder and balls to wall collisions.

The impact speed and the impulsive load of the grinding balls are the two key parameters, which determine the kinetic energy transfer [7]. The impulsive load of grinding balls is given by,

$$F = \frac{mv}{t} \quad \text{---------- (2.1)}$$

where 'm' is the ball mass, 'v' the ball velocity and 't' is the ball-vial contact time. The contact time 't' is given by,

$$t = (1+1.2\ e)\sqrt{\frac{\pi m}{30YR}} \quad \text{---------- (2.2)}$$

where 'Y' is the yield strength of the vial, 'R' is the ball radius and 'e' is the restitution coefficient typical of the vial material.

2.2.1 High-energy ball milling on $ZnFe_2O_4$ and $ZnAl_2O_4$

The high-energy ball milling was carried out on the coprecipitated $ZnFe_2O_4$ and $ZnAl_2O_4$ samples. The samples were milled for various milling time to produce a range of particle sizes. This is to investigate the finite size effects on electrical and magnetic properties of zinc ferrite and zinc aluminate.

Different types of vials and balls (tungsten carbide for ferrite system and dye steel for aluminate system) were utilized. The milling intensity was also different for $ZnFe_2O_4$ (650 rpm for dry milling and 360 rpm for wet milling) and $ZnAl_2O_4$ (200 rpm for both wet and dry milling). Both dry milling and wet milling (with toluene as medium) were employed. The details of the samples prepared are summarized in table 1.1.

2.3 X-ray diffraction studies

The identification of the phase as well as evaluation of structural parameters were carried out by X-ray diffraction technique. Phase identification was carried out by comparing the observed structural parameters with that of the standard values reported in the literature (JCPDS standards). The powder diffractograms of the samples were recorded on a Rigaku Dmax-C model X ray diffractometer using Cu K_α radiation (λ = 1.5418 Å). From the XRD pattern obtained the 'd' values are calculated using the relation $2d \sin\theta = n\lambda$. Then the lattice parameter (a) was calculated assuming cubic symmetry by using the relation,

$$a = d(\sqrt{h^2 + k^2 + l^2}) \quad \text{---------- (2.3)}$$

The particle size was also calculated from the XRD data using Scherrer formula, which is given by

Sample	Milling medium	Vial and balls used	Ball to powder weight ratio	Milling intensity (rpm)	Milling times
$ZnFe_2O_4$	Dry milling	Tungsten carbide	10:1	650	5minutes, 30minutes, 5 hours, 10 hours
$ZnFe_2O_4$	Wet milling-toluene	Tungsten carbide	8:1	360	5minutes, 30minutes, 5 hours
$ZnAl_2O_4$	Dry milling	Dye steel	10:1	200	5minutes, 30minutes, 5 hours
$ZnAl_2O_4$	Wet milling-toluene	Dye steel	10:1	200	5minutes, 30minutes, 5 hours

Table 1.1 Preparative conditions employed for the synthesis of ultrafine particles.

$$D = \frac{0.9\lambda}{\beta \cos\theta} \quad \text{---------} \quad (2.4)$$

where D is the particle size, β is the angular width which is equal to the full width at half maximum (FWHM) in radians and λ is the wavelength of X-ray radiation which is equal to 1.5418 Å [8].

The grain size and the strain developed during the milling process can be calculated from the linewidth (FWHM in radian) of XRD lines given below[8].

$$FWHM(\beta) = \lambda/(d_g \cos\theta)+4\varepsilon \tan\theta \quad \text{---------} \quad (2.5)$$

where θ is the bragg angle, ε is the strain developed and d_g the grain size [9].

Rewriting the above equation,

$$\beta \cos\theta = \varepsilon(4\sin\theta) + \lambda/d_g \quad \text{---------} \quad (2.6)$$

This equation represents a straight line between βcosθ (Y-axis) and 4sinθ(X-axis). The slope of this line gives the strain and d_g can be calculated from the intercept of this line on the Y-axis.

2.4 Transmission electron microscopy (TEM)

Grain size and morphological studies were carried out on zinc ferrite system by transmission electron microscopy method by employing JEOL-JEM 2000 FX_{II}. Transmission electron microscopy is a direct derivative of the compound light microscope making use of the shorter wavelength electron illumination [10]. Here a thin specimen is irradiated with an electron beam of uniform current density. Electrons are emitted from an electron gun and illuminate the specimen through a two or three stage condenser lens system. The electron intensity distribution behind the specimen is magnified with a three or four stage lens system and viewed on a fluorescent screen. The image can be recorded by direct exposure of a photographic film.

It is to be noted that the specimen for TEM investigations should be able to transmit sufficient electrons to form an image with nominal energy loss, must be stable under electron impingement in vacuum and must fit the sample holder. The interaction between the electron beam and specimen is necessary inorder to produce image detail, inelastic encounters resulting in energy loss by the electrons degrade the quality of the image because of the chromatic aberration in lenses [10].

Advanced versions of TEM namely High Voltage TEM (HVTEM) and High Resolution TEM (HRTEM) are the state of the tools to carry out elemental and crystallographic microanalysis [10].

2.5 Energy dispersive X-ray analysis (EDX)

Energy dispersive X-ray analysis is a chemical microanalysis technique used for elemental composition analysis. This technique is used in conjunction with scanning electron microscopy (SEM). The EDX technique detects X-rays emitted from the sample during bombardment by an electron beam to characterize the elemental composition.

When the sample is bombarded by the SEM's electron beam, electrons are ejected from the atoms comprising the sample's surface. The resulting electron vacancies are filled by electrons from a higher state, and an X-ray is emitted to balance the energy difference between the two electronic states. The X-ray energy is characteristic of the element from which it was emitted. The spectrum of X-ray energy versus counts is evaluated to determine the elemental composition of the samples.

EDX analysis of zinc aluminate system was carried out by using the model Link 10,000.

2.6 Vibrating sample magnetometry

This method is used to derive the hysteresis loop parameters namely Saturation magnetisation (M_s), Coercive field (H_c), Remanence (M_r) and Squareness ratio (M_r/M_s). When a magnetic sample is placed in a uniform magnetic field, a dipole moment proportional to the product of the sample susceptibility times the applied field is induced in the sample. If the sample is allowed to vibrate sinusoidallly, an electrical signal can be induced in a suitably located stationary pick up coils. This signal which is at the vibration frequency is proportional to the magnetic moment, vibration amplitude and vibration frequency. This means, of producing an electrical signal proportional to the magnetic moment of a sample material is used in the model EG&G PAR 4500 VSM. The material under study is contained in a sample holder, which is centered in the region between the pole pieces of an electromagnet. A slender vertical sample rod connects the sample holder with a transducer assembly located above the magnet, which in turn supports the transducer assembly by means of sturdy adjustable support rods.

The transducer converts a sinusoidal ac drive signal provided by a circuit located in the console in to a sinusoidal vertical vibration of the sample rod and the sample is thus made to undergo a sinusoidal motion in a uniform magnetic field. Coils mounted on the pole pieces of the magnet pick up the signal resulting from the sample motion. This ac signal at the vibrating frequency is proportional to the magnitude of the moment induced in the sample. However, it is also proportional to the vibration amplitude and frequency. A servo system maintains constancy in the drive amplitude and frequency so that the output accurately tracks the moment level without degradation due to variation in the amplitude and frequency of vibration.

This technique depends on the ability of a vibrating capacitor located beneath the transducer to generate an ac control signal, which varies solely with the vibration amplitude and frequency. This signal, which is at the vibration frequency, is fed back to the oscillator where it is compared with the drive signal so as to maintain a constant drive output. It is also phase adjusted and routed to the signal demodulator where it function as the reference drive signal. The signal originating from the sample in the pick up coils is then buffered, amplified and applied to the demodulator. Then it is synchronously demodulated with respect to the reference signal derived from the moving capacitor assembly. The resulting dc output is an analog of the moment magnitude alone, uninfluenced by vibration amplitude changes and frequency drifts. A cryogenic setup attached to the sample permits low temperature measurements.

The dipole moment is induced in the sample when it is placed in a uniform magnetic field be M. Then the amount of magnetic flux linked to the coil placed in the vicinity of this magnetic field is given by

$$\phi = \mu_0 n \alpha M \text{ ---------- } (2.7)$$

where 'μ_0' is the permeability of free space, 'n' the number of turns per unit length of coil and $\propto$ represents the geometric moment decided by position of moment with respect to coil as well as shape of coil.

Anharmonic oscillator of the type,

$$Z = Z_0 + A\exp(j\omega t) \text{ .....(2.8)}$$

induces an emf in the stationary detection coil. The induced emf is given by

$$V = -\frac{d\phi}{dt} = -j\omega\mu_0 nMA(\frac{\partial\alpha}{\partial z})e^{j\omega t} \quad \text{.....(2.9)}$$

If amplitude of vibration (A), frequency and $\frac{\partial\alpha}{\partial z}$ are constant over the sample zone then induced voltage is proportional to the magnetic moment of the sample. This is the basic idea behind VSM [11-13]

The magnetic properties of samples under temperature variations were studied in two cooling procedures: zero field cooled (ZFC) and field cooled (FC) conditions. These ZFC-FC magnetisation measurements (ZFC-FC curves) are very useful in studying superparamagnetism and spin glass behaviour in materials [14].

2.7 AC magnetic susceptibility studies

Figure 2.3 shows the schematic diagram of the instrumental set up used for ac susceptibility measurements consisting of a cryostat assembly and coil systems [15]. Here the change in the mutual inductance of a primary and two identical but oppositely wound secondary coils is measured when a sample is placed in it. This change is a measure of the magnetic susceptibility of the sample.

The length of the glass cryostat is around 300mm. The lower tail of the glass cryostat is a double walled cylinder of inner diameter 7mm and length 200mm. The glass cryostat is attached to a tube through a glass-to-metal seal. This tube has a Wilson seal at the top to introduce the sample rod to the cryostat. There is a glass valve in the tube to facilitate the change of the sample without disturbing the vacuum. The evacuated glass cryostat along with the coil system is dipped into a glass dewar filled with liquid N_2. Primary and a set of secondary coils are wound on separate hylum formers. Hylum was chosen for its thermal and mechanical properties. The secondary coils are generally kept inside the primary coil for a maximum filling factor of the secondary and the sample. The offset voltage, which is undesirable, is minimized by unwinding a few turns of the secondary while construction of the coil assembly. Even then a small offset voltage will remain which is compensated by an electronic offset compensation circuit. Here a voltage tapped with the primary coil is phase resolved using Butterworth filters, and is attenuated to generate voltages that are equal in magnitude and opposite in sign to the offset voltage. The sample holder is a sapphire plate of length 70mm and width 4mm. It is attached to a

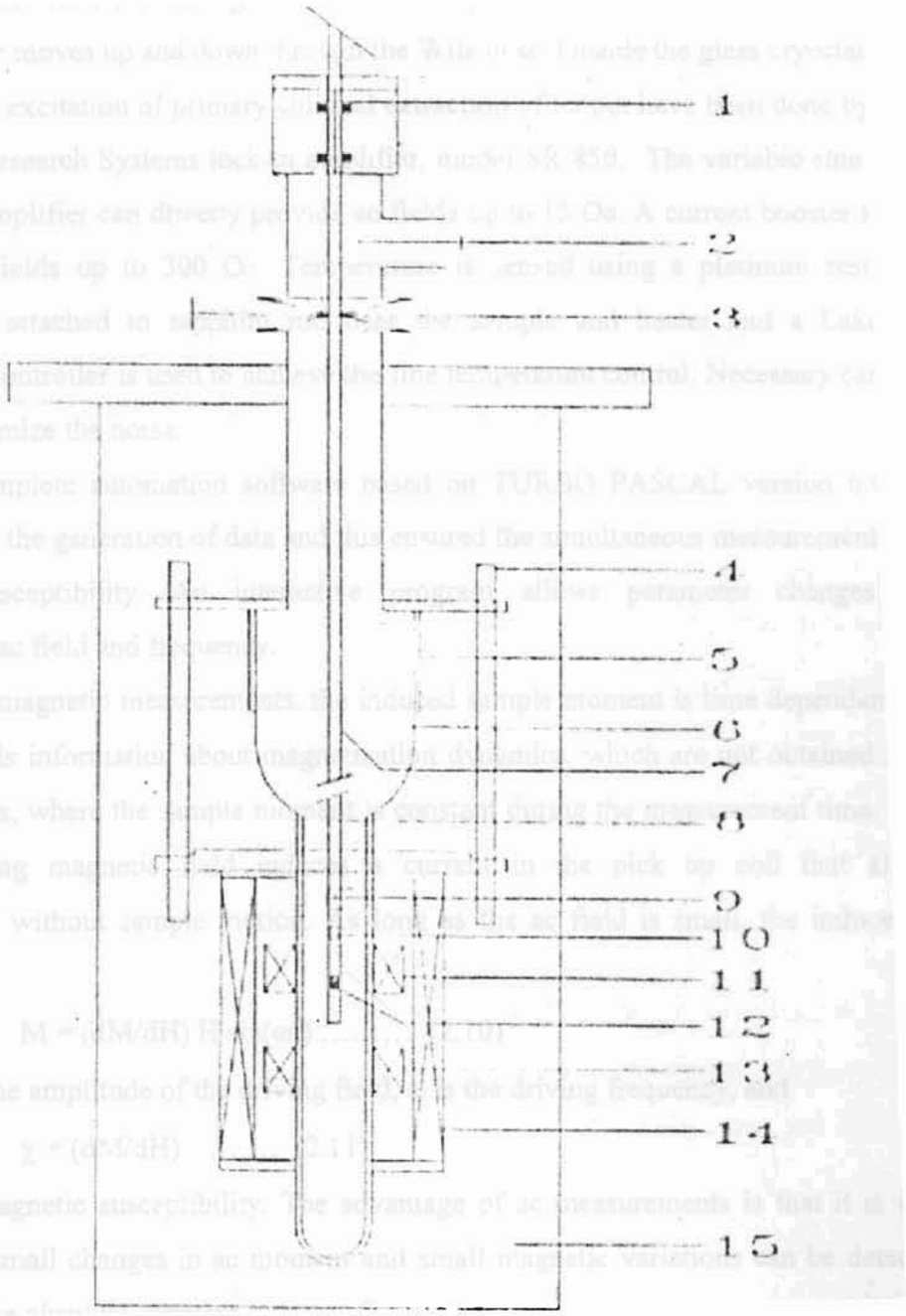

Figure 2.3 Cryostat assembly with coil system. 1.Wilson seal 2.Vacuum port 3.Gate valve 4.Hanging hylum rods 5.Glass to metal seal 6.Glass cryostat 7.Stainless steel rod 8.Sapphire plate 9.Heater wire 10.Platinum resistance thermometer 11. Secondary coil S_1 12.Sample 13.Secondary coil S_2 14.Primary coil and 15.Cryogen.

hollow stainless steel rod through a nonmetallic hylum extension of 60mm length. The sample holder moves up and down through the Wilson seal inside the glass cryostat.

Initial excitation of primary coil and extraction of output have been done by using a Standard Research Systems lock-in amplifier, model SR 850. The variable-sine out of the lock-in amplifier can directly provide ac fields up to 15 Oe. A current booster is used to generate fields up to 300 Oe. Temperature is sensed using a platinum resistance thermometer attached to sapphire rod near the sample and heater and a Lakeshore temperature controller is used to achieve the fine temperature control. Necessary care was taken to minimize the noise.

A complete automation software based on TURBO PASCAL version 6.0 was employed for the generation of data and this ensured the simultaneous measurement of ac magnetic susceptibility. An interactive program allows parameter changes like temperature, ac field and frequency.

In ac magnetic measurements, the induced sample moment is time dependant and hence it yields information about magnetization dynamics, which are not obtained in dc measurements, where the sample moment is constant during the measurement time. Here the ac driving magnetic field induces a current in the pick up coil that allows measurement without sample motion. As long as the ac field is small, the induced ac moment is

$$M = (dM/dH)\, H \sin(\omega t) \ldots\ldots\ldots \quad (2.10)$$

Where H is the amplitude of the driving field, ω is the driving frequency, and

$$\chi = (dM/dH) \ldots\ldots\ldots \quad (2.11)$$

is called magnetic susceptibility. The advantage of ac measurements is that it is very sensitive to small changes in ac moment and small magnetic variations can be detected even when the absolute moment is large. Generally ac magnetic measurements yield two quantities, magnitude of the susceptibility χ and phase shift φ. Alternatively, susceptibility can be represented by a real component $\chi^{(r)}$ and an imaginary component $\chi^{(i)}$. The two representations are related by

$$\chi^{(r)} = \chi\cos\varphi \ldots\ldots\ldots \quad (2.12)$$

$$\chi^{(i)} = \chi\sin\varphi \ldots\ldots\ldots \quad (2.13)$$

The third order susceptibility values were evaluated by the Sherrington-Kirkpatrikc model and the Bethe approximation according to which, the magnetisation of a specimen in the presence of an external oscillating magnetic field H can be represented as

$$M= M_0+\chi_1 H+\chi_2 H^2+\chi_3 H^3+..... \quad (2.14)$$

Where M_0 is the spontaneous magnetisation and χ_1,χ_2 and χ_3 are the first, second and third order susceptibilities respectively [16-19].

χ_1,χ_2 and χ_3 are measured using a mutual inductance bridge. Measurements were carried out using a susceptometer for various applied fields [16-19].

2.8 Mössbauer studies

The phenomenon of the emission of a γ-ray photon without loss of energy due to recoil of the nucleus and without thermal broadening is known as Mössbauer effect [20-21]. Since the gamma emission is recoil-free, it can be resonantly absorbed by stationary atoms. It was discovered by Rudolph Mössbauer in 1957 and it has tremendous application in materials research. The direct application of the Mössbauer effect to materials research arises from its ability to detect the slight variations in the energy of interaction between the nucleus and the extra nuclear electrons, variations which had previously been considered negligible.

The Mössbauer effect has been detected in a total of 88 γ-ray transitions in 72 isotopes of 42 different elements. Although in theory it is present for all excited state-ground state γ-ray transitions, its magnitude can be so low as to preclude detection with current techniques. The useful Mössbauer isotopes so far found out are iron, tin, antimony, tellurium, iodine, xenon, europium, gold and neptunium and to a less extent nickel, ruthenium, tungsten and iridium. Among all these elements, the largest recoil free resonant cross section occurs for the isotope Iron 57. The resonant energies are extremely narrow which allows the observation of the hyperfine interactions between the nucleus and the surrounding electrons. The link between the Mössbauer spectrum and the electron structure of the sample can be exploited in the study of many types of materials.

Figure 2.4 shows the decay of $_{26}Fe^{57}$ from its parent nuclei $_{27}Co^{57}$. By an electron capture $_{27}Co^{57}$ whose half-life is 270 days gets decayed to $_{26}Fe^{57}$. Approximately 90% of

the $_{26}Fe^{57}$ nuclear excited state decays through the intermediate level to produce 14.4 keV gamma radiation. These gamma photons can then be absorbed by Fe^{57} in a sample.

To use the Mössbauer source as a spectroscopic tool, we must be able to vary its energy over a significant range. For this the gamma ray source is mechanically vibrated back and forth to Doppler shift the energy of the emitted gamma radiation. Figure 2.5 shows a transmission Mössbauer experiment. As the energy of the gamma radiation is scanned by Doppler shifting, the detector records the frequencies of gamma radiation that are absorbed by the sample. Moving the source at a velocity of 1 mm/s toward the sample will increase the energy of the photons by 14.4 keV (v/c), which is equal to 4.8×10^{-8} eV. The 'mm/s' is a convenient Mössbauer unit and is equal to 4.8×10^{-8} eV for Fe^{57}.

Mössbauer spectrum reflects the hyperfine interactions of the sample [20-21]. The total interactions between the nucleus and the electrons can be represented by the Hamiltonian,

$$H = H_0 + E_0 + M_1 + E_2 + \ldots \quad \text{---------} \quad (2.15)$$

where H_0 represents all terms in the Hamiltonian for the atom except the hyperfine interactions being considered; E_0 represents the electric monopole interactions between the nucleus and the electrons; M_1 represents the magnetic dipole hyperfine interactions; and E_2 refers to the electric quadrupole interactions. Higher terms are usually negligible.

Figure 2.6 gives an outline of the different interactions that produce different types of Mössbauer spectra. The E_0 coulombic interaction alters the energy separation between the ground state and the excited state of the nucleus, thereby causing a slight shift in the position of the observed resonance line. The shift will be different in various chemical compounds, and for this reason is generally known as the chemical isomer shift (δ). This may be written as

$$\delta = K \{\Sigma_s |\psi(0)|^2 - \Sigma_a |\psi(0)|^2\} \quad \text{---------} \quad (2.16)$$

where K is a positive constant depending on the change in the nuclear radius, $\Sigma_s |\psi(0)|^2$ is the electron density at the source nucleus and $\Sigma_a |\psi(0)|^2$ is the electron density at the absorber nucleus. Thus isomer shift gives an idea about the electron density in the sample. Thus Mössbauer spectroscopy becomes an important means by which atomic

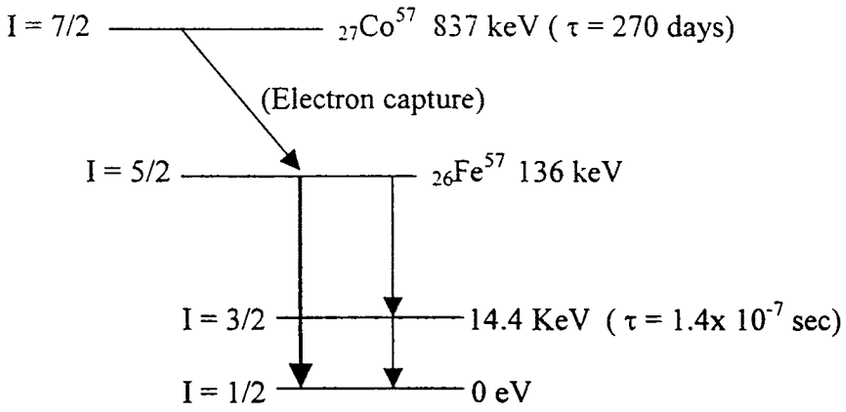

Figure 2.4. The production of gamma rays for Mössbauer spectroscopy.

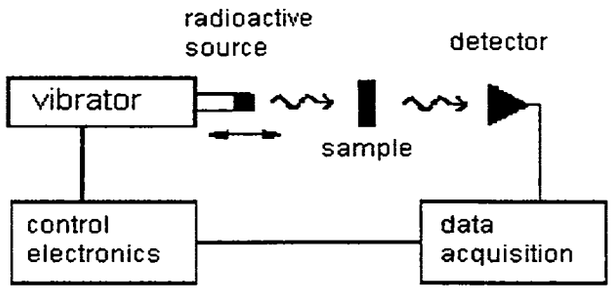

Figure 2.5 A Typical Transmission Mössbauer Experimental Setup.

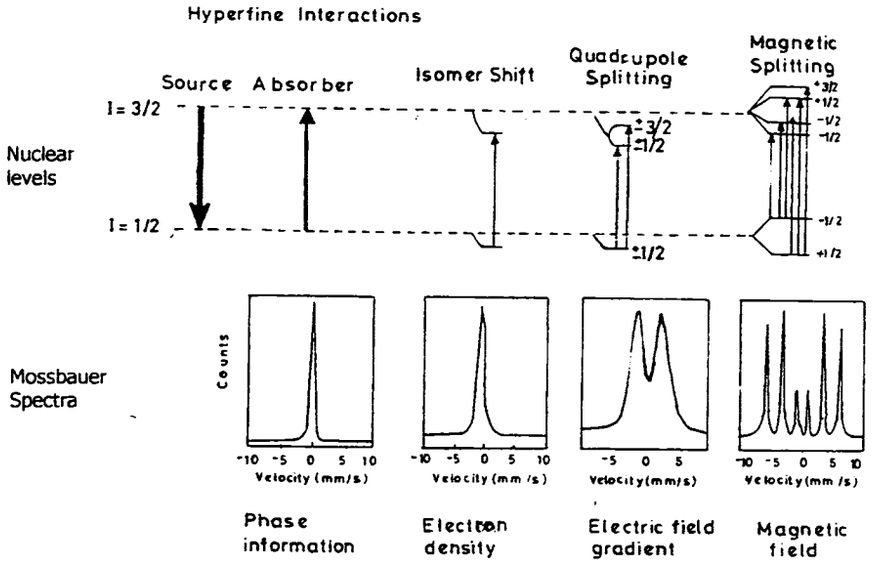

Figure 2.6 Different Interactions in a Mössbauer Spectrum.

oxidation state can be detected, which are sometimes very difficult to determine by other techniques. The electronic contribution to the isomer shift is essentially temperature independent and the observed decrease at high temperatures is due to the relativistic second order Doppler effect.

While discussing isomer shift, it is assumed that the nuclear charge distribution is spherical. However, nuclei in states with a nuclear angular momentum quantum number $I > 1/2$ have non-spherical charge distributions, which are characterised by a nuclear quadrupole moment [20]. When the nuclear quadrupole moment experiences an electric field gradient (ie an asymmetric electric field produced by an asymmetric electronic charge distribution), an electric quadrupole interaction occurs which gives rise to a splitting of the nuclear energy levels. In the case of Fe^{57} the excited state has $I = 3/2$, and in the presence electric field gradient this splits into two sub states as shown in figure 2.6. This situation leads to a two line spectrum, with the two lines separated by the quadrupole splitting Δ. This gives information relating to the electronic population of various orbitals, isomerisation phenomenon, short-lived reaction intermediates, semiconductor properties and the defect structure of solids.

When a nucleus is placed in a magnetic field, there is a magnetic dipole interaction between any nuclear magnetic moment and the magnetic field. The interaction splits the nuclear state with spin quantum number I into 2I+1 equally spaced and non-degenerate substates. The selection rule limits and appropriates the Mössbauer γ-ray to six possible transitions and hence it leads to a Mössbauer spectrum with six absorption lines (Figure 2.6). Magnetic hyperfine fields are observed in the Mössbauer spectra of magnetically ordered systems, or of paramagnetic systems when the electron spin relaxation times are long. Since the splitting of the spectral lines is directly proportional to the magnetic field experienced by the nucleus. Mössbauer spectroscopy provides a very effective means by which this field may be measured. The transition probabilities between the nuclear substates affect the intensities of the lines in the Mössbauer spectrum, which can therefore give information on the relative orientation of the magnetic field at the nucleus and the direction of propagation of the γ-ray beam.

2.9 DC conductivity studies

DC conductivity studies on the ultrafine ferrites and aluminates were carried out to evaluate the conduction mechanism and its temperature dependence. Computer controlled keithley 236 source/measure unit is used to apply a potential to the sample and measure the current across the sample. The conductivity cell (figure 2.7) has provisions for sensing and controlling the temperature and pressure. The dry milled zinc ferrite and zinc aluminates were subjected to dc conductivity studies in the temperature range 300 K to 393 K.

The temperature dependence of the electrical conductivity is given by the relationship,

$$\sigma T = \sigma_0 \exp(-E_a/kT) \quad \text{---------} \quad (2.17)$$

Where E_a is the activation energy for conduction and k the Boltzmann constant. Hence the slope of the $10^3/T$ Vs ln (σT) graph will give an idea about the activation energy.

2.10 Dielectric permittivity and ac conductivity studies

These studies give an idea about the conduction mechanism of these nanomaterials. A material is said to be dielectric if it has the ability to store energy when an external electric field is applied. If a dc voltage source is placed across a parallel plate capacitor, more charge is stored when a dielectric material is inserted between the plates than if no material is between the plates. The dielectric material increases the storage capacity of the capacitor by neutralizing charges at the electrodes, which ordinarily would contribute to the external field.

In any dielectric material there will be some power loss because of the work done to overcome the frictional damping forces encountered by the dipoles during their rotations. If an ac sinusoidal voltage source is placed across the capacitor, the resulting current will be made up of a charging current and a loss current that is related to the dielectric permittivity. Here we are interested only in the relative permitivity (ε_r) of the material. Relative permittivity describes the interaction of a material with an electric field. The complex relative permittivity is given by

$$\varepsilon_r^* = \frac{\varepsilon^*}{\varepsilon_0} = \frac{\varepsilon^1 - j\varepsilon^{11}}{\varepsilon_0} \quad \text{----------} \quad (2.18)$$

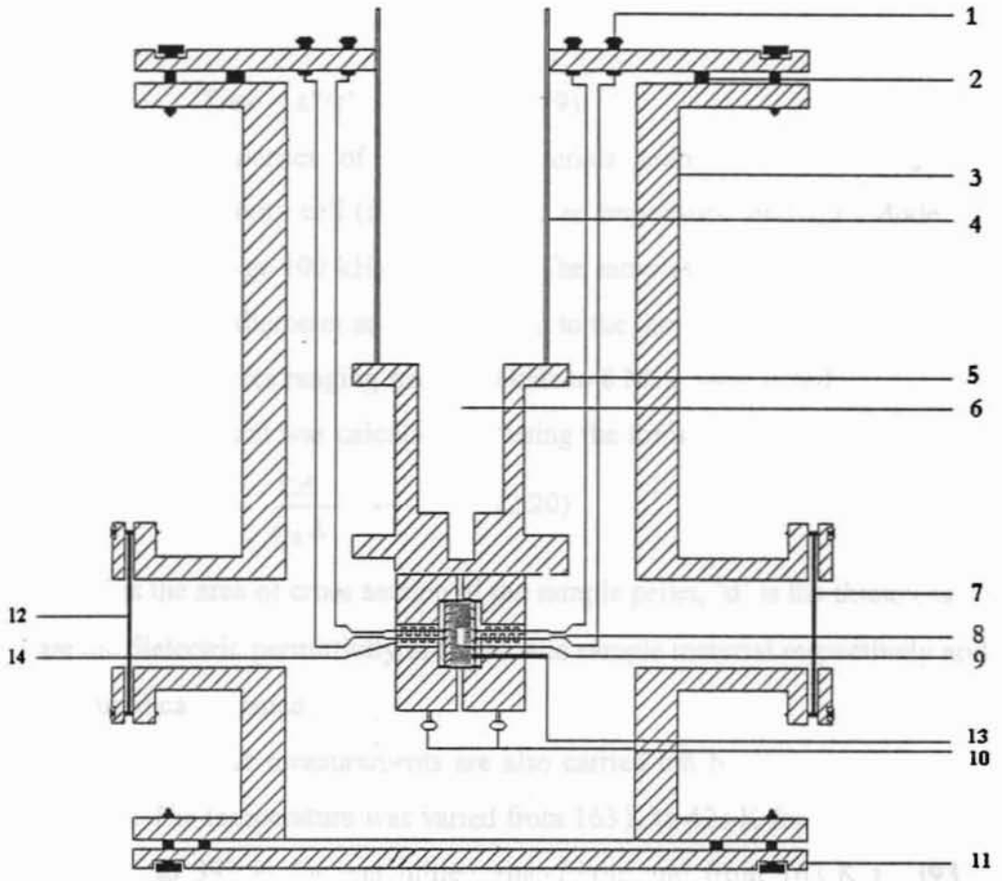

1. BNC
2. Neoprine O Ring
3. MS Chamber
4. SS Pipe
5. Sample Holder
6. Liq. Nitrogen Cavity
7. Optical Window
8. Copper Electrodes
9. Sample
10. Fixing Screws
11. MS Flange
12. To Vacuum pump
13. Thermo couple
14. Spring

Figure 2.7 Conductivity cell.

Where 'ε_0' is the dielectric permittivity of free space, which is 8.854 x 10^{-12} F/m in SI units. The real part of dielectric permittivity (ε^1) is a measure of how much energy from an external electric field is stored in a material. The imaginary part of the dielectric permittivity (ε_r") is called the loss factor. It is a measure of the energy dissipation or heat generation in the material when an external electric field is applied. The dielectric loss is given by,

$$\text{Tan}\delta = \varepsilon''/\varepsilon' \quad \text{----------} \quad (2.19)$$

The dielectric properties of the nanomaterials prepared were studied by using a homemade conductivity cell (figure 2.7) and an impedance analyzer (Model: HP 4285A) in the frequency range 100 kHz to 8 MHz. The samples prepared were made in the form of pellets of 12mm diameter and is loaded in to the dielectric cell. The capacitance values at different frequencies ranging from 100 kHz to 8 MHz were noted.

The dielectric constant was calculated by using the formula

$$\varepsilon_r = \frac{Cd}{\varepsilon_0 A} \quad \text{----------} \quad (2.20)$$

where 'A' is the area of cross section of the sample pellet, 'd' is the thickness, 'ε_0' and 'ε_r' are the dielectric permittivity of the air and sample material respectively and 'C' is the measured capacitance.

The dielectric measurements are also carried out by changing the temperature of the samples. The temperature was varied from 163 K to 423 K for dry milled zinc ferrites, from 300 K to 393 K for wet milled zinc ferrite and from 163 K to 393 K for zinc aluminates.

The entire data acquisition and evaluation of the dielectric constant were automated by using a package called LabVIEW which in turn is based on G programming. LabVIEW is a programming language for data acquisition, analysis, simulation or computer control of instruments, techniques or processes. LabVIEW is an acronym for Laboratory Virtual Instrument Engineering Workbench and is a proprietary item owned by National Instruments. LabVIEW is an object-oriented language and its style, syntax and data flow is different from conventional linear programming languages. Appropriate modifications were incorporated in the software so as to enable the data acquisition automatic and visual observation of the graphs on the computer screen. It has

been possible to acquire 20,000 data points or more in a matter of 5 to 10 minutes by using the modified package. The details of the experimental set up and automation are cited elsewhere [22].

A capacitor when charged under an ac voltage will have some loss current due to ohmic resistance or impedance by heat absorption. If 'Q' is the charge in coulombs due to a potential difference of 'V' volts between two plates of a capacitor of area of A and inter plate distance is 'd' , then ac conductivity (σ_{ac}) due to ac voltage v ($v_0 e^{j\omega t}$) is given by the relation

$$\sigma_{ac} = \frac{J}{E} \quad \text{---------} \quad (2.21)$$

where 'J' is the current density and 'E' is the electric field strength vector. But we know that the electric field vector

$$E = \frac{D}{\varepsilon} \quad \text{----------} \quad (2.22)$$

where 'D' is the displacement vector of the dipole charges. 'ε' is the complex permittivity of the material. Also the electric field intensity (E) for a parallel plate capacitor is the ratio of potential difference between the plates of the capacitor and the inter plate distance. i.e.

$$E = \frac{V}{d} \quad \text{---------} \quad (2.23)$$

Since the current density $J = \frac{dq}{dt}$ where q is given by $\frac{Q}{A} = \frac{V\varepsilon}{d}$

$$\therefore J = \frac{dq}{dt} = \frac{d}{dt}\left(\frac{V\varepsilon}{d}\right) = \frac{\varepsilon}{d}\frac{dV}{dt}$$

$$\therefore J = \frac{\varepsilon}{d} V j\omega \quad \text{----------} \quad (2.24)$$

Substituting for E and J in equation (2.24)

$$\sigma_{ac} = \frac{J}{E} = \varepsilon j\,\omega \quad \text{---------} \quad (2.25)$$

Since 'ε' being a complex quantity

$$\sigma_{ac} = (\varepsilon' - j\varepsilon'')\, j\,\omega = \varepsilon' j\,\omega + \omega\,\varepsilon'' \quad \text{----------} \quad (2.26)$$

To make ac conductivity a real quantity the term containing 'j' has to be neglected hence

$$\sigma_{ac} = \omega \varepsilon'' \text{ --------- } (2.27)$$

Substituting ε'' from equation (2.19)

$$\sigma_{ac} = \omega \varepsilon' \tan\delta \text{ --------- } (2.28)$$

Putting $\varepsilon' = \varepsilon_0\varepsilon_r(\omega)$ as a frequency dependant term, and substituting $\omega = 2\pi f$,

$$\sigma_{ac} = 2\pi f \tan\delta \ \varepsilon_0 \varepsilon_r(\omega) \text{ --------- } (2.29)$$

This equation is used to calculate the ac conductivity by employing the values of dielectric constant and tan δ at a given frequency.

From the above it is clear the evaluation of capacitance by employing LCR meter and subsequent estimation of σ_{ac} is completely automated. This is made possible with LabVIEW and hence the evaluation of dielectric permittivity and ac conductivity at various frequencies and temperatures is simultaneously carried out.

References:

1.G C Hadjpanayis, R W Siegel 1994 *Proceedings of the NATO Advanced study institute on Nanophase materials-syntheses, properties and applications, Kluwer academic publishers* pXIV

2.A M A Bennet, T Douglas, K M Unruh, S I Shah and K H Theopold 994 *Proceedings of the NATO Advanced study institute on Nanophase materials-syntheses, properties and applications, Kluwer academic publishers* p29

3.J P Jolivet, E.Tronc and L.Vayssieres 1994 *Proceedings of the NATO Advanced study institute on Nanophase materials-syntheses, properties and applications, Kluwer academic publishers* p45

4.H.J.Fecht 1994 *Proceedings of the NATO Advanced study institute on Nanophase materials-syntheses, properties and applications, Kluwer academic publishers* p125

5.Suryanarayana C, Guo-Hao Chen and Sam Froes F H 1992 *Scripta Metallurgica* **26** p1727

6.Young –Soon Kwon, Konstantin B.Gerasimov and Sok-keel Yoon 2002 *J.Alloys and compounds* **346** p276

7.Diego Basset, Paolo Matteazzi and Fabio miani 1994 *Proceedings of the NATO Advanced study institute on Nanophase materials-syntheses, properties and applications, Kluwer academic publishers* p145

8.B D Cullity, 1978 *Elements of X-ray diffraction* 2^{nd} *edition, Addison Weisley Publishing Company Inc., Phillipines*

9. Manojkumar and Sekhon S S 2001 *J.Phys.D.Appl.Phys* **34** p2995

10.I M Watt 1997 *The principles and practice of electron microscopy, second edition, Cambridge university press* p60

11.Joseph A. Pesch, *Rev. Sci. Instrum,* Vol.54, No.4 (1983)p480

12.E P Giannelis, V Mehrotra, J K Vassiliou, R D Shull, R D MacMichael, R F Ziolo 1994 *Proceedings of the NATO Advanced study institute on Nanophase materials-syntheses, properties and applications, Kluwer academic publishers* p617

13.Simon Foner, *Rev. Sci. Instrum.* Vol. 30, No.7 (1959) p548-557

14.R.V.Krishnan and A.Banerjee, *Rev. Sci. Instrum.*, Vol.70 No.1 (1999)p85

15. A.Bajpai and A.Banerjee 1997 *Rev.Sci.Instru.* **68(11)** p4075

16.Sunil Nair and A.Banerjee *Phys.Rev B* 68, 094408 (2003)

17.A.Bajpai and A.Banerjee *Phys.Rev B* 55(18), 12439 (1997)

18.A.Bajpai and A.Banerjee *J.Phys.: Condens.Matter* 13 (2001) 637-647

19.A.Bajpai and A.Banerjee *Phys.Rev B* 62(13), 8996 (2000)

20.N N Greenwood and T C Gibb, *Mössbauer spectroscopy, Chapman and Hall Ltd, London* p1

21.Dominic P E Dickson and Frank J Berry, *Mössbauer spectroscopy, Cambridge university press, Cambridge* p9

22.E M Mohammed, *PhD thesis, Dept.of Physics, Cochin University of Science & Technology, Cochin-22,* 2001

CHAPTER 3

EFFECT OF DRY AND WET MILLING ON THE STRUCTURAL PROPERTIES OF ZINC FERRITE

3.1 Introduction

Zinc ferrite crystallizes in the normal spinel structure and exhibits no net magnetisation at room temperature. This is the case if this is prepared in the micron regime. However, as has been pointed out in the introduction and motivation in chapter 1, this material when prepared in the ultrafine regime displays anomalous magnetic behaviour and has been subjected to detailed investigations by various researchers. Though they are antiferromagnetic with a T_N = 10 K, in the nanoregime, zinc ferrite exhibits a net magnetisation at room temperature. It has been thought that this is a clear case of finite size effect on the magnetic property of this material. This has given rise to lot of speculation and so many hypotheses exist.

It is known that superparamagnetism, single domain, spin glass, spin glass clusters, quantum magnetisation, quantum tunnelling, spin polarized tunnelling are all manifestations of finite size effects. In order to validate any of the hypothesis, it is necessary to prepare ultrafine zinc ferrite. Once phase pure materials are prepared, structural characterization in terms of lattice parameter evaluation, identification of planes, and particle size estimation are crucial. It is in this context that this chapter is a prelude to further studies and will surely help to correlate both magnetic and electrical properties. In this chapter, the investigation carried out using XRD and TEM are highlighted. Transmission electron microscopy is used as a supporting tool to establish the particle size of these materials and also to determine the distribution that exists in these materials.

3.2 X-ray diffraction studies on dry milled zinc ferrites

Unmilled and dry milled zinc ferrites were subjected to X-ray diffraction studies and the XRD patterns are shown in figure 3.1. XRD pattern indicates the presence of small amounts of α-Fe_2O_3 in all milled samples whose percentage is found to be increasing with milling time. In 10 hours milled sample ZnO phase is also detected suggesting decomposition of $ZnFe_2O_4$ to α-Fe_2O_3 and ZnO. The broad shape of the diffraction peaks indicates the formation of fine particle structure with small

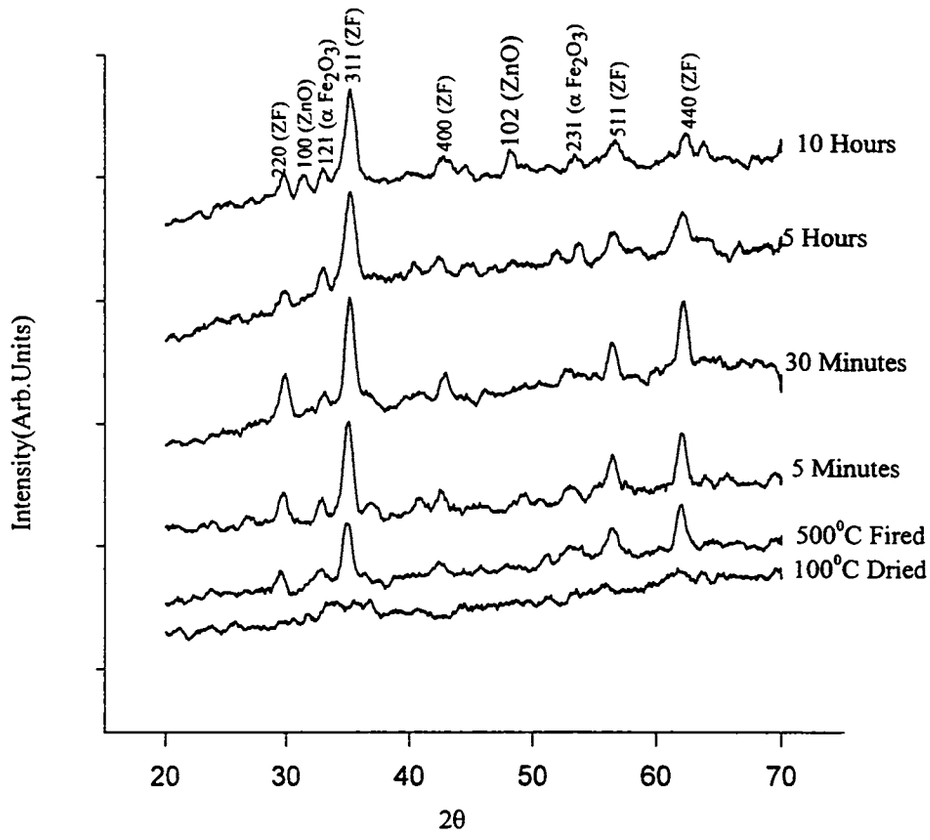

Figure 3.1 XRD patterns of dry milled and unmilled zinc ferrite.

crystallite size distribution and existence of strong internal lattice strains which is introduced during high energy ball milling [1].

Average size of the particle is calculated by Debye Scherrer formula, and they are in the nanometer range and found to be decreasing with milling time (figure 3.2). With 10 hours milling, size reduces to around 11nm while the initial coprecipitated sample was with a grain size of around 16nm. This decrease in particle size with increase in milling time is due to the fact that the kinetic energy generated by the series of collisions among balls is transferred to the zinc ferrite powder. The sudden decrease in grain size is not achieved in this case as in the case of particles prepared by the solid state reaction methods. The reason is that the coprecipitated zinc ferrite, which is the starting material, itself is of nanometer sized when subjected to initial milling. Also there are reports that within 24 minutes of milling, size reduction may attain its maximum [2]. A great reduction in size with prolonged milling is not achievable due to the high local temperature and pressure generated during the combustion as a result of the high energy ball milling [3]. Also the difficulty in maintaining the very high stress during milling (discussed in section 2.2) slows down reduction of grain size.

Assuming cubic symmetry for these materials, lattice parameter was calculated and the variation of lattice parameter with milling time is determined and shown in figure 3.3. The lattice parameter calculated from XRD data for unmilled sample was around 8.46 Å. Milling reduces this value and with 10 hours of milling the lattice parameter of the sample reduces to 8.40 Å. This reduction in lattice parameter clearly suggests possible lattice shrinkage [2]. This may be due to the high surface tension of the particle since fine particle surface area is large. The strong internal strains in the lattice initiated by high energy ball milling may also influence the lattice to shrink. Lattice shrinkage also points to cation redistribution between tetrahedral (A) and octahedral (B) sites [4]. There are reports saying that as inversion parameter increases, lattice parameter decreases [5]. Since Zn^{2+} has a large ionic radius compared to Fe^{3+}, this site reversal will cause a decrease of lattice constant [4]. This effect has not been observed in sintered (ceramic) ferrite. It is also possible that the cation distributions do differ between those present near the particle's surface and those of non-surface atoms. This situation is highly probable for the materials with a

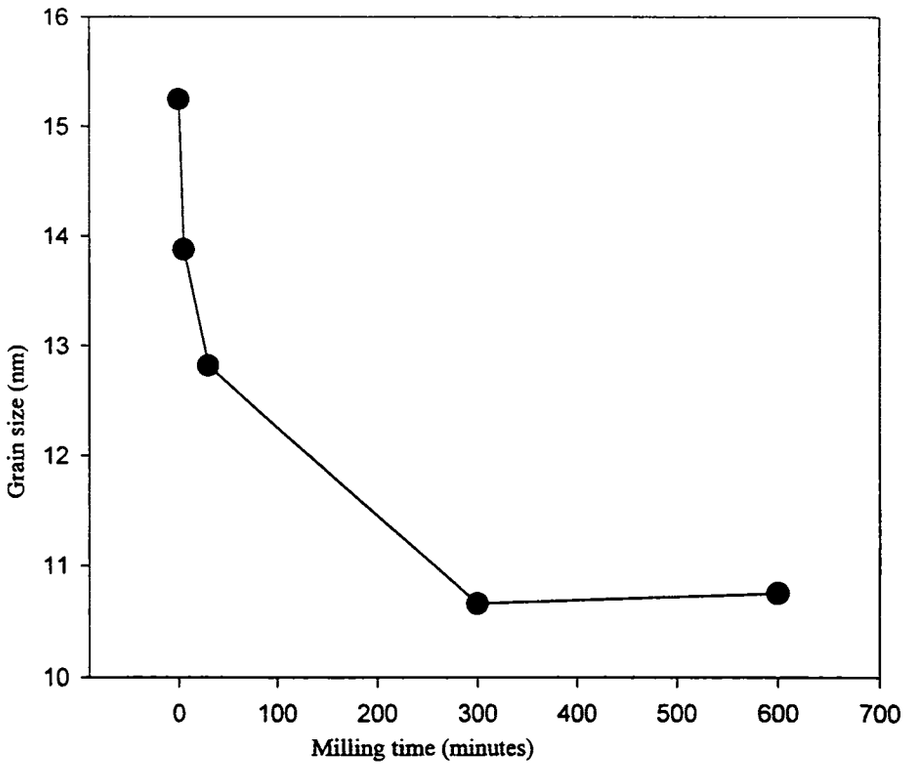

Figure 3.2 Particle size variation with milling time for dry milled zinc ferrite.

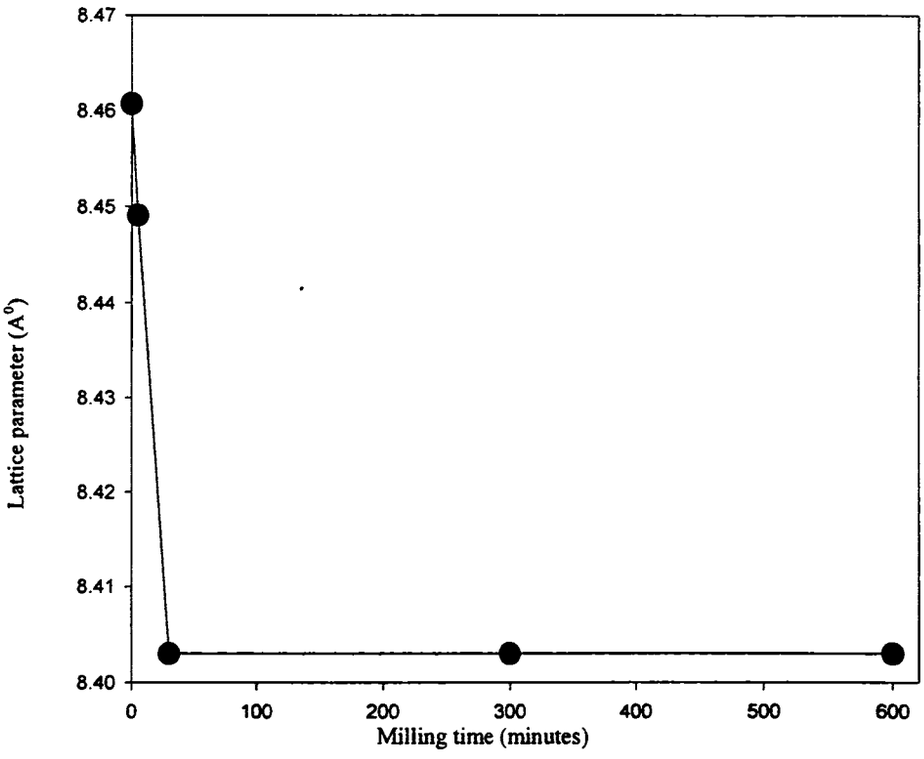

Figure 3.3 Lattice parameter variation with milling time for dry milled zinc ferrite.

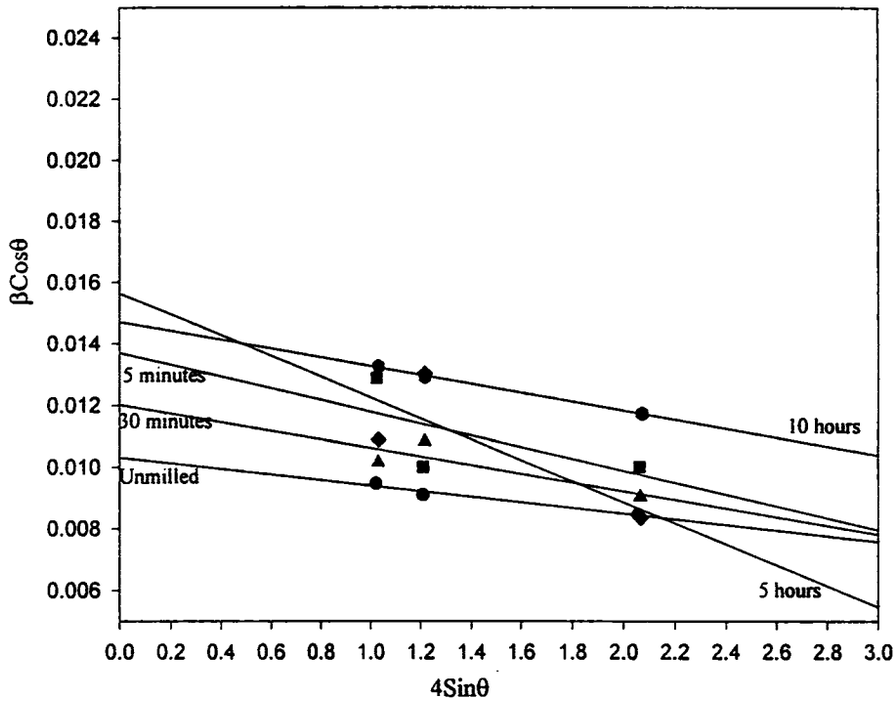

Figure 3.4 4Sinθ Vs βCosθ curves for unmilled and dry milled zinc ferrites

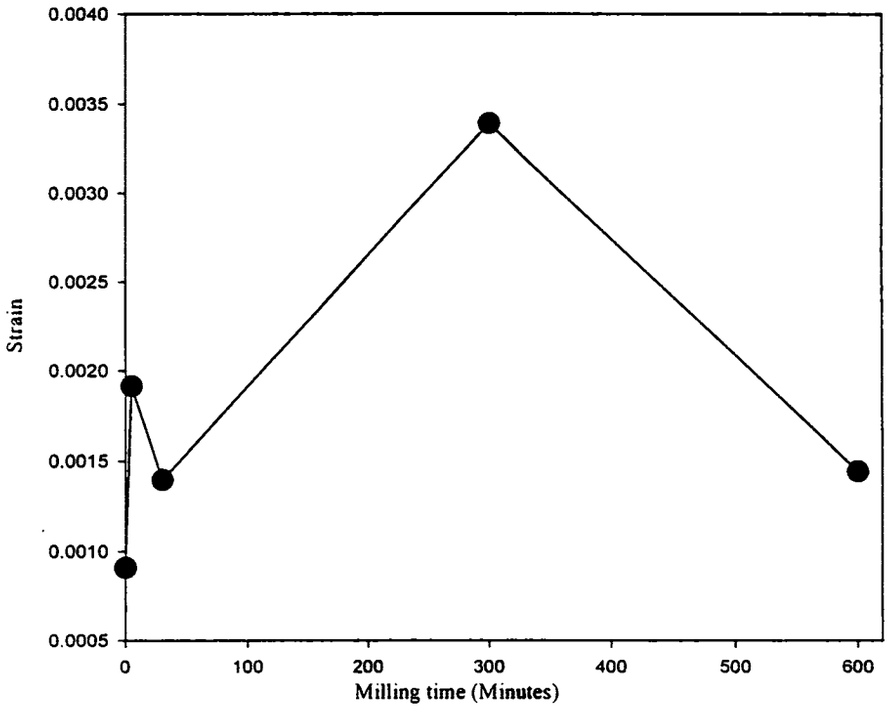

Figure 3.5 Strain calculated from XRD data for dry milled zinc ferrites

large number of defects in which O^{2-} ions are missing from normally occupied sites and/or in which Fe^{3+} occupies normally unoccupied sites.

As discussed in section 2.3, line broadening of the XRD peaks is attributed to mainly three factors namely thermal, strain and particle size. This can be calculated from the line width (FWHM in radian) of XRD lines using the following relation [6].

$$FWHM(\beta) = \lambda/(d_g \cos\theta)+4\varepsilon \tan\theta \quad \ldots (3.1)$$

where θ is the bragg angle, ε is the lattice strain developed and d_g the grain size. Rewriting the above equation,

$$\beta \cos\theta = \varepsilon(4\sin\theta) + \lambda/d_g \quad \ldots (3.2)$$

This equation represents a straight line between $\beta \cos\theta$ (Y-axis) and $4\sin\theta$ (X-axis). The slope of this line gives the strain parameter (ε) and d_g can be calculated from the intercept of this line on the Y-axis. The broadening due to the instrumental effect also contributes to diffraction peak broadening, but since it is very small, is neglected here.

Figure 3.4 shows $4\sin\theta$ vs. $\beta\cos\theta$ lines of unmilled and milled samples. The grain sizes calculated from this graphs are comparable with the one calculated by Scherer formula for the most intense (311) line. Strain values calculated are found to be increasing with milling time and are plotted in figure 3.5. It is observed that the prolonged milling reduces the strain. As reported [7], when the grain size reduces beyond a certain limit, the individual grains rotate with respect to each other, thus reducing the overall strain.

3.3 TEM studies on dry milled zinc ferrites

Figure 3.6 and 3.7 shows the transmission electron micrographs (TEM) of 5 hours milled and 10 hours milled zinc ferrite samples. TEM images show the microstructure of ball milled zinc ferrites. The microstructure clearly indicates that grain size is in the nanometer range and it is around 10 nm. TEM graphs indicate that the particles are more or less ultrafine in size and they are almost spherical in shape. There are reports [8] indicating that ammonia used for the precipitation of zinc ferrite is a facilitator for the formation of spherical particles.

3.4 X-ray diffraction studies on wet milled zinc ferrites

XRD pattern indicates presence of small amounts of α-Fe_2O_3 in all the three samples whose percentage first decreases and then increases with milling time (figure 3.8). Since milling was carried out in a wet medium of toluene, unlike as in the case

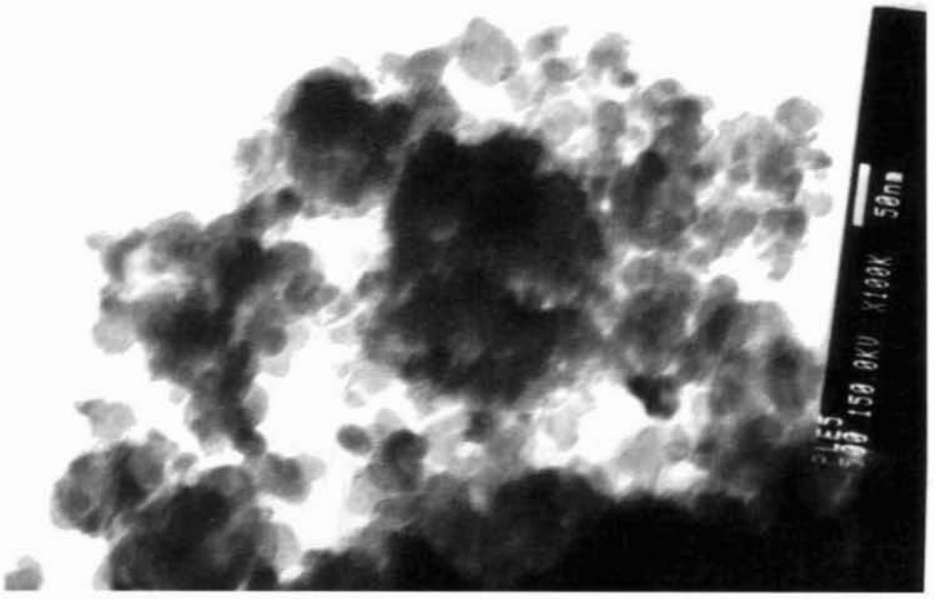

Figure 3.6 Transmission electron micrograph for 5 hours dry milled zinc ferrite.

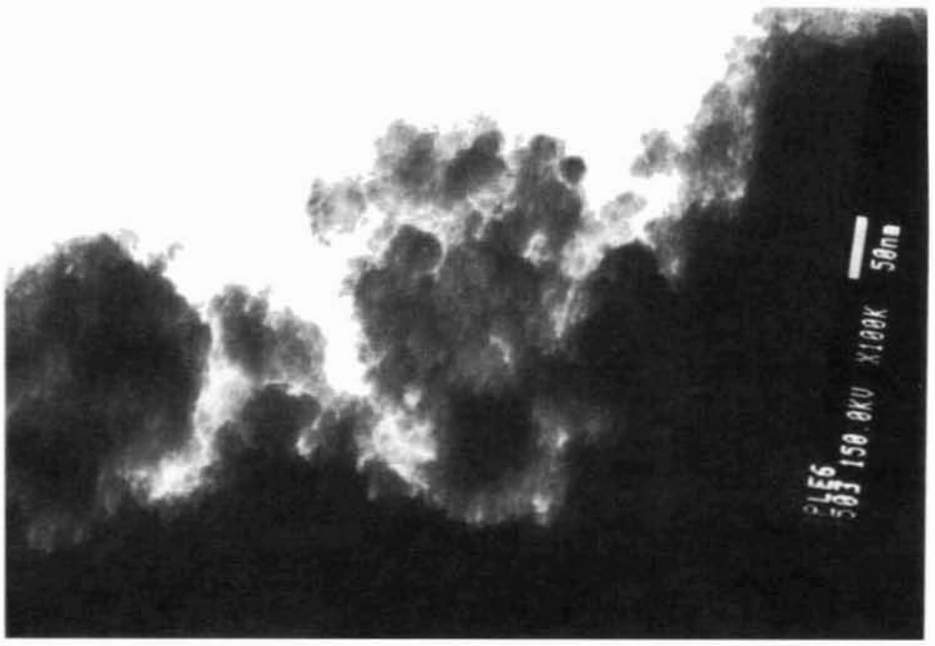

Figure 3.7 Transmission electron micrograph for 10 hours dry milled zinc ferrite.

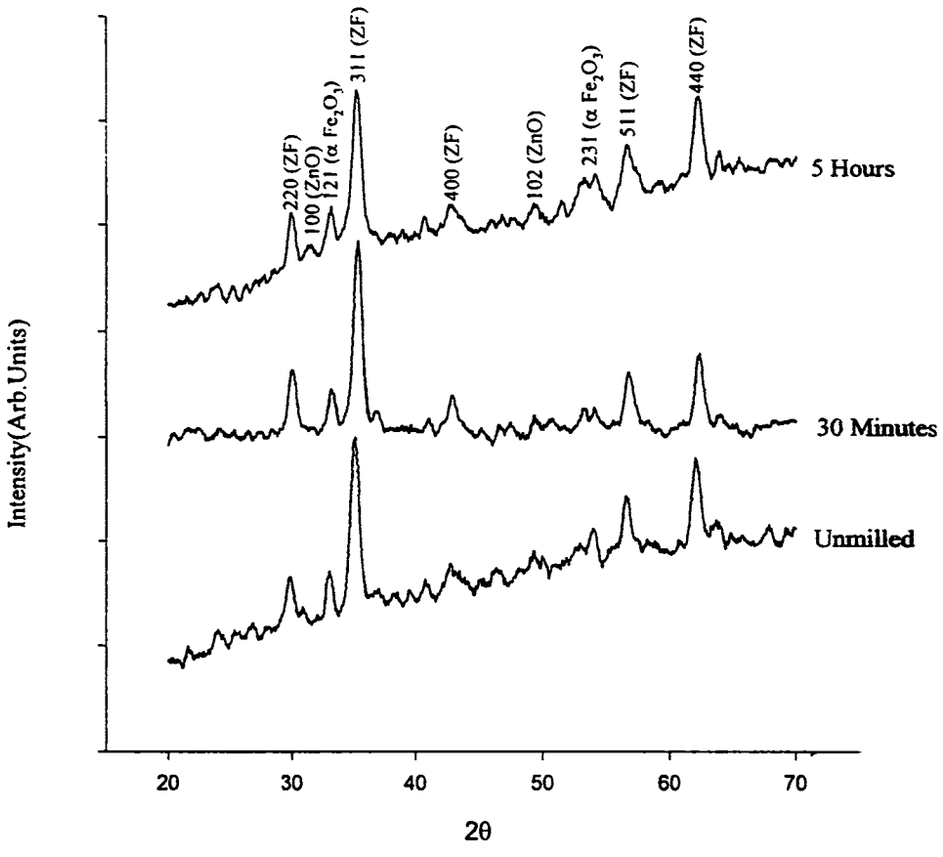

Figure 3.8 XRD patterns of wet milled and unmilled zinc ferrite.

of dry milling, the chances of recombination of some unreacted salts to yield a substantial amount of zinc ferrite exists and hence there is an the overall reduction of hematite percentage in the initial stage of milling. Hence during first stage of milling, may be, some unreacted ferric and zinc salts and the α-Fe_2O_3 present will react to form $ZnFe_2O_4$ and thereby α-Fe_2O_3 line gets less intense during 30 minutes milling. But during prolonged milling, due to nanometer sized grains, high local pressures and temperatures during collisions with balls and vial, and the subsequent kinetic energy produced will lead to a decomposition of $ZnFe_2O_4$ in the milling process [2,5]. There are reports of production of Fe_3O_4 (by product of α-Fe_2O_3) as a result of prolonged milling [9]. But in our present study no traces of Fe_3O_4 was detected by XRD.

An interesting feature is that for wet milling, we have employed a low rpm of 360 compared to 650 rpm for dry milling. But careful analysis of XRD patterns (figure 3.1 and 3.8) shows a speedy decomposition of zinc ferrite to zinc oxide and hematite in toluene based wet milling. From figure 3.8, it is evident that from XRD the emergence of 100% peak corresponding to zinc oxide took only 5 hours during wet milling whereas in dry milling, it took 10 hours for the appearance of the same 100% peak corresponding to zinc oxide.

As in the case of dry milling, here also broad shape of the diffraction peaks signals the formation of fine particle structure with small crystallite size distribution and existence of strong internal lattice strains which is introduced during high energy ball milling [1]. Average size of the particles, which is calculated by Debye Scherrer formula, are plotted against the milling time (figure 3.9). Here also there is no sudden reduction in particle size with milling which is akin to the results obtained for dry milled samples.

Lattice parameter reduction (figure 3.10) and the lattice strain (figure 3.12) calculated from $4\sin\theta$ vs. $\beta\cos\theta$ plots (figure 3.11) are in tune with the results obtained for dry milled zinc ferrite.

3.5 Conclusions

XRD results indicate that the particles formed are ultrafine and associated with strains. Strain increases with milling producing an atomic disorder due to displacement of the position of both anions and cations. This is confirmed by the lattice parameter reduction with milling. Particle size measured show that they are around 10nm, which is confirmed by transmission electron micrographs for dry milled

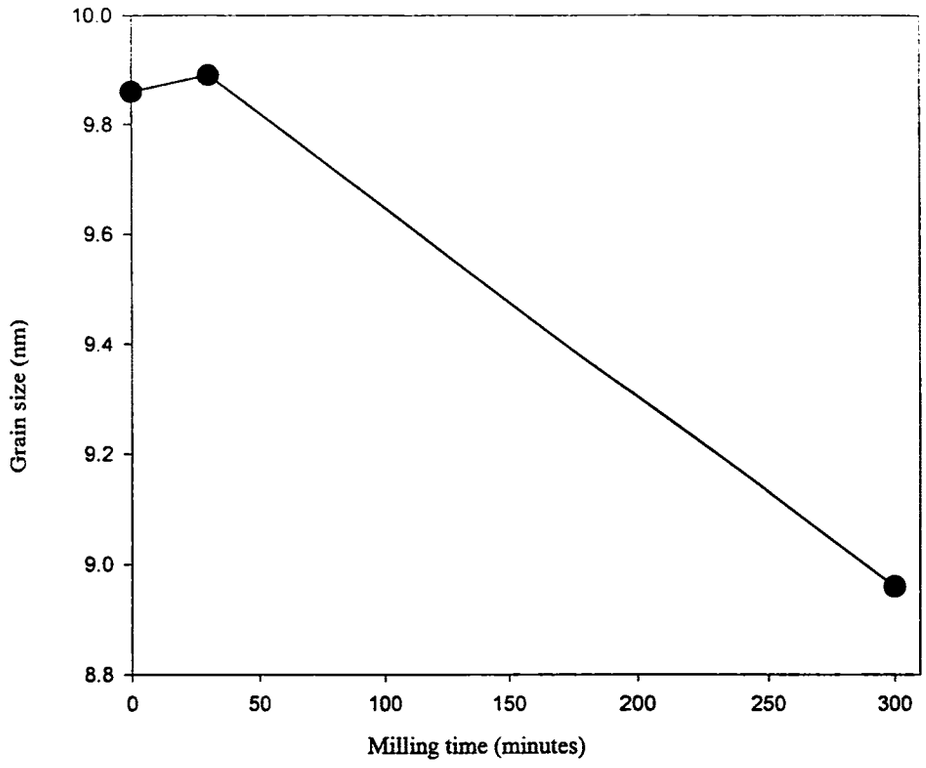

Figure 3.9 Particle size variation with milling time for wet milled zinc ferrite.

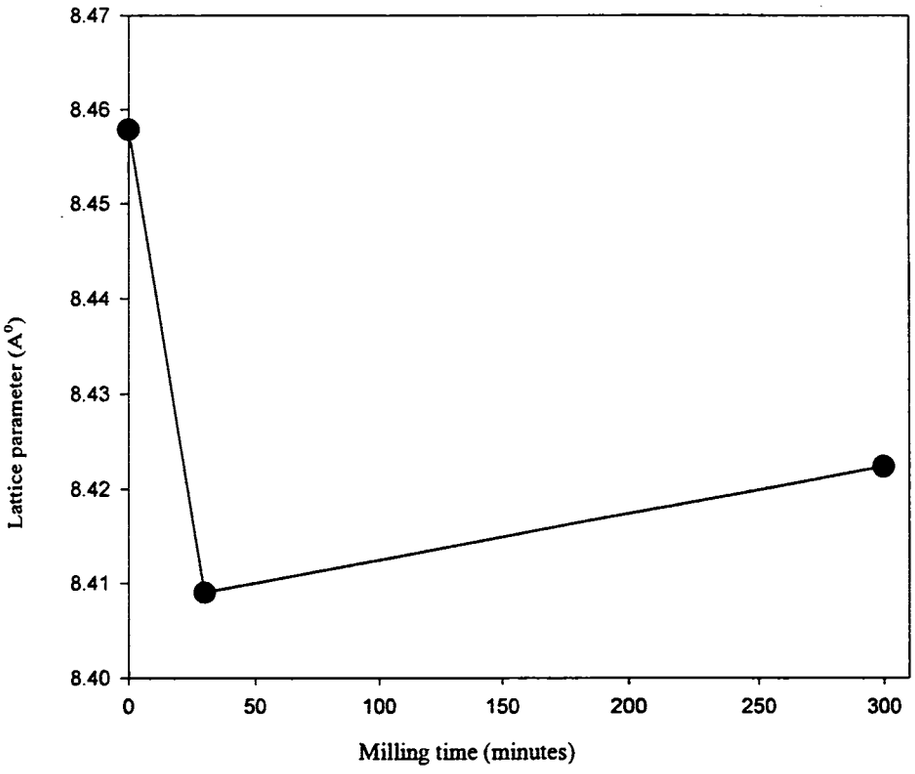

Figure 3.10 Lattice parameter variation with milling time for wet milled zinc ferrite.

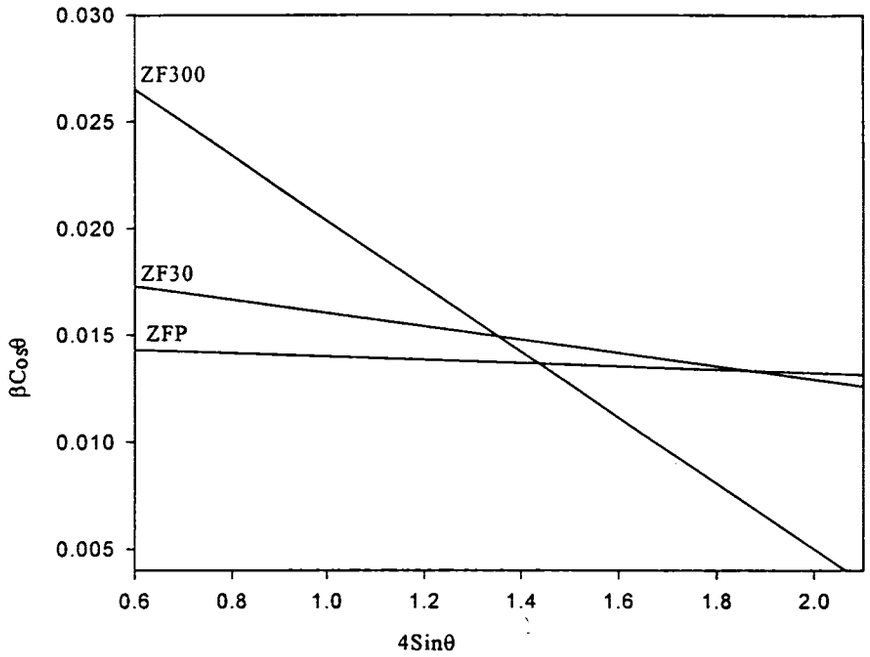

Figure 3.11 4Sinθ Vs βCosθ for unmilled and wet milled zinc ferrites.

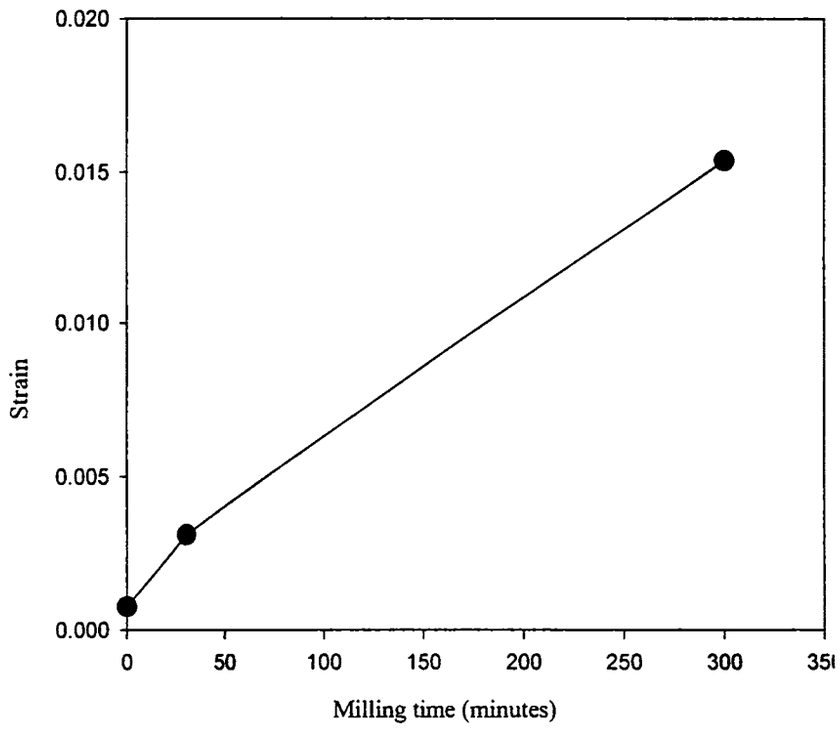

Figure 3.12 Strain calculated from XRD data for wet milled zinc ferrites

specimens. Prolonged milling does not yield further reduction in size due to the high local temperature and pressure produced during the milling.

References:

1.Arcos D, Valenzuela R, Vazquez M and Vallet-Regi M 1998 *J.Solid State Chem* **141** 10

2.Sepelak V, Tkacova K, Boldyrev V V, Wibmann S and Becker K D 1997 *Physica B* **234-236** 617

3.Young –Soon Kwon, Konstantin B.Gerasimov and Sok-keel Yoon *J. of Alloys and Compounds* 346 (2002) 276

4.T Sato 1970 *IEEE Trans.Magn mag-6* 795

5.Q. Chen, A.J. Rondinone, B.C. Chakoumakos, J.Z. Zhang, *J.Magn.Magn.Mater.* 194 (1999) 1

6.Manojkumar and Sekhon S S 2001 *J.Phys.D.Appl.Phys* **34** 2995

7.H.J.Fecht 1994 *Proceedings of the NATO Advanced study institute on Nanophase materials-syntheses, properties and applications, Kluwer academic publishers* p125

8.Pannaparayil T, Komarneni S, Marande R and Zadarko M 1990 *J.Appl.Phys* **67** 5509

9.G.F. Goya, H.R. Rechenberg, J.Z. Jiang , *J.Appl.Phys.* 84 (1998) 1101

CHAPTER 4

FINITE SIZE EFFECTS ON THE MAGNETIC PROPERTIES OF DRY AND WET MILLED ULTRAFINE ZINC FERRITE

4.1 Introduction

Fine magnetic particle systems like $ZnFe_2O_4$ evoked renewed interest in the last few years because of the possibilities of applications in the nanostructured materials technology. Nanosized magnetic particles have properties, which are drastically different from those of the corresponding bulk materials. High energy ball milling is an excellent tool to tune the grain size and modify the magnetic properties of ferrite materials [1-16].

As described in chapter 1, the spinel ferrites have the general formula $\{(M)_{\delta}(Fe)_{1-\delta}\}[(M)_{1-\delta}(Fe)_{1+\delta}]\ O_4$. The divalent metal ion M (eg:- Zn, Mg, Mn, Fe, Co, Ni or a mixture of them) can occupy either tetrahedral(A) or octahedral(B) sites as depicted by curled and square brackets respectively. In the above formula when $\delta = 1$, it is called a normal spinel. $ZnFe_2O_4$ and $CdFe_2O_4$ are examples of normal ferrites. When $\delta = 0$, it is called an inverse spinel and examples are $NiFe_2O_4$, $CoFe_2O_4$, $CuFe_2O_4$ etc. When $\delta = 1/3$, it is called a random spinel.

The origin of the magnetic properties of ferrites arise from the spin magnetic moment of the unpaired transition metal 3d electrons coupled by the superexchange interaction via the oxygen separating them [1]. It has long been known that the A-O-B exchange interaction is much stronger than the B-O-B and the A-O-A interactions [17-21]. The systems where one or both the sublattices are populated with magnetic ions, the competing exchange interactions may lead to topological frustration, yielding a magnetic structure that may include states of antiferromagnetic order, local spin canting, spin glass behaviour, disordered phases and ferrimagnetic order. Experimental studies on spinel ferrites have shown that they are replete with this rich variety of magnetic ordering that ranges from classical ferrimagnetic ordering to spin glass behaviour [1].

The magnetic behaviour of the particle surface differs from that of the corresponding core, because of distinct atomic coordination, compositional gradients and, concentration and nature of defects present in both the regions. Thus, whereas the core usually displays a spin arrangement similar to that of the bulk material, a much

higher magnetic disorder is present on the surface, giving rise to magnetic behaviour which cover from that of a dead magnetic layer to that of a spin-glass like [22]. Many researchers have invoked this hypothesis of dead layer, especially, for explaining the anomaly in the magnetic properties exhibited by ultrafine nickel ferrites. However literature reports by various researchers are at variance [1-6,10-13,15,23-29].

Superparamagnetism and spin-glass like properties, have wide applications from the technological point of view. Superparamagnetism is a finite size effect since the particle anisotropy is generally proportional to its volume and has important applications in the thermal and time stability of the bits written in recording media [22]. Spin glass property also has some relevant applications in memory devices. Spin glass is a substance in which electron spins are in a random direction below its glass transition temperature (T_G). It contains many metastable states separated by the potential barrier of k_BT_G. Once it falls into one of the metastable states, it cannot have a more stable state at a thermal energy below T_G. However the addition of some external field, for example, light irradiation, will turn the metastable state into a more stable state. This feature is exclusively used in magneto optical memory devices [30]. However, generally, in spin glass, the T_G is very low, far below room temperature. To utilize a spin glass as an actual magnetic memory device, a spin glass with a higher T_G at least approximately near room temperature is desired.

In this chapter the magnetisation studies on wet milled and dry milled ultrafine zinc ferrite are described. Thermomagnetisation studies are conducted under zero field cooled and field cooled environments on selected samples. This is to ascertain the nature of magnetic ordering and spin-glass like properties of these materials. AC magnetic susceptibility measurements are also carried out on these samples in order to distinguish between ferromagnetic/superparamagnetic/spin-glass transitions.

4.2 Magnetisation studies on wet milled zinc ferrites by VSM

Figure 4.1 represents the magnetisation curves for wet milled zinc ferrites at two different temperatures, room temperature (300 K) and at a lower temperature (83 K). Room temperature curves show typical superparamagnetic behaviour with no hysteresis. That is, both retentivity and coercivity are zero, which is in tune with the results obtained by other researchers [28,31-34].

Table 4.1 summarizes the saturation magnetisation and coercivity values at both room temperature and low temperature. The strain associated with fine particles, as a result of milling, produces a disorder by displacement of ions, which is one cause

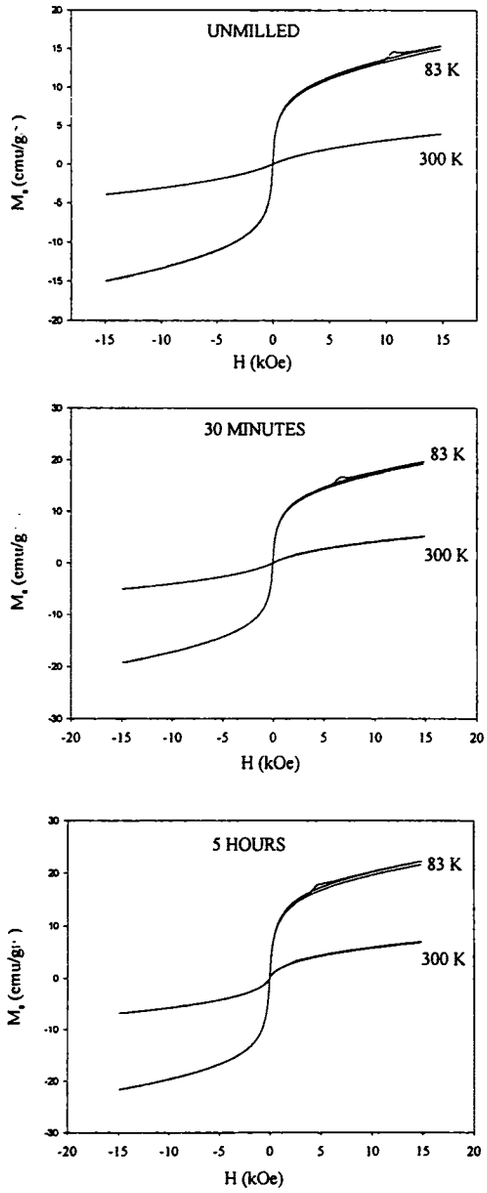

Figure 4.1 Magnetisation curves for wet milled zinc ferrite samples at 300 K and at 83 K.

Sample	M_s (emu/g...) 300 K	M_s (emu/g...) 83 K	H_c (Oe) 300 K	H_c (Oe) 83 K
Unmilled	3.9	15.1	20	4
30 Minutes	5.1	19.3	13	6
5 Hours	6.9	21.9	6	7

Table 4.1 Saturation magnetisation (M_s) and coercivity (H_c) values of wet milled zinc ferrite at 300 K and 83 K.

for an increase in magnetisation. In ultrafine particles large fractions of atoms are located on the surface and therefore the surface effects, which include surface energy and surface tension as well as the change in position of anions and cations, will favour an increase of magnetisation, although hematite percentage may increase. Furthermore, hematite may be acting as a facilitator in producing magnetic zinc ferrite, which is magnetic due to the strain and surface effects. This can be written in the following form,

$$\alpha\text{-}Fe_2O_3 + ZnFe_2O_4 \rightarrow \alpha\text{-}Fe_2O_3 + \text{magnetic } ZnFe_2O_4$$

From figure 3.12, it is evident that the strain increases tetra fold for 5 hours milled sample when compared to 30 minutes milled sample. But from table 4.1, one doesn't observe a corresponding increase in magnetisation for 300 minutes milled sample. Though strain produces disorder and thereby contributes to overall magnetisation (could be because of surface spins), there is another possibility. Since we are seeing M_s in emu/gm, the overall increase in magnetisation may be masked by the increased amount of α-Fe_2O_3, which increases with milling as evidenced by XRD.

The hysteresis behaviour completely vanishes at room temperature. Short range magnetic ordering of Fe spins at 83 K contributes to magnetic hysteresis loops. Long range ordering is expected at liquid helium temperature. These powders exhibit a net magnetisation and are magnetically ordered at much higher temperature than that of normal zinc ferrite. It may be noted here that for mechanically milled sample, T_N has been reported to be ~ 115 K [23]. The magnetic ordering starts with the formation of superparamagnetic clusters whose size gradually increases with lowering of temperature, superparamagnetic clusters present are heterogeneous at room temperature but get ordered at lower temperature to contribute to magnetisation [2].

Superparamagnetic relaxation time τ, which is the average time required for the particle to jump from one axis of magnetisation to another is given by the relation,

$$\tau=\tau_0 \exp (K_{eff}V/k_BT_B) \quad \ldots\ldots (4.1)$$

where k_BT_B is the thermal energy, K_{eff} is the effective anisotropy constant and V the particle volume. τ increases with decreasing temperature resulting in an enhanced magnetisation. Also the saturation magnetisation (M_s) is governed by the equation [35],

$$M_s=\frac{2K}{H_c}\,[1-(25k_BT/KV)^{1/2}] \quad \ldots\ldots (4.2)$$

According to the above relation, M_s increases with decrease of temperature and this is in agreement with our results.

Coprecipitation results in large structural and chemical disorder. Ball milling will produce greater atomic disorder due to mechanical displacement of ions under high stress and shear. This order may contribute to magnetisation [2,4,10].

As the particle size (hence the volume) decreases the probability of thermally activated magnetisation increases. Surface effects become increasingly important as the particle volume decreases. So surface effects could not be ruled out in fine particle systems [27,36-37].

As the inversion increases, the material makes the transition to ferromagnetism through complex magnetic states [2]. One complex state is the distribution of Fe^{3+} and Fe^{2+} ions and the oxygen vacancies resulting from milling which can create the superexchange paths and induce spin disorder [23]. Cation distribution may also differ between those present near the particle's surface and those of non-surface atoms [22,25]. This FM ordering coupled with the antiferromagnetically (AFM) ordered α-Fe_2O_3 may produce FM-AFM exchange interaction that can modify magnetic properties as suggested by various researchers [38-39]. But the dispersion of FM clusters in an AFM matrix is ruled out here since α-Fe_2O_3 percentage is small [40].

Figure 4.2 represents the thermomagnetisation curves for wet milled samples in the temperature range 80 K to 300 K at 50 Oe field. The experiment was carried out in zero field cooled conditions. No characteristic spin glass like transition is observed in wet milled samples. This suggests reduced surface spin disorder, which actually is due to the dearth of oxygen deficiencies in these samples. This is in conformity with the dielectric results obtained for these samples, where wet milling does not contribute in enhancing the dielectric permittivity unlike in the case of dry milled samples (discussed in chapter 6).

4.3 Room temperature magnetisation studies on dry milled zinc ferrites by VSM

Figure 4.3 represents the magnetisation curves for dry milled zinc ferrites at room temperature. All samples show superparamagnetic properties at room temperature with low coercivity [24,41]. Table 4.2 summarizes the saturation magnetisation (M_s) and coercivity (H_c) values of dry milled zinc ferrite samples. An enhancement in saturation magnetisation can be observed in 5 hours milled sample.

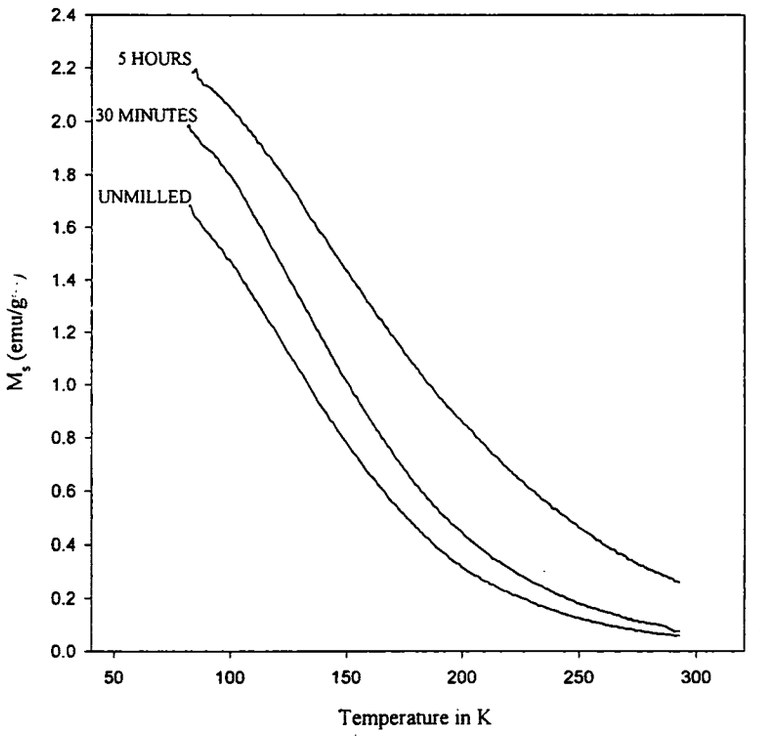

Figure 4.2 Thermomagnetisation curves for unmilled, 30 minutes and 5 hours wet milled zinc ferrite samples at 50 Oe field (zero field cooled conditions).

However, 10 hours milled sample shows no much increase in saturation magnetisation compared to 5 hours milled sample.

The grain size of 10 hours milled sample is slightly greater than 5 hours milled sample. But the M_s value does not decrease for 10 hours milled sample. Hence a direct relation between grain size and saturation magnetisation is not possible from the present results. However, it can be said that milling time strongly influences the saturation magnetisation [10-11].

The high saturation magnetisation value for milled zinc ferrites cannot be explained by superparamagnetism alone, but there exists some other magnetic ordering together with superparamagnetism that contribute to magnetisation. A ferrimagnetic ordering that is short range can develop inside the core of the particle as a result of cation redistribution [5-6,11-12, 26-29,42]. This forms magnetic clusters in the core. Inside the clusters, a Fe^{3+} ion in A site and its twelve nearest neighbours in B sites are coupled through AB spin interaction. This leads to magnetic behaviour, which is responsible for the residual magnetisation in milled sample. The formation of magnetic clusters as a result of cation redistribution is highly probable in coprecipitated samples, which are produced at low temperature within a short period of time [5]. This result is in accordance with the results obtained by various researchers [1-6, 10-11]. X-ray photoelectron spectroscopy studies by V.Sepelak and co-workers indicated the migration of Fe^{3+} ions to A sites with milling [6].

A marginal increase in α-Fe_2O_3 is observed with milling from XRD results. α-Fe_2O_3 is antiferromagnetic and the occurrence of α-Fe_2O_3 during milling should reduce the magnetisation in milled samples [14]. But the increase of M_s suggests that the cation redistribution contributes much more to saturation magnetisation compared with the increase of α-Fe_2O_3 content in the material. But the possibility of α-Fe_2O_3 acting as a facilitator inducing cation redistribution in zinc ferrite cannot be ruled out.

The surface of the particle may behave differently and is capable of modifying the magnetic properties of nanoparticles. In these materials the superexchange interaction occurs through O^{2-} ions. The absence of the oxygen ions on the surface results in broken exchange bonds between Fe^{3+} ions, which induces surface spin disorder [23,25,30,43]. This modifies the magnetic properties of nanoparticles where surface to volume ratio is high. Thus surface effects dominate the magnetic properties of fine particles since decreasing the particle size increases the ratio of surface spins

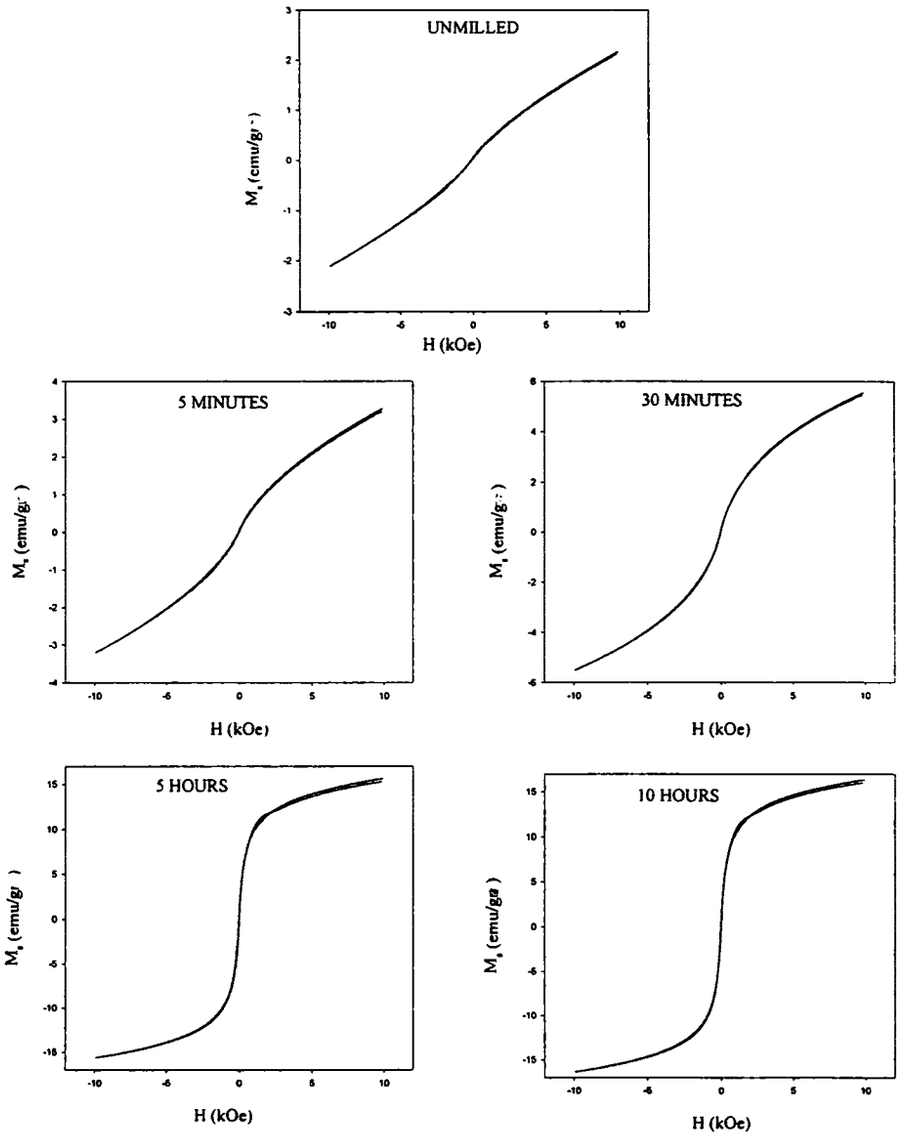

Figure 4.3 Magnetisation curves for dry milled zinc ferrite samples at room temperature.

Sample	M_s (emu/g.)	H_c (Oe)
Unmilled	2.196	25.05
5 minutes	3.298	36.92
30 minutes	5.558	23.07
5 hours	15.547	23.07
10 hours	16.410	23.12

Table 4.2 Saturation magnetisation (M_s) and coercivity (H_c) values of dry milled zinc ferrite at room temperature.

to the total number of spins. There are reports suggesting that high energy ball milling produces spin-glass like surface disorder [22,26].

A mixed ferrimagnetic and superparamagnetic behaviour is probable at room temperature and the role of surface spin disorder and spin-glass like properties could be more pronounced at low temperatures. Figure 4.3 clearly shows nonsaturation of magnetisation curves for all samples even at an applied magnetic field of 10 kOe. This suggests the coexistence of superparamagnetism and ferrimagnetism in our samples [31,41,44]. The ferrimagnetic part tends to saturate, whereas the superparamagnetic part increases linearly, resulting in nonsaturation. The saturation magnetisation and coercivity values indicate that ferrimagnetic contribution is nominal in these samples and the dominance of superparamagnetism is more probable. Low temperature magnetisation studies will throw more light on these aspects. This is discussed in the following section.

4.4 Thermomagnetisation studies on dry milled zinc ferrites by VSM

Thermomagnetisation studies were carried out in the temperature range 80-300 K, on three representative samples of dry milled zinc ferrite by employing vibrating sample magnetometer. Here the samples were cooled under zero field cooled conditions and measurements were carried out at 50 Oe field. The samples selected for this study are unmilled sample, 30 minutes milled sample and 10 hours milled sample. The results are shown in figure 4.4. It can be noticed that 10 hours milled sample shows a broad transition within the temperature range of experiments while a transition in other two samples are expected at lower temperatures.

Since a spin glass like transition was observed in 10 hours milled sample, ZFC- FC thermomagnetisation experiments were conducted. The results are shown in figure 4.5. The curves show a spin glass like behaviour suggesting the existence of magnetic spin clusters at the surface and establishes a short range ferrimagnetic ordering [30,41,44-46]. The deviation from ideal spin glass property may be due to the size distribution of spin clusters and the dominance of superparamagnetic ordering at the core. The broad transition peak of ZFC curve lies at around 170 K. Below this spin glass transition temperature electron spins are in a random direction and the clusters occupy different metastable states. Also below the transition temperature the intra sublattice exchange interactions that are predominantly antiferromagnetic plays a major role to decrease the magnetisation [2,41,44,47]. These B-B and A-A antiferromagnetic interactions compete with the

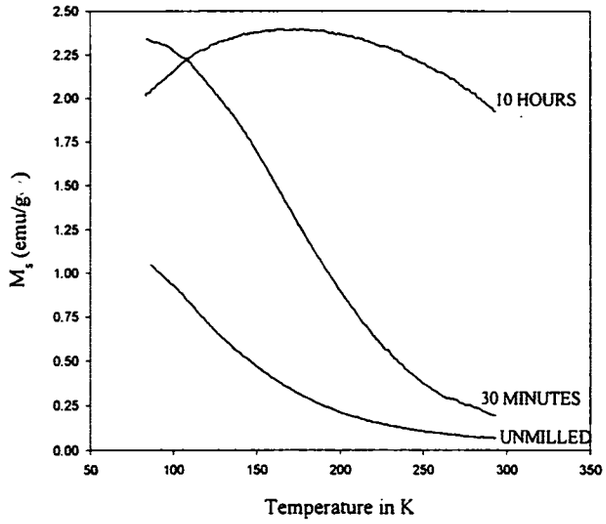

Figure 4.4 Thermomagnetisation curves for unmilled, 30 minutes and 10 hours dry mille zinc ferrite samples at 50 Oe field (zero field cooled conditions).

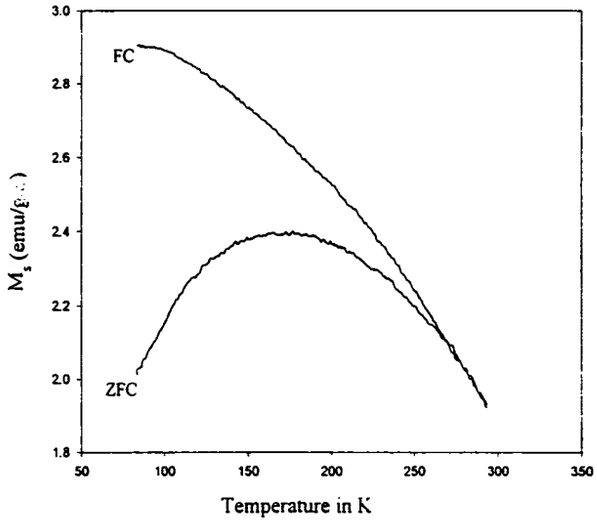

Figure 4.5 Thermomagnetisation curves (FC-ZFC) for 10 hours dry milled zinc ferrite sample at 50 Oe field.

ferrimagnetic interactions and freeze the clusters below the transition temperature. The magnetic clusters at the surface are as a result of broken O^{2-} superexchange bonds, which increase with milling. Thus the oxygen deficiency will increase the transition temperature [25,30,43,48].

In the field cooled magnetisation curve, a continuous increase of magnetisation is observed on decreasing the temperature and finally stabilises at around 80 K. This is due to the strong A-A and B-B antiferromagnetic interactions, which is reduced by the orientation of the clusters along the field direction [41]. Antiferromagnetic A-A interaction and B-B interaction will not be possible at room temperatures since these interactions are so weak that the thermal energy at room temperature will destroy the ordering. Hence usually antiferromagnetic ordering in zinc ferrites occurs only at low temperatures.

From the above discussion based on thermomagnetisation studies in field cooled and zero field cooled conditions, suggest a possible cation redistribution, which increases with milling. These observations support a spin glass like layer at the surface of the nanoparticles. Thus the ZFC-FC curves of 10 hours milled sample is attributed to cation redistributed ferrimagnetically ordered core and spin glass like surface layer. The surface properties predominate at lower temperatures. The role of antiferromagnetic A-A and B-B interactions also play a role at lower temperatures.

4.5 AC magnetic susceptibility studies on dry milled zinc ferrites

Figure 4.6 represents the ac magnetic susceptibility graphs for dry milled zinc ferrites in the temperature range of 80 K to 300 K. The experiments were carried out at 2 Oe field at a frequency of 133.33 Hz. A transition is observed for 30 minutes milled, 5 hours milled and 10 hours milled samples. A transition at lower temperatures is expected for unmilled and 5 minutes milled samples.

Since the milling decreases the particle size, which is well established by our XRD and TEM studies (figure3.1, 3.2, 3.6 and 3.7), and if the transition is due to the superparamagnetic blocking it should decrease with milling [32,33,35]. Table 4.3 shows the particle size estimated from XRD studies and the approximate transition temperature derived from ac susceptibility studies. It is a well-established theory that the superparamagnetic blocking temperature is directly proportional to particle volume and can be represented as

$$T_B = KV/25k_B \quad \ldots\ldots\ldots\ldots \quad (4.3)$$

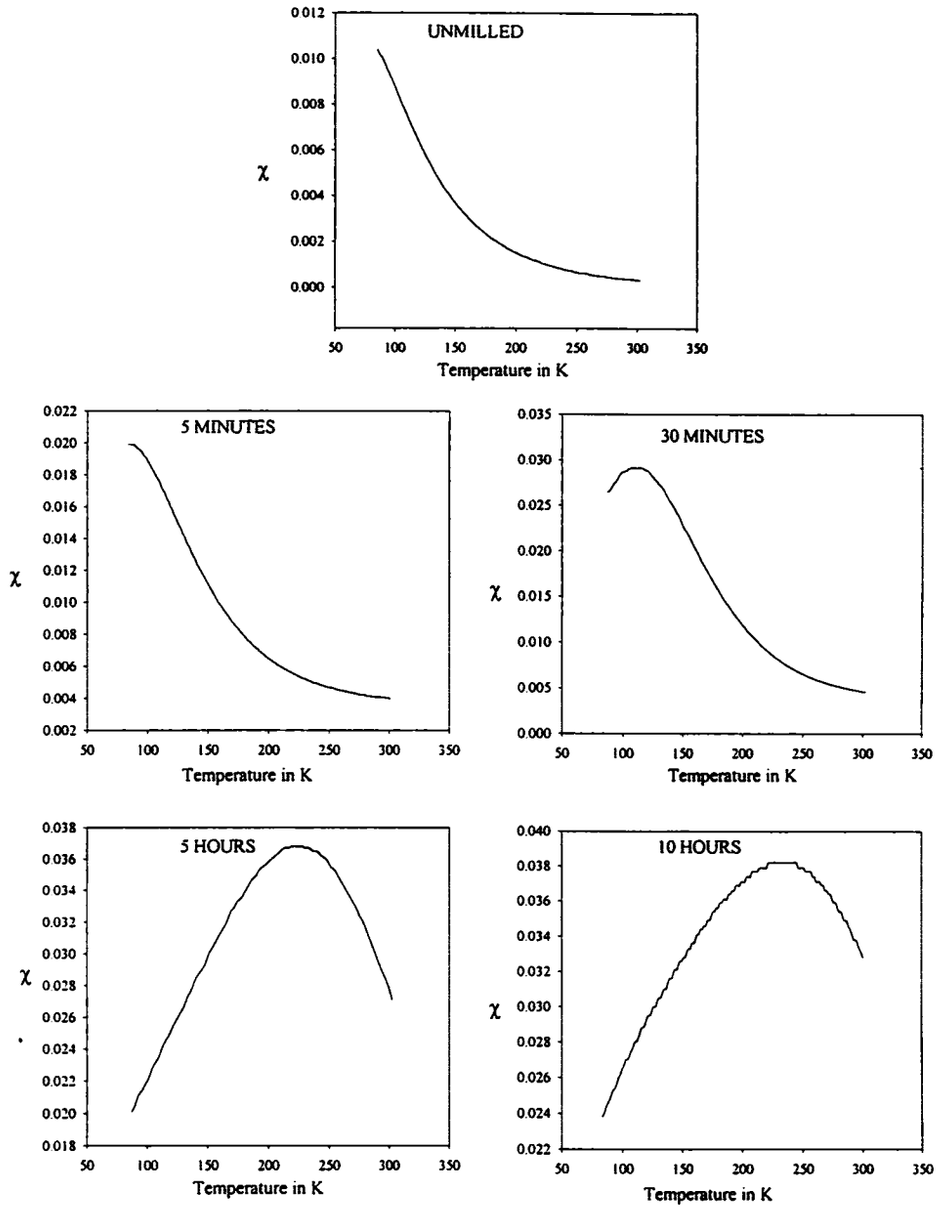

Figure 4.6 Temperature dependence of ac magnetic susceptibility of dry milled zinc ferrites at 2 Oe field and 133.33 Hz frequency.

Sample	Grain size (nm)	Transition temperature (K)
Unmilled	15.25	-
5 minutes	13.88	85
30 minutes	12.82	107
5 hours	10.66	225
10 hours	10.75	235

Table 4.3 Grain size and transition temperature (from temperature-χ graph) for dry milled zinc ferrite.

where T_B is the superparamagnetic blocking temperature, K is the crystalline anisotropy constant, V the particle volume and k_B the Boltzmann constant [35]. The results, which are summarized in table 4.2, are not in accordance with equation (4.3) and hence the transition cannot entirely be due to superparamagnetic blocking, but may also be due to the freezing of spin clusters resulting in a spin glass like feature. Below the broad maximum, spin clusters randomly freeze to decrease the magnetisation. A substantial amount of susceptibility at transition temperature is due to the short-range ferrimagnetic ordering, as a result of cation redistribution. The ac magnetic susceptibility increases with milling which is an indication of the fact that the high energy ball milling facilitates the cation redistribution.

4.6 Higher order ac magnetic susceptibility studies on unmilled and 10 hours dry milled zinc ferrite

ZFC-FC studies on unmilled and 10 hours dry milled samples give inconclusive evidence as regard the nature of the transitions vis-à-vis ferrimagnetic, superparamagnetic, spin glass like occuring at near room temperature. In order to gain a clear understanding of the nature of the transition and ordering taking place, alternate and complementary tools are required to probe this phenomenon. It has been reported in literature [49-52] that higher order susceptibility measurements will help to identify these transitions to a certain extent. With this motive in mind higher order ac magnetic susceptibility measurements were carried out using the same apparatus as described in chapter 2. This is based on a model proposed by the Sherrington-Kirkpatrikc and the Bethe approximation [49-52]. In that it is assumed that the magnetisation of a specimen in the presence of an external oscillating magnetic field H can be represented as

$$M= M_0+\chi_1 H+\chi_2 H^2+\chi_3 H^3+\ldots \quad \ldots\ldots (4.4)$$

Where M_0 is the spontaneous magnetisation and χ_1,χ_2 and χ_3 are the first, second and third order susceptibilities respectively [49-52]. Evaluation of the third order susceptibility measurements can be employed to investigate complex magnetic phases in nanosized magnetic particles.

Figure 4.7(a) and figure 4.7(b) represents first order (real component) and third order (imaginary component) ac magnetic susceptibility graphs for 10 hours dry milled samples at different applied fields. The small shift in the peak with ac field establishes that spin glass/superparamagnetic behaviour is exhibited by the milled

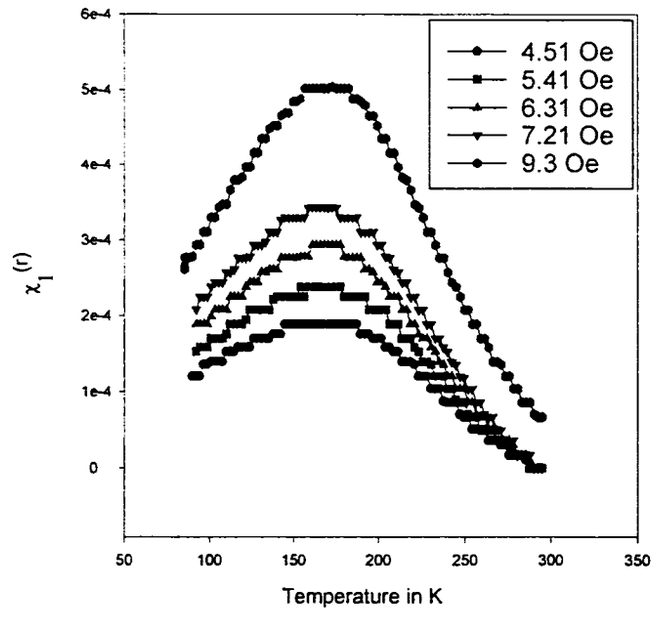

Figure 4.7(a) First order ac magnetic susceptibility (real component) graphs for 10 hours dry milled zinc ferrite at different applied fields.

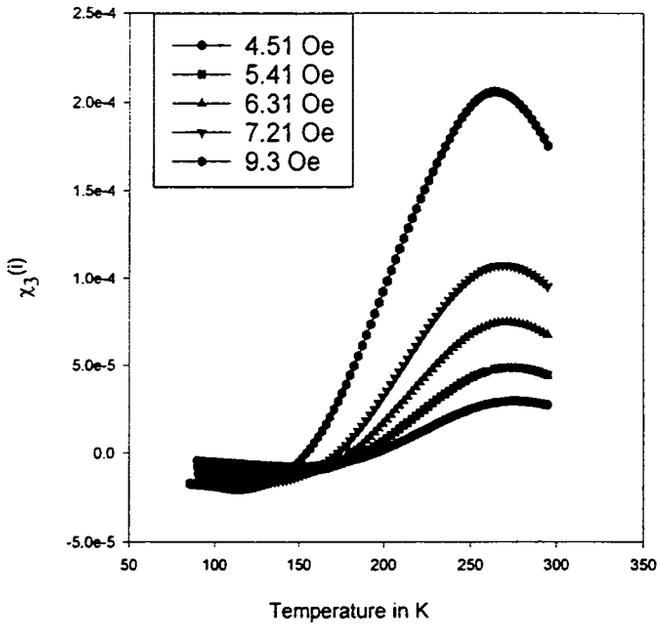

Figure 4.7(b) Third order ac magnetic susceptibility (imaginary component) graphs for 10 hours dry milled zinc ferrite at different applied fields.

sample [50]. Spin glass phase is partial since the curves do not merge above the transition [50]. Figure 4.8 represents the variation of third order susceptibility with applied field. The graph clearly establishes the predominance of superparamagnetic feature over spin glass, since when $H \rightarrow 0$, $\chi_3^{(r)} \rightarrow 0$, which is characteristic of a superparamagnetic ordering [51].

Figures 4.9(a)-4.9(c) depicts the real and imaginary susceptibility plots against temperature for different applied fields. The first, second and third order susceptibility variations are separately plotted in each case. $\chi_1^{(i)}$ practically remains zero in the entire experimental temperature range indicating that there is no magnetic loss [50]. The broad transition confirms the superparamagnetic ordering instead of a ferrimagnetic ordering [50]. In the case of pristine zinc ferrite, it is seen that they too display low magnetic loss characteristics, however, the nature of magnetic ordering occuring in this temperature range could not be ascertained.

4.7 Scrutiny of superparamagnetic signatures from Langevin fitting

A clear picture of superparamagnetic characteristics could be obtained by fitting the magnetisation curve with the theoretically derived Langevin function.

The Langevin function for a magnetic material can be expressed as

$$L(a) = \coth a - \frac{1}{a} \quad \ldots\ldots\ldots\ldots \quad (4.5)$$

Where $a = \mu H/k_B T$. μ represents the magnetic moment of the sample, H represent the applied field, T the temperature in degree absolute and k_B the Boltzmann constant. Expressing in terms of a series, Langevin function can be rewritten as

$$L(a) = \frac{a}{3} - \frac{a^3}{45} + \frac{2a^5}{945} - \ldots\ldots \quad \ldots\ldots\ldots\ldots \quad (4.6)$$

The total magnetisation M can be written as,

$$M = n\mu L(a) \quad \ldots\ldots\ldots\ldots \quad (4.7)$$

where n is the number of particles. In superparamagnetic materials, the evaluation of L(a) using the μ_B estimated from saturation magnetisation (M_s), should represent a paramagnetic characteristic with a large magnetic moment [18]. Hence the magnetisation becomes comparable to that of a ferrimagnetic material with the number of dipoles becoming equal to the number of particles, which is of the order of 10^{18}.

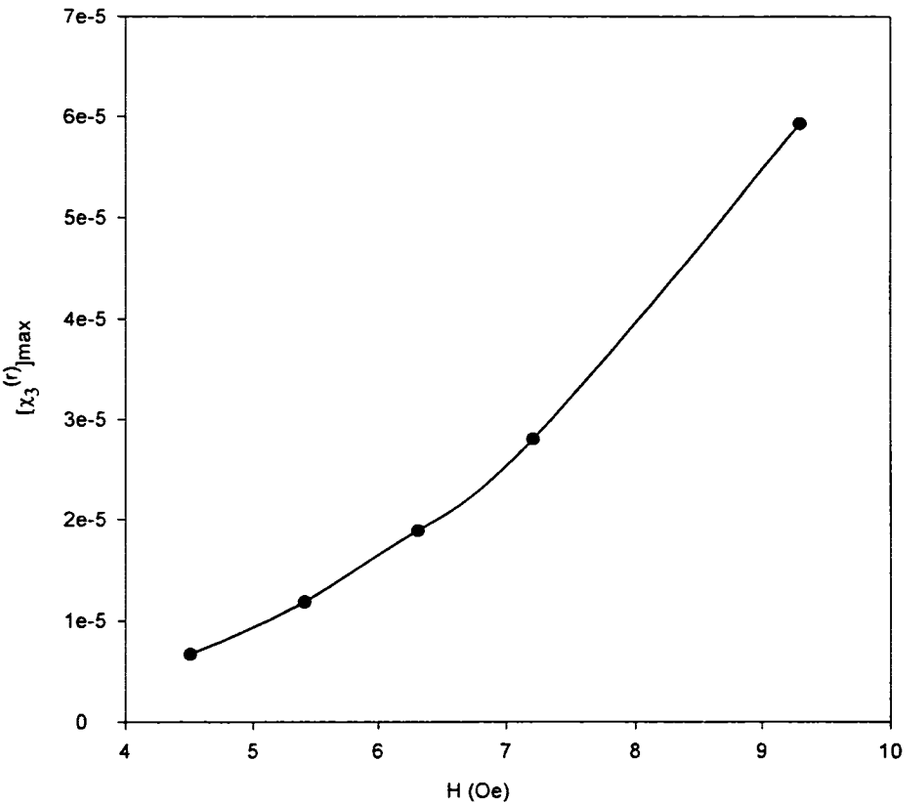

Figure 4.8 Variation of third order ac magnetic susceptibility (real component) for 10 hours dry milled zinc ferrite for different applied fields.

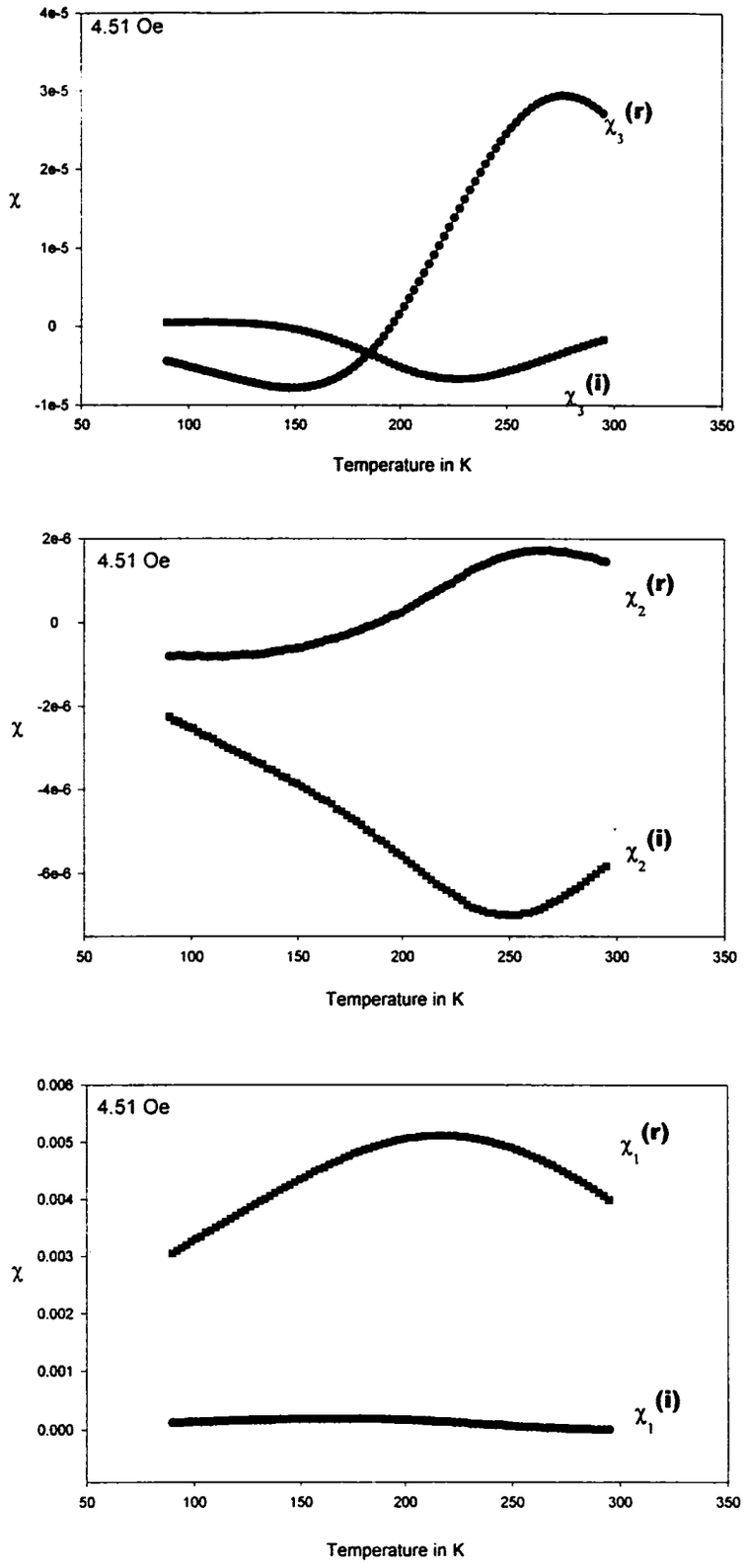

Figure 4.9(a) Real and imaginary components of first, second and third order ac magnetic susceptibility plots at an applied field of 4.51 Oe for 10 hours dry milled zinc ferrite.

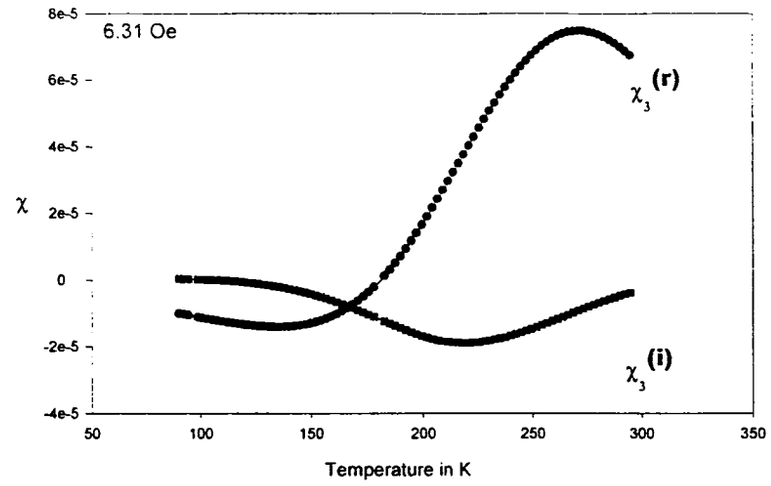

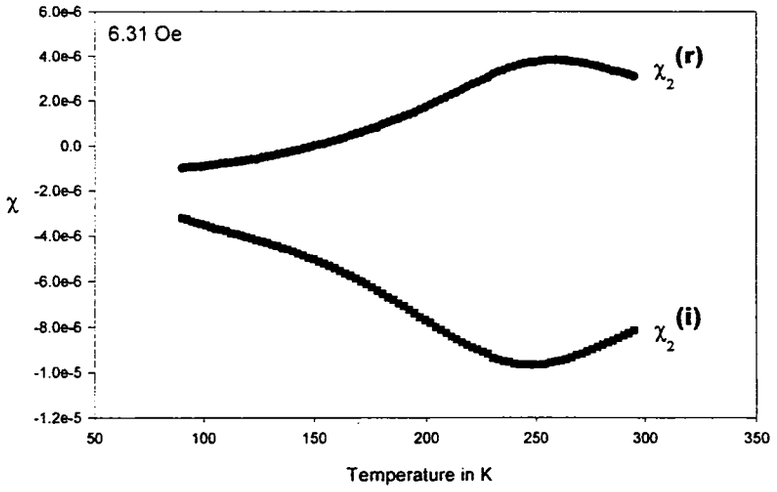

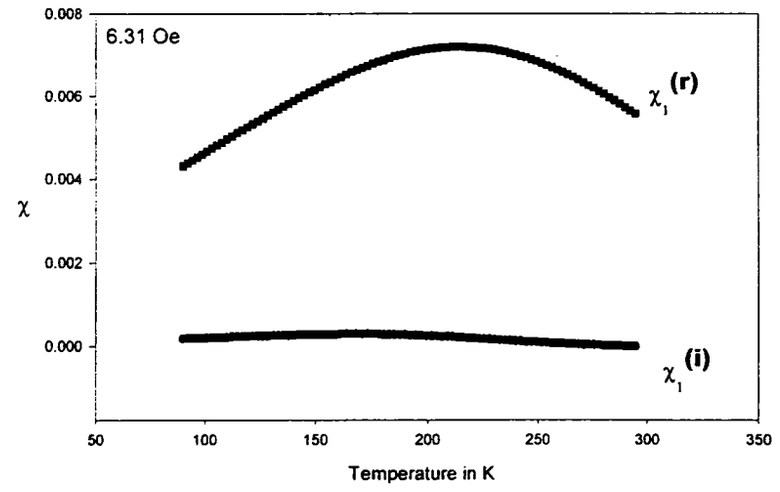

Figure 4.9(b) Real and imaginary components of first, second and third order ac magnetic susceptibility plots at an applied field of 6.31 Oe for 10 hours dry milled zinc ferrite.

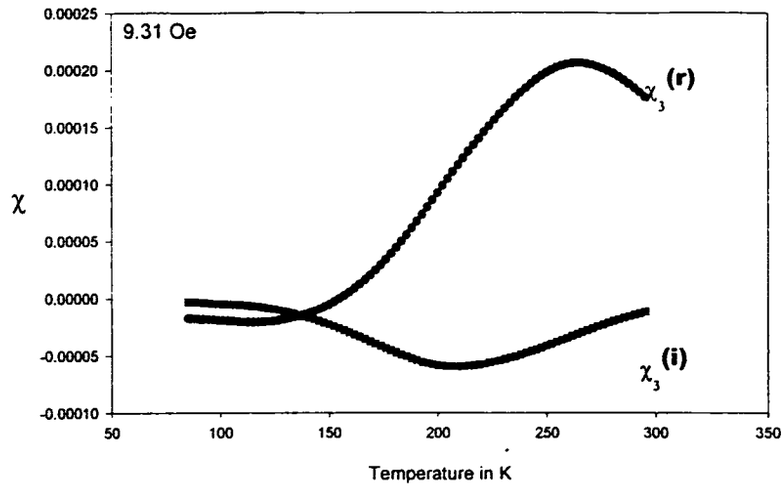

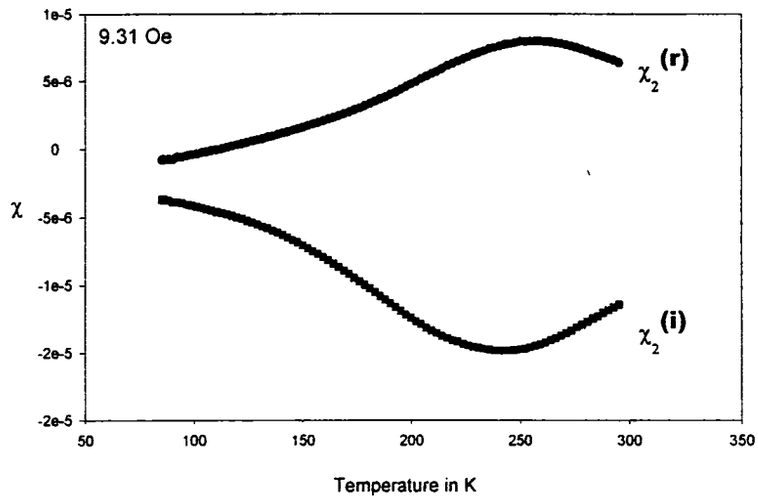

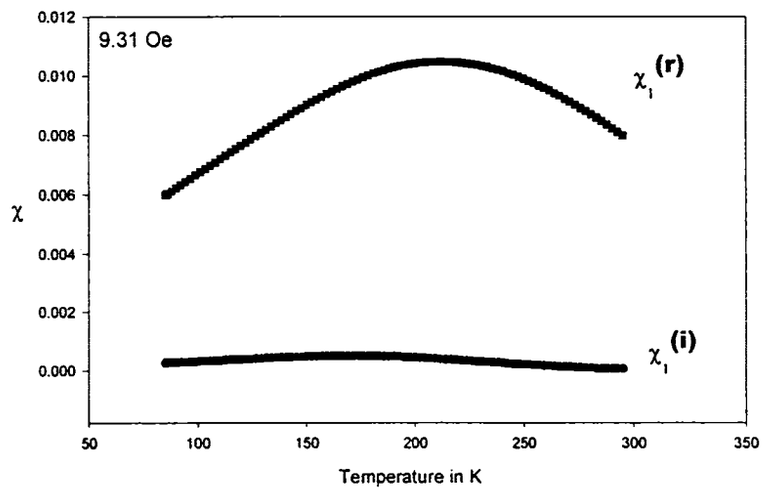

Figure 4.9(c) Real and imaginary components of first, second and third order ac magnetic susceptibility plots at an applied field of 9.31 Oe for 10 hours dry milled zinc ferrite.

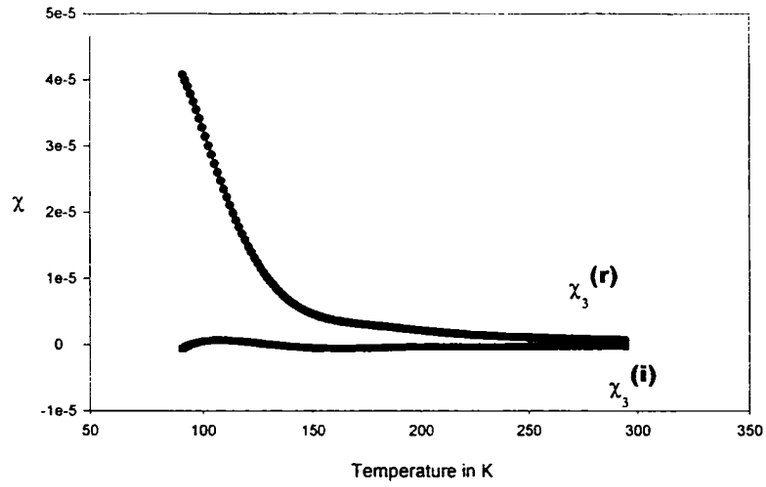

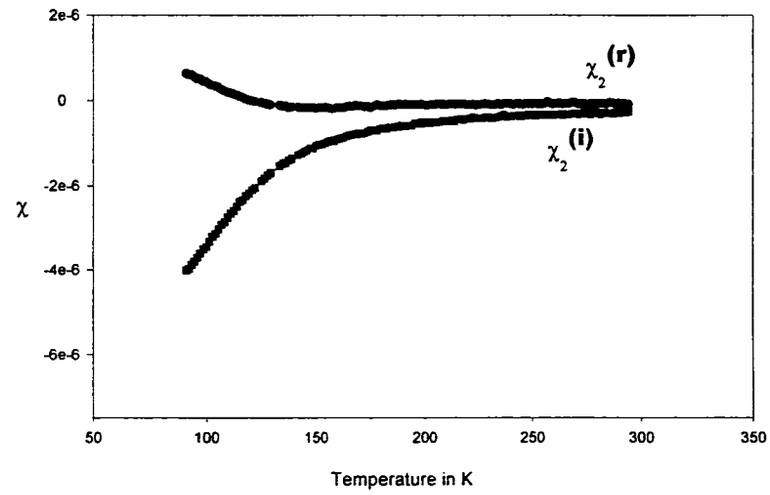

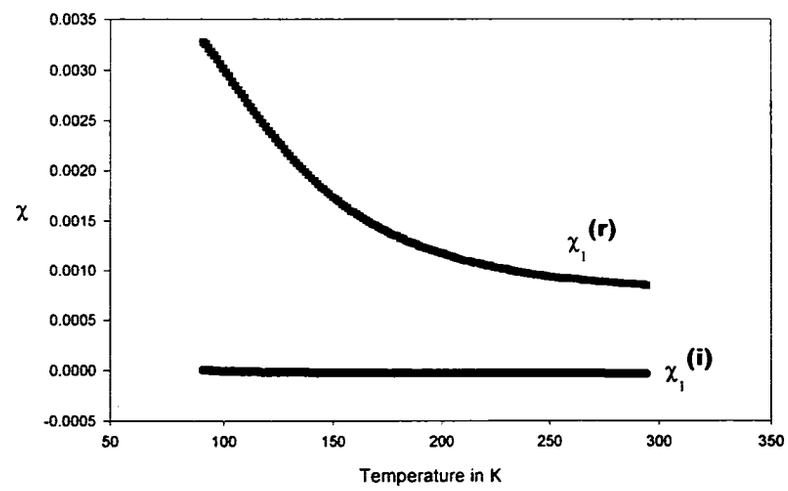

Figure 4.10 Real and imaginary components of first, second and third order ac magnetic susceptibility plots for unmilled zinc ferrite.

A linear response (figure 4.11) in magnetisation with applied field is exhibited by unmilled samples, which is a signature of antiferromagnetic ordering [25,44]. But with prolonged milling, this antiferromagnetic ordering is shifted to superparamagnetic ordering. In 10 hours dry milled samples, the theoretical and experimental magnetisation curves show signs of similar trend (figure 4.12).

4.8 Conclusions

Cation redistribution causes a short range ferrimagnetic ordering in dry milled and wet milled zinc ferrites that forms magnetic clusters, which contribute to the total magnetisation of the samples. Superparamagnetic clusters coupled with ferrimagnetic clusters are thought to be responsible for the nonsaturation exhibited by the hysteresis loops, even at a field of 10 kOe. The α-Fe_2O_3 formed during milling may be acting as a facilitator to redistribute the cations. The oxygen deficiency produced by the high energy ball milling causes the superexchange bonds to break, which results in spin disorder especially on the surface. This surface spin disorder also contributes to magnetisation. Thermomagnetisation studies on dry milled zinc ferrites establish partial cation redistribution and spin glass like surface layer. A-A and B-B interactions do play a role at lower temperatures. A-A and B-B interactions reduce the magnetisation below the transition temperature in zero field cooled condition. In field cooled conditions, the antiferromagnetic ordering is suppressed by the applied field which orients the clusters in the field direction. AC magnetic susceptibility results are also in tune with VSM results. Lack of spin glass like properties and less enhancement of saturation magnetisation in wet milled zinc ferrite is due to the resistance offered by the milling medium (toluene) to the direct kinetic energy transfer from balls to powder.

It has been found that in the case of dry milled samples, there is a tendency for the transition temperature (T_G/T_B) to shift towards room temperature with a further decrease in particle fineness. This is important from the applications point of view. If this represents a metastable state and if ultrafine zinc ferrite can be made into a thin film, the possibilities of employing thin films based on $ZnFe_2O_4$, for magneto optical applications is very bright. This is possible because at room temperature, the metastable states can be easily switched by a laser of appropriate wavelength and power. From third order susceptibility measurements it was possible to confirm the dominance of superparamagnetic particles in determining the overall magnetic

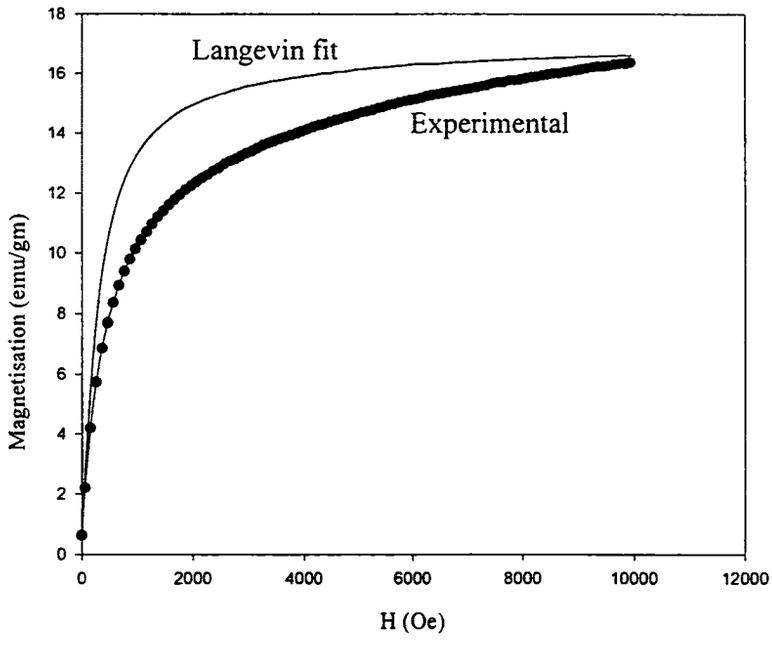

Figure 4.11 Theoretical (Langevin) and experimental magnetisation curves for 10 hours dry milled zinc ferrite.

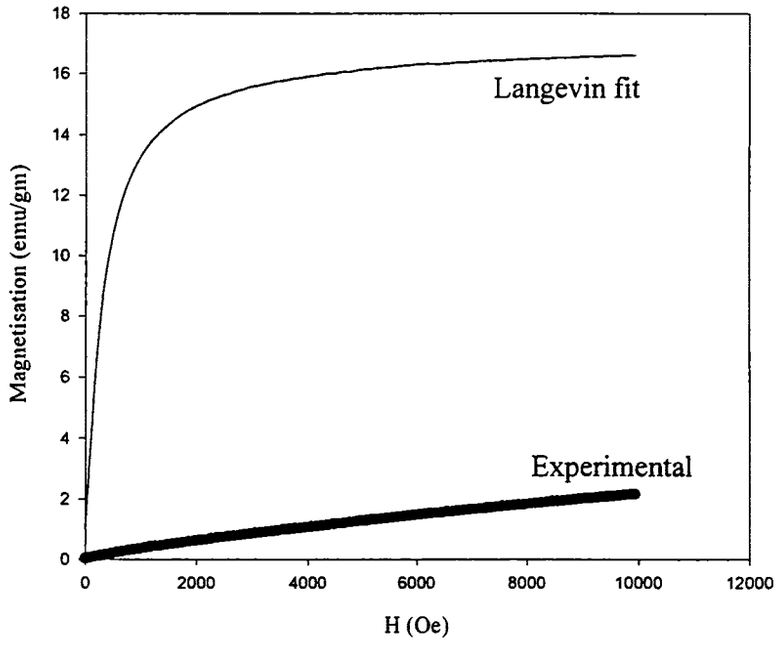

Figure 4.12 Theoretical (Langevin) and experimental magnetisation curves for unmilled zinc ferrite.

properties of ultrafine zinc ferrites. The theoretical Langevin function almost matches with that of experimentally fit values and confirm the dominance of superparamagnetic particles in zinc ferrite in deciding the overall magnetisation.

References:

1.H.Hamdeh, J.C.Ho, S.A.Oliver, R.J.Willey, G.Oliveri, G.Busca 1997 *J.Appl.Phys* **81** 1851

2.J.C.Ho,H.H.Hamdeh, Y.S.Chen, S.H.Lin, Y.D.Yao, R.J.Willey, S.A.Oliver 1995 *Phys.Rev.B* **52** 10122

3. T.Kamiyama, K.Haneda, T.Sato, S.Ikeda, H.Asano 1992 *Sol.state.communi.***81** 563

4.H.H.Hamdeh, J.C.Ho, S.A.Oliver, R.J.Willey, J.Kramer, Y.Y.Chen, S.H.Lin, Y.D.Yao, M.Daturi, G.Busca 1995 *IEEE Trans.magn.* **31** 3808

5.B.Jeyadevan, K.Tohji, K.Nakatsuka 1994 *J.Appl.Phys* **76** 6325

6.C.N.Chinnasamy, A.Narayanasamy, N.Ponpandian, R.Justin Joseyphus, B.Jeyadevan, K.Tohji and K.Chattopadhyay 2002 *J.Magn.Magn.mater* **238** 281

7.Hishan M. Widatallah and Frank J.Berry 2002 *J. Sol. State. Communi.* **164** 230

8.Fatemi D J, harris V G, Chen M X, Malik S K, Yelon W B, Long G J and Mohan A 1999 *J.Apl.Phys* **85(8)** 5172

9.M H M Mahmoud, H H Hamdeh, J C Ho, M J O'Shea and J C Walker 2000 *J.Magn.Magn.Mater.* **220** 139

10.G.F.Goya, H.R.Richenberg, M.Chen, W.B.Yelon 2000 *J.Appl.Phys.* **87** 8005

11.Goya G F, Rechenberg H R and Jiang J Z 1998 *J.Appl.Phys* **84** 1101

12.Arcos D, Valenzuela R, Vazquez M and Vallet-Regi M 1998 *J.solid state Chem* **141** 10

13.Sepelak V, Tkacova K, Boldyrev V V, Wibmann S and Becker K D 1997 *Physica B* **234-236** 617

14.M Pardavi-Horvath , L Takacs 1993 *J.Appl..Phys* 73(10) 6958.

15.Ding J, Tsuzuki T, McCormick P G and Street R 1996 *J.Magn.Magn.Mater.* **162** 271

16.Rosales M I, Ayala-Valenzuela O and Valenzuela R 2001 *IEEE Trans.Magn* **37** 2373

17. Murthy V R K and Viswanathan B 1990 *Ferrite Materials Science and Technolgy, Narosa Publishing House, New Delhi-15* 8

18. B.D.Cullity, *Introduction to magnetic materials , 1972 Addison Wesley publishing Company* 159

19. Soshin Chikazumi, *Physics of magnetism , 1964 John Wiley and sons, Inc., New York* 9

20. Ronald F.Soohoo, *Theory and application of ferrites, 1960 Prentice hall Inc, New Jersey* 46

21.J.Smit, and H.P.J. Wijn, 1959 *Ferrites, Philips Technical Library* 33

22.Xavier Battle and Amilcar Laborta 2002 *J.Phys.D.Appl.Phys* **35** R15

23.G.F.Goya, H.R.Rechenberg 1999 *J.Magn.Magn.Mater* **196-197** 191

24.Pannaparayil T, Komarneni S, Marande R and Zadarko M 1990 *J.Appl.Phys* **67** 5509

25.Ted Clerk M and Evans B J 1997 *IEEE Trans magn* **33** 3745

26.Chinnasamy C N, Narayanasamy A, Ponpandian N, Chattopadhyay K, Shinoda K, Jeyadevan B, Tohji K, Nakatsuka K, Furubayashi T and Nakatani I 2001 *Phy.Rev.B* **63** 184108

27.Upadhyay R V 1997 *Pramana* **49** 309

28.Sato T, Haneda K, Seki M and Iijima T 1990 *Appl.Phys. A* **50** 13

29.Sepelak V, Tkacova K, Boldyrev V V, Wibmann S and Becker K D 1997 *Physica B* **234-236** 617

30.Youhei Yamamoto, Hidekazu Tanaka and Tomoji kawai 2001*Jpn.J.Appl.Phys* **40** L545

31.Masheva V, Grigorova M, Valkov N, Blythe H J, Midlarz T, Blaskov V, Geshev J and Mikhov M 1999 *J.Magn.Magn.Mater*. **196-197** 128

32.Qi Chen, Adam.J.Rondinone, Bryan.C.Chakoumakos, Z.John.Zhang 1999 *J.Magn.Magn.Mater* **194** 1

33.Qi Chen and John.Zhang Z 1998 *Appl.Phys.lett*. **73** 3156

34.M. Zheng, X.C. Wu, B.S. Zou, Y.J. Wang, *J.Magn.Magn.Mater.* 183 (1998) 152

35. B.D.Cullity, *Introduction to magnetic materials , 1972 Addison Wesley publishing Company* 414

36.K. Haneda, *Can.J.Phys.* 65 (1987) 1233

37.A.H. Morrish, K. Haneda, X.Z. Zhou, *Proceedings of the NATO Advanced study institute on Nanophase materials-syntheses, properties and applications, Kluwer academic publishers, Netherlands (*1994) 515

38.J. Sort, J. Nogues, X. Amils, S. Surinach, J. S.Munoz, M.D. Baro, *Appl. Phys. Lett.* 75 (1999) 3177

39.J. Sort, J. Nogues, S. Surinach, J. S. Munoz, M. D. Baro, E. Chappel, F. Dupont, G. Chouteau, *Appl. Phys. Lett.* 79 (2001) 1142

40.W. A. Kaczmarek, B. Idzikowski, K. H. Muller, *J.Magn. Magn. Mater.* 177-181 (1998) 921

41.Bhowmik R N and Ranganathan R 2002 *J.Magn.Magn.Mater* **248** 101

42.M Andres-Verges, C de Julian, J m Gonzalez and C J Serna 1993 *J.Mat.Sci* **28** 2962

43.C Caizer 2002 *Sol.State.Communi.* **124** 53

44.Bhowmik R N and Ranganathan R 2002 *J.Magn.Magn.Mater* **247** 83

45.P S Anilkumar, P A Joy and S K Date 2000 *Bull.Mater.Sci* **23(2)** 97

46.G Balaji, N S Gajbhiye, G Wilde and J Weissmuller 2002 *J.Magn.Magn.Mater* **242-245** 617

47.W.Schiessel, W.Potzel,H.Karzel, M.Steiner, G.M.Kalvius, A.Martin, M.K.Krause, I.Halevy, J.Gal, W.Schafer, G.Will, M.Hillberg, R.Wappling 1996 *Phys.Rev B* **53** 9143

48.Hiroshi Yahiro, Hidekazu Tanaka, Youhei Yamamoto, Tomoji Kawai 2002 *Sol.State.Communi.* **123** 535

49.Sunil Nair and A.Banerjee *Phys.Rev B* 68, 094408 (2003)

50.A.Bajpai and A.Banerjee *Phys.Rev B* 55(18), 12439 (1997)

51.A.Bajpai and A.Banerjee *J.Phys. Condens.Matte*r 13 (2001) 637-647

52.A.Bajpai and A.Banerjee *Phys.Rev B* 62(13), 8996 (2000)

CHAPTER 5

ROOM TEMPERATURE AND LOW TEMPERATURE MÖSSBAUER SPECTROSCOPIC INVESTIGATIONS ON ULTRAFINE ZINC FERRITE

5.1 Introduction

A detailed investigation by employing various tools like vibrating sample magnetometry, ac magnetic susceptibility and ZFC-FC measurements on ultrafine zinc ferrite brought out various possibilities in finding an explanation for the anomalous magnetic properties exhibited by ultrafine zinc ferrite. For example, it was possible to establish the fact that prolonged milling in zinc ferrite samples induces cation redistribution and inversion. This results in a ferrimagnetic ordering in the core. However, ZFC-FC measurements carried out on dry milled zinc ferrite samples give conclusive evidence for the presence of a superparamagnetic component along with spin glass clusters. These spin glass clusters are the result of the freezing of spins on the surface. From third order ac magnetic susceptibility measurements, it was possible to detect the presence of both superparamagnetic and spin glass components in dry milled samples. Mössbauer spectroscopy is an effective tool to investigate the magnetic properties of ferro/ferri and the paramagnetic systems. It is also a complementary tool to gather confirmative evidence on the nature of magnetic ordering. The detection of superparamagnetic particles in milled samples is also possible by Mössbauer investigations [1-46]. A systematic study on the variation of Mössbauer hyperfine parameters with milling and with temperature was carried out. This will throw more light on the magnetic properties exhibited by zinc ferrite in the ultrafine regime.

For bulk zinc ferrite, which is prepared by conventional ceramic method, well-established Mössbauer parameters exist. The Mössbauer spectrum of a bulk $ZnFe_2O_4$ at 298 K exhibits a single quadrupole doublet, as expected for a paramagnetic phase with an isomer shift of 0.35 mm/s and a quadrupole splitting of 0.33 mm/s. These parameters are characteristic of Fe^{3+} ion occupying octahedral sites [1-4]. In ultrafine zinc ferrite samples, inversion of the spinel structure occurs as a result of cation redistribution [2-19].

When magnetic hyperfine splitting occurs, a Fe^{57} Mössbauer spectrum consists of six absorption lines (sextet) [20-21]. If the hyperfine splitting occurs by the cation redistribution, the Fe ions occupy both tetrahedral and octahedral sites. Then the Mössbauer spectrum will consists of two sextets but in an overlapping configuration corresponding to the tetrahedral and octahedral coordinations [22,37].

Mössbauer spectra were recorded for unmilled and all dry milled samples at room temperature (Fig 5.1-5.5). The unmilled and 10 hours dry milled samples were subjected to low temperature Mössbauer studies (Fig 5.6-5.10). The spectra were satisfactorily fitted by utilizing a software called NORMOS. While fitting the spectrum using NORMOS, it was assumed that the contribution of α-Fe_2O_3, present in the samples is negligible and its possible effects on the spectrum are neglected.

5.2 Room temperature Mössbauer studies on dry milled zinc ferrite

Figures 5.1 to 5.5 represents the Mössbauer spectra of unmilled and dry milled (5 minutes, 30 minutes, 5 hours and 10 hours respectively) zinc ferrite samples at room temperature. All spectra were satisfactorily fitted with a sextet, a doublet and a distribution component representing nanocrystalline and amorphous component of ultrafine particles.

The superparamagnetic component, the doublet, is due to the electric field gradient (EFG) existing at the site of Fe atom. Charges on neighbouring ions, which surround this Fe atom, will contribute to EFG. In ultrafine particles, a large fraction of the Fe ions are situated on the surface and since surface represents a discontinuity with respect to the core, marked changes in symmetry and strong EFG can be expected here [2,14]. The doublet was found to be getting broadened with milling. This is an indication that different Fe environments are present in the sample [2]. This supports the theory of cation redistribution and super exchange path breakage between Fe atoms occuring at the surface that leads to different Fe environments. The different isomer shift values (refer table 5.1) supports the different electron densities around Fe atoms confirming the above results [1-2]. The quadrupole splitting values get modified with milling. Thus the broadening of the doublet and the change in isomer shift and quadrupole splitting values provides a very clear evidence of considerable changes in the quadrupole interaction and indicates the presence of a wide distribution of EFG at the Fe^{3+} nucleus. All these observations gathered from the Mössbauer

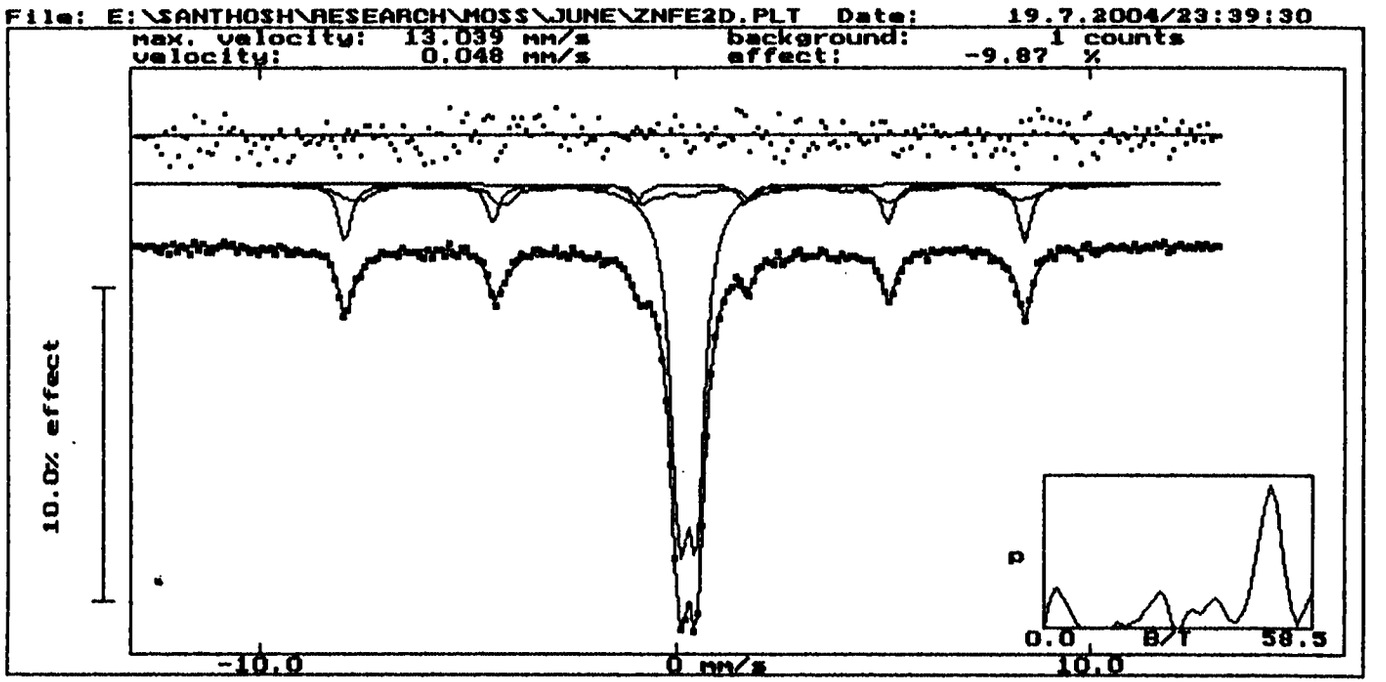

Figure 5.1. Mössbauer spectrum for unmilled zinc ferrite at room temperature.

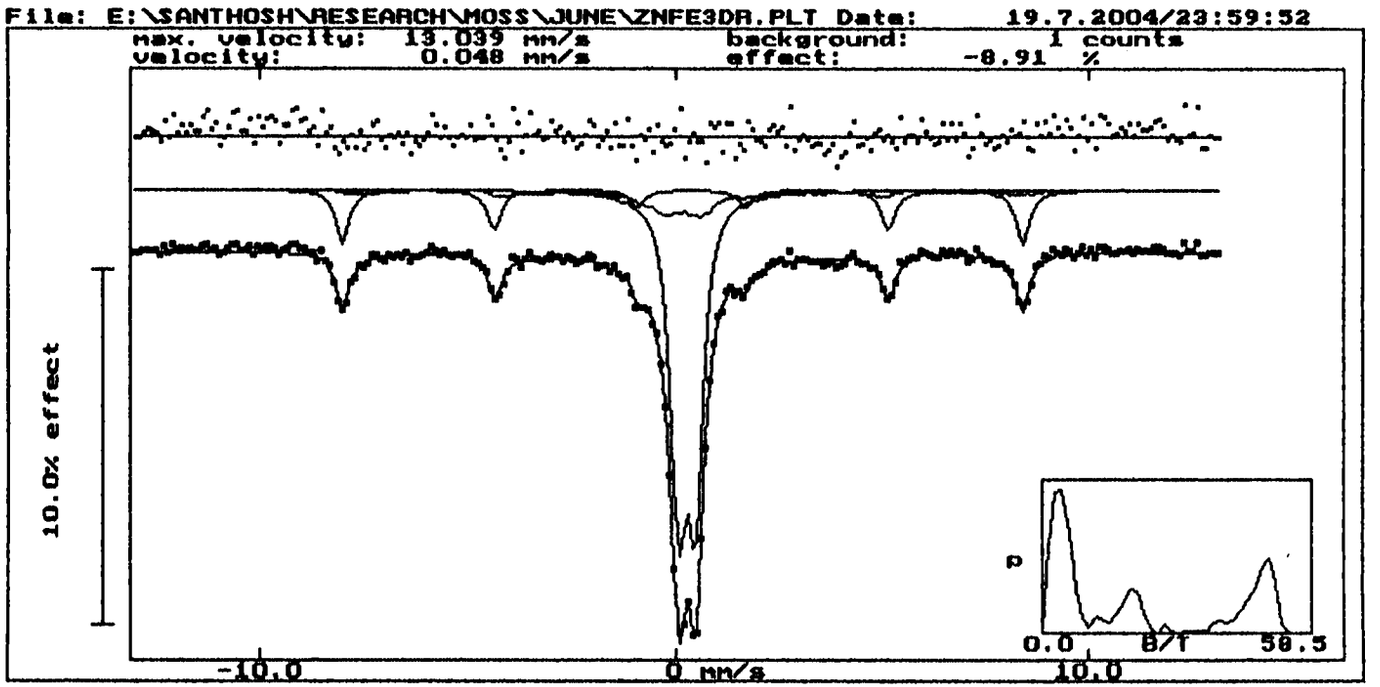

Figure 5.2. Mössbauer spectrum for 5 minutes dry milled zinc ferrite at room temperature.

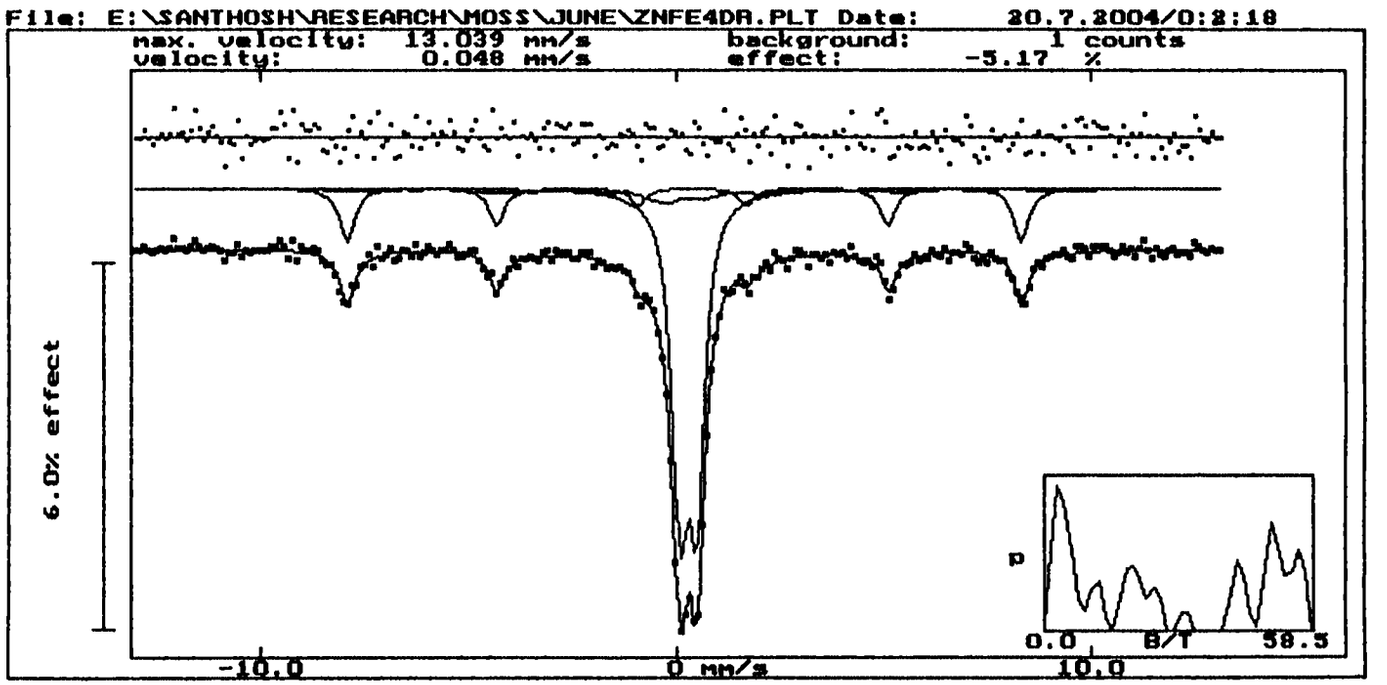

Figure 5.3. Mössbauer spectrum for 30 minutes dry milled zinc ferrite at room temperature.

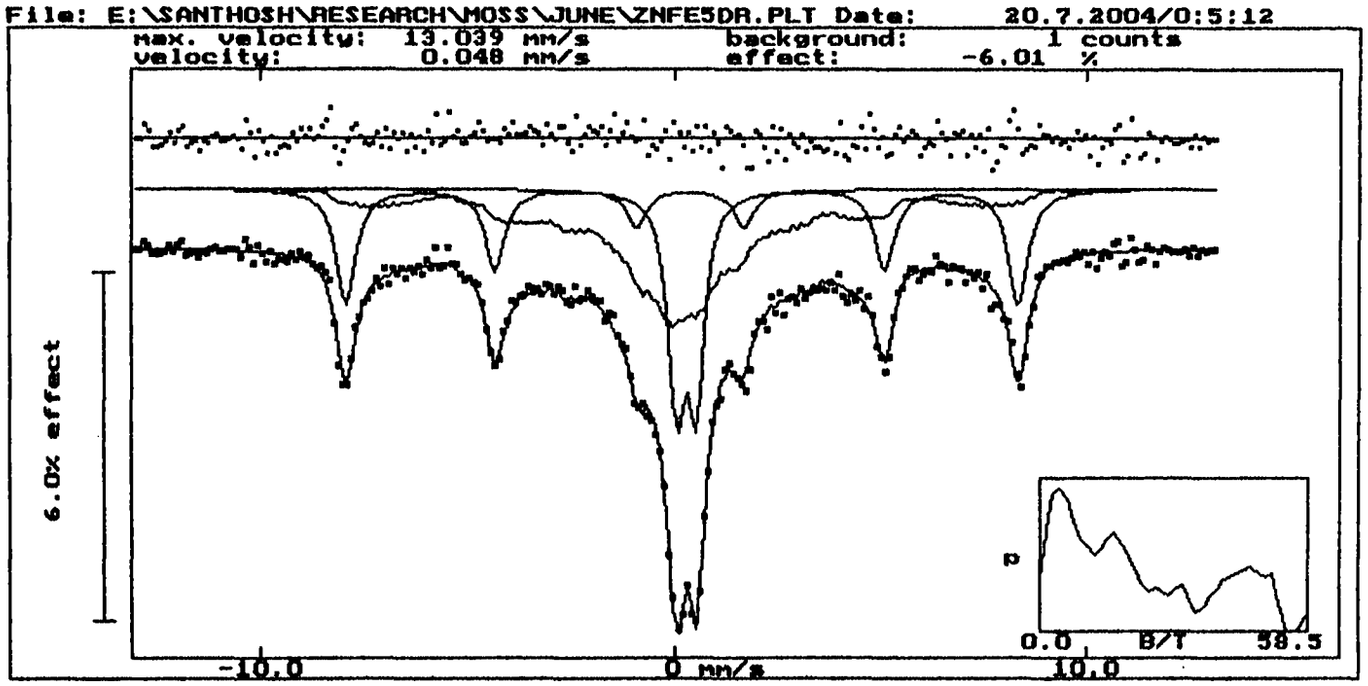

Figure 5.4. Mössbauer spectrum for 5 hours dry milled zinc ferrite at room temperature.

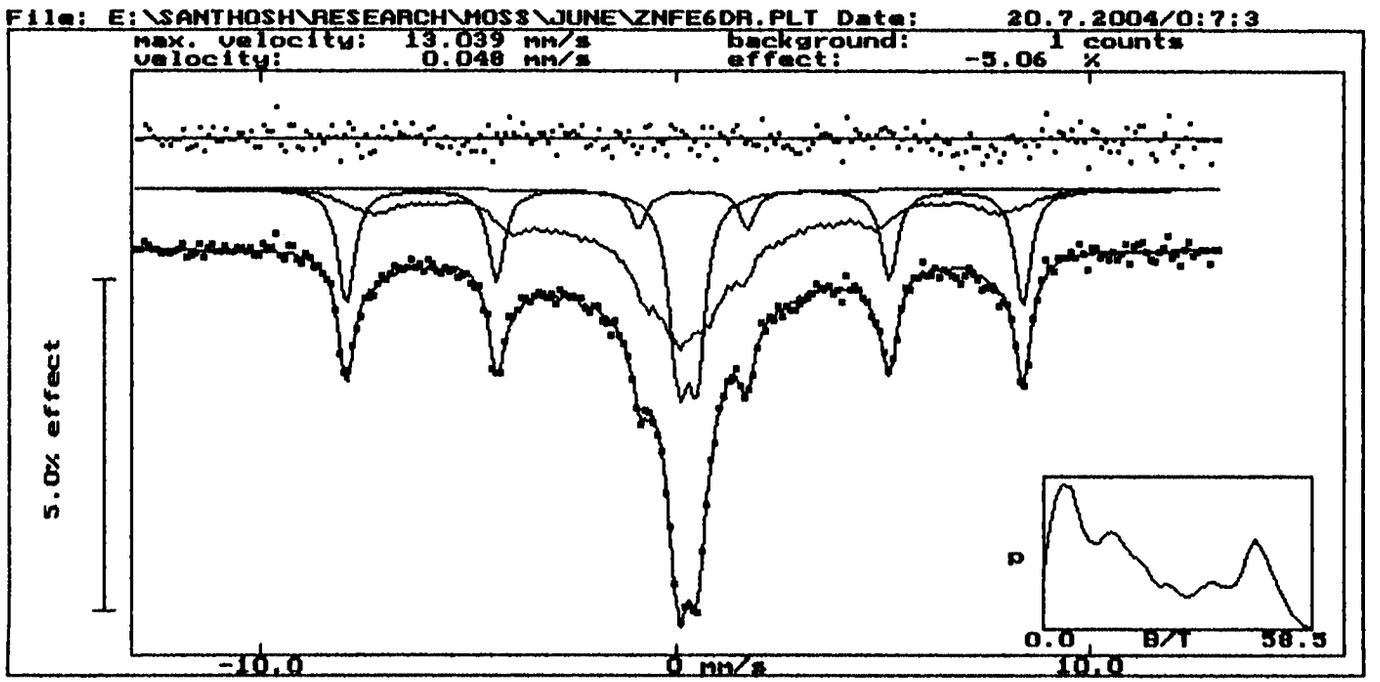

Figure 5.5. Mössbauer spectrum for 10 hours dry milled zinc ferrite at room temperature.

Sample	Distribution area (%)	Sextet area (%)	Doublet area (%)	Line width (mm/s)	Sextet IS (mm/s)	Sextet QS (mm/s)	Doublet IS (mm/s)	Doublet QS (mm/s)	Hyperfine field (T)
Unmilled	19.83	18.56	61.61	.24	.342	.142	.337	.387	50.57
5 minutes	15.02	22.16	62.82	.24	.353	.211	.337	.387	50.65
30 minutes	10.84	23.83	65.33	.24	.351	.198	.336	.388	50.13
5 hours	49.39	30.15	20.46	.24	.351	.184	.349	.455	50.23
10 hours	57.45	25.03	17.52	.24	.370	.208	.332	.410	50.39

Table 5.1 Mössbauer fitted data for unmilled and milled zinc ferrites at room temperature.

spectra are convincing and clinching evidences to the assumption that milling induces cation redistribution.

Although the variant isomer shift and quadrupole splitting values of doublet gives information about the anomalous feature of ultrafine particle, it is the sextet which directly gives the presence of a magnetic ordering in these samples. The isomer shift values, which lie around 0.35 mm/s suggests that only Fe^{3+} is present in these samples and the chances for the occurrence of Fe^{2+} is completely ruled out [2-20]. From the spectra, it can be observed that the percentage of sextet and doublet area at around 18.56% and 61.61% respectively. Upon milling, the sextet area increases marginally from 18.56% to 30.15% and then decreases for the 10 hours milled sample. It is to be noted here that the doublet in the case of 5 hour milled sample reduces to 20.46%. It is also to be taken note of the fact that in the case of 5 hours milled and 10 hours milled samples, the amorphous component as indicated by the spectra is a result of the disconnected superexchange paths.

The detection of the presence of an amorphous component in the spectra of 5 hours and 10 hours milled sample could be because of the short range ordering occuring out of bond breakage at the surface, which possibly, results in the creation of spin glass like clusters on the surface. It may be noted here that there exists evidence from ac magnetic susceptibility and ZFC-FC measurements for this finding. So Mössbauer spectroscopy provides supportive evidence for the presence of a spin glass component along with ferrimagnetism and superparamagnetism. This spin glass component could be in the form of spin glass like clusters resulting out of the freezing of spins.

The hyperfine field lie around 51 T for all samples. This hyperfine field is typical of a spinel configuration resulting in ferrimagnetism. It must be noted here that for Fe_3O_4 and γ-Fe_2O_3, the hyperfine field is 51 T nearly. Careful observation of the Mössbauer pattern suggests an asymmetry between first and sixth, second and fifth, and, third and fourth line in the spectra and this trend increases with milling. This confirms the distribution of Fe^{3+} ions over A and B sites that result in the anomalous magnetic properties of ultrafine zinc ferrite particles [1,3]. This is also observed in hyperfine magnetic field distributions, which shows a wide distribution suggesting different Fe environments [3-4,8,12-13]. A totally different HMF distribution is found in milled samples, which is due to the displacement of more Fe^{3+} ions towards

tetrahedral sites. This cation redistribution is accompanied by a decrease in unit cell dimension (figure 3.3). Lattice contraction resulting out of cation redistribution can alter the A-O or B-O bond angles [2,7,12,19].

5.3 Mössbauer studies on unmilled zinc ferrite samples at different temperatures

Figure 5.1 and 5.6 represents the Mössbauer spectra of unmilled zinc ferrite sample at room temperature and at 16 K. There exists a significant superparamagnetic component at 16 K even though the quadrupole splitting is low. This clearly suggests That the Neel temperature is not attained at 16 K in unmilled sample. This supports the results obtained by various researchers that the T_N of zinc ferrite lies below 10 K.

The presence of a doublet and a sextet in this large temperature range is due to the coexistence of superparamagnetism and the ferrimagnetism in zinc ferrite. The superparamagnetic blocking temperature (T_B), which is a finite size property and a volume dependant term, is different for different sized particles. Since, in our samples, a wide particle size distribution exists, which results in the wide range of T_B. This could be yet another reason for the coexistence of both the doublet and sextet in this wide range of temperatures [24-26]. Table 5.2 depicts the fitted Mössbauer parameters for unmilled sample at different temperatures.

5.4 Mössbauer studies on 10 hours dry milled zinc ferrite samples at different temperatures

Figure 5.5, 5.7, 5.8, 5.9 and 5.10 represents the Mössbauer spectra of 10 hours dry milled zinc ferrite sample at room temperature, 190 K, 150 K, 100 K and 16 K respectively. The superparamagnetic doublet almost disappears at 16 K suggesting an antiferromagnetic ordering well above Neel temperature. Hence it can be inferred that high energy ball milling enhancing the magnetic ordering temperature. Table 5.3 shows the fitted Mössbauer parameters for 10 hours dry milled sample at different temperatures.

5.5 Conclusions

The Mössbauer spectra taken at room temperature and at low temperatures were satisfactorily fitted by a superparamagnetic doublet, a ferrimagnetic sextet and an amorphous component typical of nanocrystalline materials. The different isomer shift values, quadrupole splitting values, the broadening of the doublet, asymmetry of

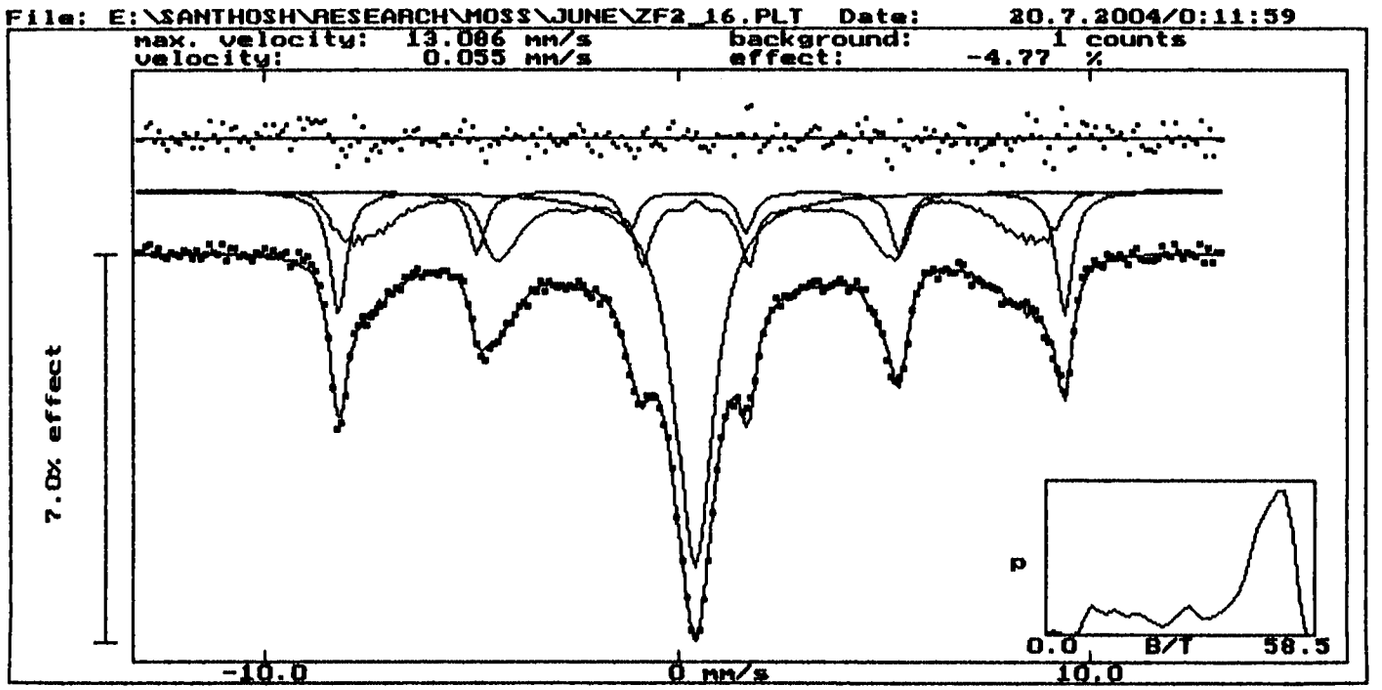

Figure 5.6. Mössbauer spectrum for unmilled zinc ferrite at 16 K.

Temp	Distribution area (%)	Sextet area (%)	Doublet area (%)	Line width (mm/s)	Sextet IS (mm/s)	Sextet QS (mm/s)	Doublet IS (mm/s)	Doublet QS (mm/s)	Hyperfine field (T)
300 K	19.83	18.56	61.61	.24	.342	.142	.337	.387	50.57
16 K	37.21	21.57	41.22	.24	.470	.314	.456	.050	54.21

Table 5.2 Mössbauer fitted data for unmilled zinc ferrite at different temperatures.

the sextet lines and the wide distribution of hyperfine magnetic field suggests possible cation redistribution and surface super exchange bond breakage due to oxygen deficiency. The HEBM enhances magnetisation and the sextet area increases. Antiferromagnetic ordering is not observed in unmilled sample at 16 K. But the ferrimagnetic component is found to be increasing at the expense of the superparamagnetic component. However in 10 hours milled sample an antiferromagnetic ordering was observed at 16 K with a clear sextet pattern.

All these conclusions drawn out of Mössbauer spectroscopic studies conducted on dry milled ultrafine zinc ferrite samples are in conformity with the results obtained from various magnetisation measurements. Though most of these measurements reveal bulk characteristic of the material, from Mössbauer spectroscopic studies, there is conclusive evidence for the presence of a spin glass component in milled samples.

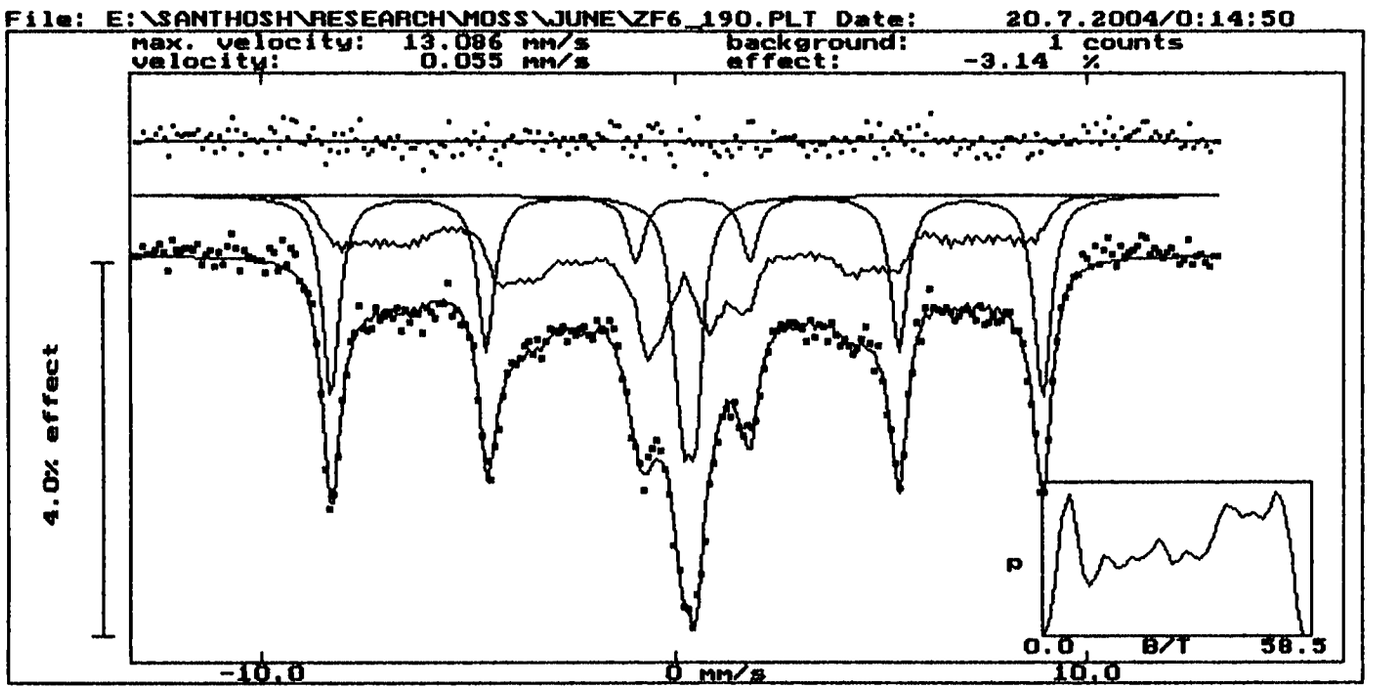

Figure 5.7. Mössbauer spectrum for 10 hours dry milled zinc ferrite at 190 K.

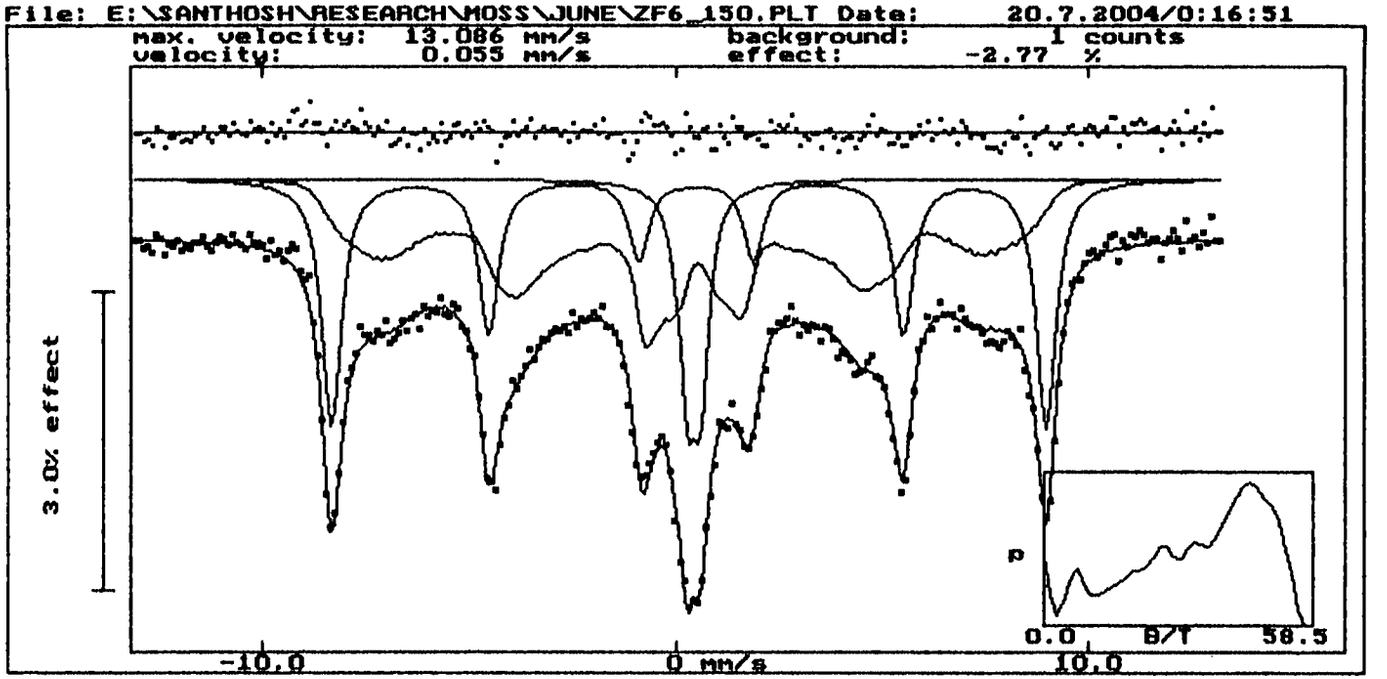

Figure 5.8. Mössbauer spectrum for 10 hours dry milled zinc ferrite at 150 K.

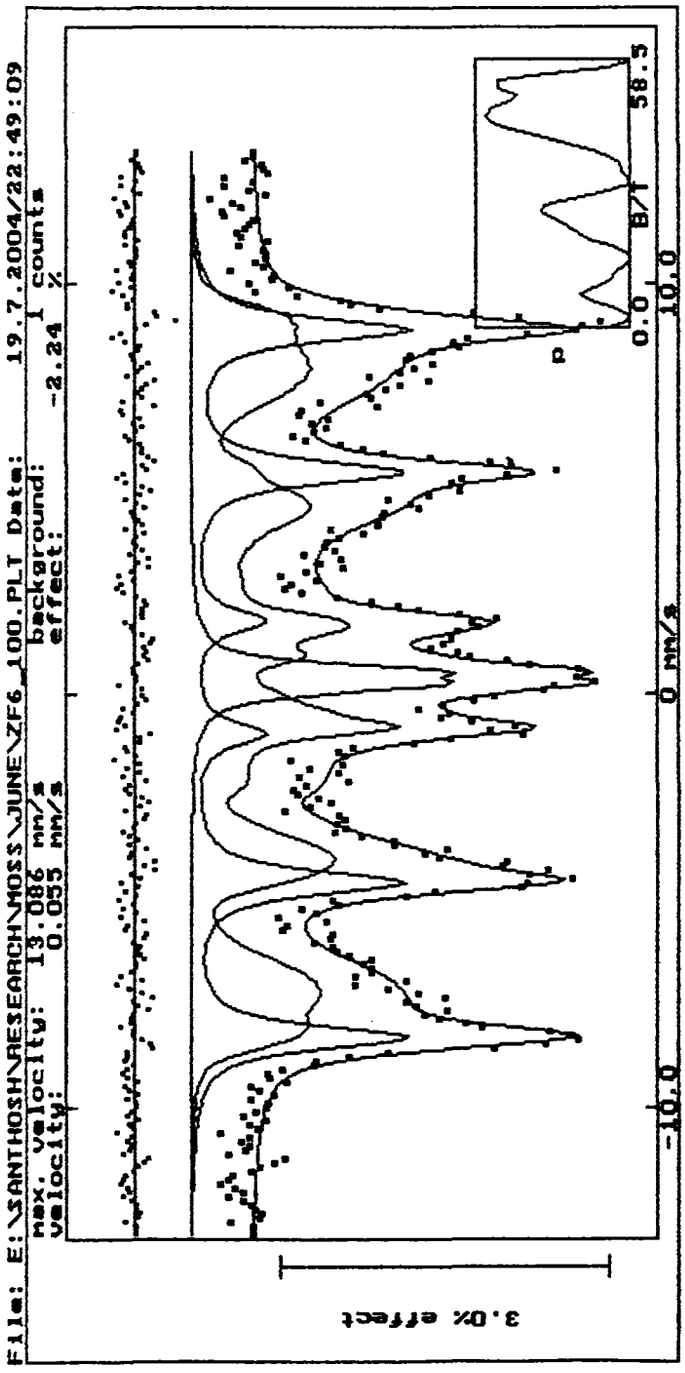

Figure 5.9. Mössbauer spectrum for 10 hours dry milled zinc ferrite at 100 K

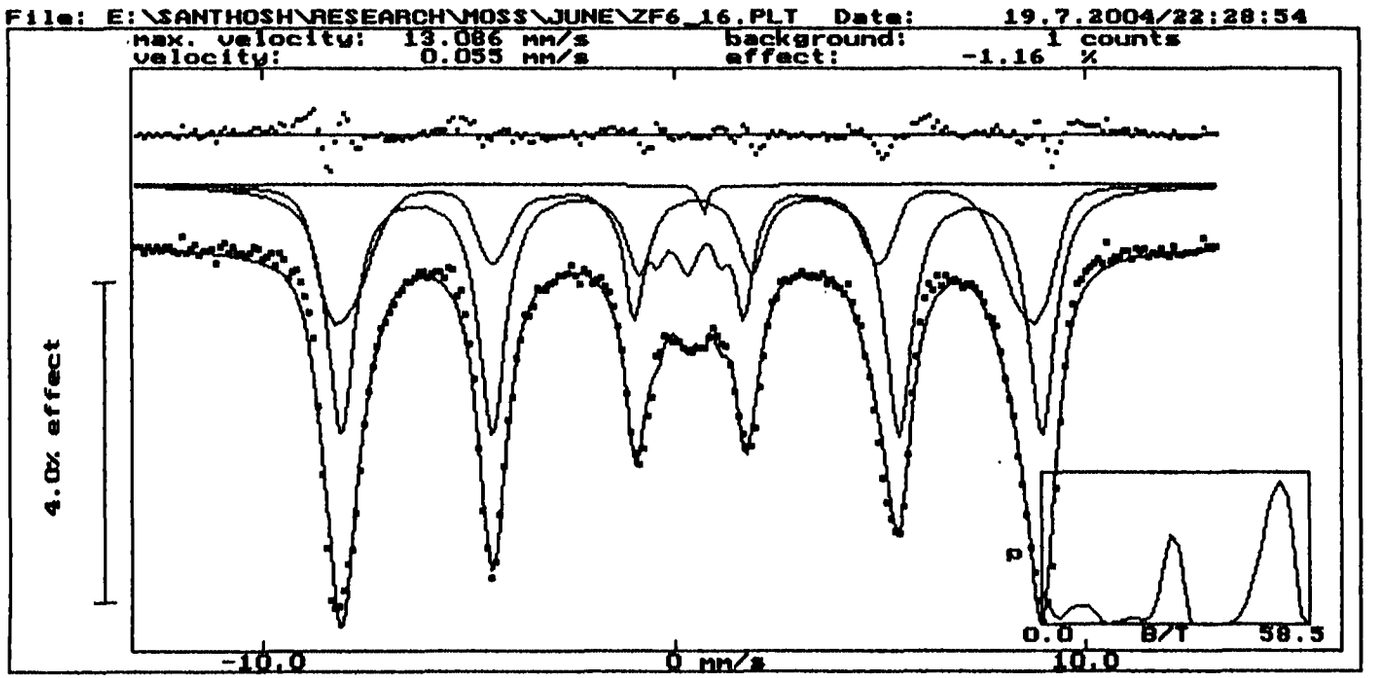

Figure 5.10. Mössbauer spectrum for 10 hours dry milled zinc ferrite at 16 K.

Temp	Distribution area (%)	Sextet area (%)	Doublet area (%)	Line width (mm/s)	Sextet IS (mm/s)	Sextet QS (mm/s)	Doublet IS (mm/s)	Doublet QS (mm/s)	Hyperfine field (T)
300 K	57.45	25.03	17.52	.24	.370	.208	.332	.410	50.39
190 K	58.44	29.53	12.03	.24	.437	.142	.386	.310	53.19
150 K	57.02	32.55	10.43	.35	.466	.174	.480	.323	53.34
100 K	55.48	35.50	9.02	.40	.425	.157	.459	.339	52.90
16 K	41.79	57.79	0.42	.41	.524	.105	.747	.002	52.51

Table 5.3 Mössbauer fitted data for 10 hours dry milled zinc ferrite at different temperatures.

References:

1.Ted Clerk M and Evans B J 1997 *IEEE Trans magn* **33** 3745

2. H.Ehrhardt, S.J.Campbell, M.Hofmann 2002 J.Alloys *and Compounds* **339** 255

3.H.H.Hamdeh, J.C.Ho, S.A.Oliver, R.J.Willey, J.Kramer, Y.Y.Chen, S.H.Lin, Y.D.Yao, M.Daturi, G.Busca 1995 *IEEE Trans.magn.* **31** 3808

4.H.Hamdeh, J.C.Ho, S.A.Oliver, R.J.Willey, G.Oliveri, G.Busca 1997 *J.Appl.Phys* **81** 1851

5.W.Schiessel, W.Potzel,H.Karzel, M.Steiner, G.M.Kalvius, A.Martin, M.K.Krause, I.Halevy, J.Gal, W.Schafer, G.Will, M.Hillberg, R.Wappling 1996 *Phys.Rev B* **53** 9143

6.S A Oliver, H H Hamdeh, J C Ho 1999 *Phy.Rev.*B **60(5)** 3400

7.Sepelak V, Tkacova K, Boldyrev V V, Wibmann S and Becker K D 1997 *Physica B* **234-236** 617

8.G.F.Goya, H.R.Richenberg, M.Chen, W.B.Yelon 2000 *J.Appl.Phys.* **87** 8005

9.C P Marshall, W A Dollase 1984 *Amer.Miner.* **69** 928

10.S Ligenza, M Lukasiak, Z Kucharski, J Suwalski 1983 *Phys.Stat.Sol(b)* **117** 465.

11.Chinnasamy C N, Narayanasamy A, Ponpandian N, Chattopadhyay K 2001 *Mater.Sci.Eng.A* **304-306** 983

12.V Sepelak, S wibmann, K D Becker 1998 *J.Mat.Sci* **33** 2845

13.M.R.Anantharaman, S.Jagatheesan, K.A.Malini, S.Sindhu, A.Narayanasamy, C.N.Chinnasamy, J.P.Jacobs, S.Reijne, K.Seshan, R.H.H.Smits, H.H.Brongersma 1998 *J.Magn.Magn.Mater* **189** 83

14.Pannaparayil T, Komarneni S, Marande R and Zadarko M 1990 *J.Appl.Phys* **67** 5509

15.Chinnasamy C N, Narayanasamy A, Ponpandian N, Chattopadhyay K, H Guerault, 2000 J M Greneche *J.Phys.Condens.Matter* 12 7795

16.Y T Pavlyukhin, Y Y Medikov, V V Boldyrev 1984 *J.Sol.State.Chem.* **53** 155

17.G.F.Goya, H.R.Rechenberg 1999 *J.Magn.Magn.Mater* **196-197** 191

18.Sato T, Haneda K, Seki M and Iijima T 1990 *Appl.Phys. A* **50** 13

19.V Sepelak, U Steinike, D C Uecker, S wibmann, K D Becker 1998 *J.Sol.State Chem.* **135** 52

20.N N Greenwood and T C Gibb, *Mössbauer spectroscopy, Chapman and Hall Ltd, London*

21.Dominic P E Dickson and Frank J Berry. *Mössbauer spectroscopy, Cambridge university press, Cambridge*

22.A H Morrish, K Haneeda 1983 *J.Magn.Magn.Mater* **35** 105

23.Chinnasamy C N, Narayanasamy A, Ponpandian N, Chattopadhyay K, Shinoda K, Jeyadevan B, Tohji K, Nakatsuka K, Furubayashi T and Nakatani I 2001 *Phy.Rev.B* **63** 184108

24.S Morup 1993 *Nanomagnetism, Kluwer Academic publishers, Netherlands* 93

25.T Kodama, M Ookubo, S Miura, Y Kitayema 1996 *Mater.Res.Bull.* **31(12)** 1501

26.Qi Chen, Adam.J.Rondinone, Bryan.C.Chakoumakos, Z.John.Zhang 1999 *J.Mag.Mag.Mater* **194** 1

27.R G Gupta, r G Mendiratta 1977 *J.Appl.Phys.* **48(2)** 845

28.B J Evans, S S Hafner, H P Weber 1971 *J.Chem.Phys* **55(11)** 5282

29.A H Morrish, K Haneeda 1981 *J.Appl.Phys.* **52(3)** 2496

30.Bhowmik R N and Ranganathan R 2002 *J.Mag.Mag.Mater* **248** 101

31.W C Kin, S J Kim, Y R Uhm, C S Kong 2001 *IEEE Trans.magn.* **37(4)** 2362

32.U Herr, J Jing, R Birringer, U Gonser, H Gleiter 1987 *Appl.Phys.lett* **50(8)** 472

33.J W Young, J Smit 1971 *J.Appl.Phys.* 42(6) 2344

34.Fatemi D J, harris V G, Chen M X, Malik S K, Yelon W B, Long G J and Mohan A 1999 *J.Apl.Phys* **85(8)** 5172

35.M H M Mahmoud, H H Hamdeh, J C Ho, M J O'Shea and J C Walker 2000 *J.Mag.Mag.Mater.* **220** 139

36.D Fiorani, S Viticoli, J L Dormann, J L Tholence, A P Murani 1984 *Phys.Rev.B* **30(5)** 2776

37.K Haneeda, A H Morrish 1988 *J.Appl.Phys.* **63(8)** 4258

38.H M Widatallah, F J Berry 2002 *J.Sol.State.Chem.* **164** 230.

39.H Yang, L Shen, L Zhao, L Song, J Zhao, Z Wang, L Wang, D Zhang 2003 *Mater.Lett* **57** 2455

40.G A Petit, D W Forester 1971 *Phys.Rev.B* **4(11)** 3912

41.W Kundig, H Bommel 1966 *Phys.Rev.* **142(2)** 327

42.J L Dormann, M Nogues 1990 *J.Phys.Condens.Matter* **2** 1223

43.J M Williams, D P Danson, C Janot 1978 *Phys.Med.Biol.* **23(5)** 835

44.K J Ando, W Kundig, G Constabaris, R H Linquist 1967 *J.Phys.Chem.Sol.* **28** 2291

45.P A Dickof, P J Schurer, A H Morrish 1980 *Phys.Rev.B* **22(1)** 115

46.Goya G F, Rechenberg H R and Jiang J Z 1998 *J.Appl.Phys* **84** 1101

CHAPTER 6
ON THE ELECTRICAL PROPERTIES OF ULTRAFINE ZINC FERRITE

6.1 Introduction

The electrical properties of nanomagnetic materials are dictated by various parameters namely method of preparation, cation distribution, grain size, sintering temperature, oxygen parameter, ratio of Fe^{2+}/Fe^{3+} ions, oxygen anion vacancies and ac conductivity [1-9]. So far there exists no convincing reports on dc conductivity, dielectric permittivity and ac conductivity studies of nanoparticles ferrites, which gives a clear idea about the conduction mechanism in these materials especially in the fine particle regime.

The importance of ferrites in the present context is due to its semiconducting properties [10]. These high resistivity ferrites have wide application in electronic devices and in many other technological applications [4,7-8,10-15]. The increased demand of these ferrites resulted in a detailed investigation on the various aspects of conductivity in the nanoregime.

In ferrites, cations are surrounded by close packed oxygen anions and can be treated as isolated from each other. This localized electron model accounts for the basically insulating-semiconducting nature of these materials [10]. In ferrites, prepared by conventional solid state reaction technique with micron-sized particles, conductivity is mainly due to the hopping of Fe^{2+}/Fe^{3+} ions [1,3-8,12,14-30]. In normal zinc ferrite only a few Fe^{2+}/Fe^{3+} ion pairs are possible that contribute to the overall electrical conduction. In ultrafine particles, where the sintering temperature is very low, the probability of Fe^{2+}/Fe^{3+} ion pairs is further reduced. Hence by all means there exists some other charge carrier/conduction mechanism in fine particles, which should be investigated thoroughly. Therefore the aim of this chapter is to examine the various aspects and then to propose a model for explaining the conduction process occuring in ultrafine zinc ferrite, which are produced by HEBM.

The use of tungsten carbide vials and balls for the milling of zinc ferrite instead of steel (for milling zinc aluminates, steel vials and balls were used) is because if the steel vials were used, iron pick up in the vial and balls will take place which will influence the resistivity substantially [31]. Thus the use of tungsten carbide vials and balls for the milling of zinc ferrite is deliberate and significant in the present context of electrical studies of these ferrites.

6.2 DC conductivity studies on dry milled zinc ferrites

The dc conductivity studies are carried out in dry milled zinc ferrites for different applied voltages in the range 12-25 Volts. The V-I graphs are shown in figure 6.1, and exhibits an ohmic behaviour for all samples. These nanosized particles consists of grains of different sizes as established from TEM micrographs (figure 36 and 3.7.).

The effect of the temperature on the dc electrical conductivity (σ_{dc}) for all samples is illustrated in figure 6.2. Electrical conductivity increases with temperature and this can be attributed to increase in drift mobility of electric charge carriers that are thermally activated upon an increase in temperature [1,11,12,14-15]. This behaviour is common in semiconducting materials, which follows the Arrhenius relation

$$\sigma T = \sigma_0 \, Exp(-E_a/kT) \quad \ldots\ldots\ldots\ldots \quad (6.1)$$

Where E_a is the activation energy for conduction and k the Boltzmann constant.

Activation energy for conduction for all samples were calculated from figure 6.2 and summarized in table 6.1. The conductivity is increased (activation energy is decreased) with milling up till 5 hours milled samples and then decreased for 10 hours milled sample. Similar change is obtained for lattice strain and grain size from XRD results and hence a direct relation of conductivity with lattice strain and grain size exists [32].

The heterogeneous grain structure certainly influences the activation energy for conduction. The charge carriers that tunnel through the grains here are electrons and they presumably hop between Fe^{3+}/Fe^{2+} and due to the oxygen anion vacancies [15,33], which is produced during milling. From table 6.1 it is clear that conductivity increases with milling. This is because more and more oxygen vacancies are created during milling. With milling, the ratio of Fe^{3+}/Fe^{2+} ions can increase because of the creation of the oxygen vacancies [31]. But in the case of 10 hours milled sample, activation energy is

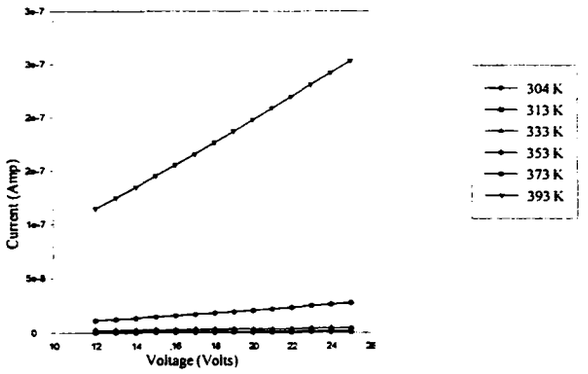

Figure 6.1(a) V-I graphs of fired unmilled zinc ferrite at different temperatures.

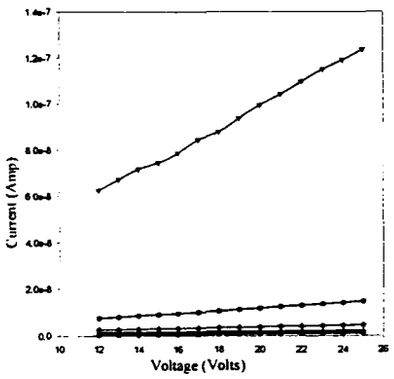

Figure 6.1(b) V-I graphs of zinc ferrite (5 minutes milled)at different temperatures.

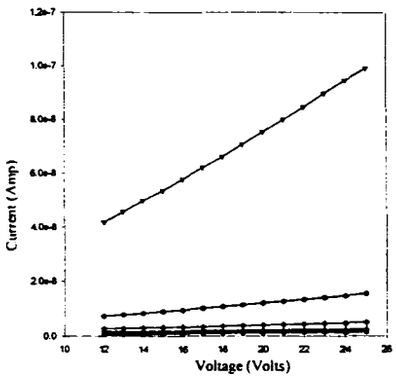

Figure 6.1(c) V-I graphs of zinc ferrite (30 minutes milled)at different temperatures.

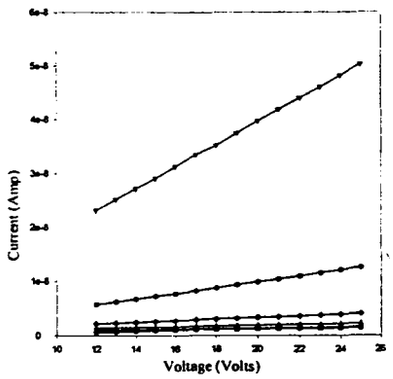

Figure 6.1(d) V-I graphs of zinc ferrite (5 hours milled) at different temperatures.

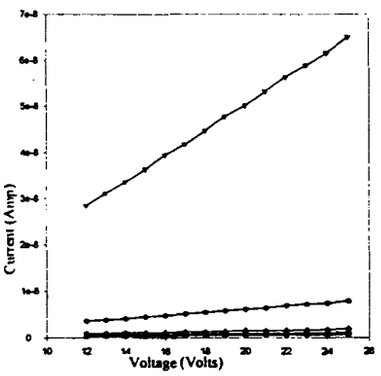

Figure 6.1(e) V-I graphs of zinc ferrite (10 hours milled) at different temperatures.

Figure 6.1 V-I graphs of dry milled zinc ferrites.

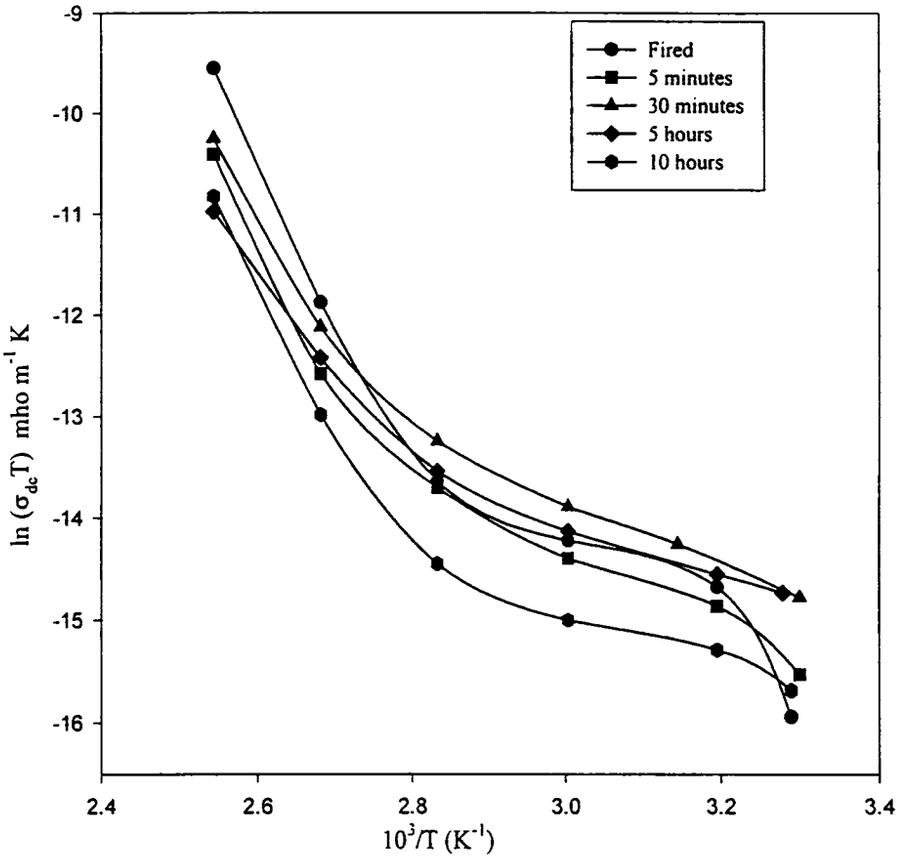

Figure 6.2 ln (σ_{dc}T) Vs 10^3/T graphs of zinc ferrite dry milled for different times.

Sample	Unmilled	30 minutes	5 hours	10 hours
Activation energy (eV)	0.6399	0.4774	0.4116	0.4991

Table 6.1 Activation energy for conduction from DC conductivity measurements for unmilled and dry milled zinc ferrite.

found to be increasing and hence conductivity is reduced. This is because by 10 hours milling the ferrite sample assumes a structure in which the grains have a greater size distribution [34]. Conduction in inhomogeneous grain structural materials are thought to be occuring due to the tunnelling of charge carriers between the grains [35]. The conductance between the grains may be expressed as

$$G_{ij} = G_0 \exp(-2\chi S_{ij} - E_{ij}/kT) \quad \ldots\ldots\ldots \quad (6.2)$$

where χ is the WKB tunnelling constant, S_{ij} denotes the tunnelling distance between the two grains and E_{ij} can be written in the following form

$$E_{ij} = \frac{1}{2}\left(\left|E_i - E_j\right| + E_i + E_j\right) \quad \ldots\ldots\ldots \quad (6.3)$$

The expression for E_{ij} is the result of considering both the probability of having a charge carrier at grain i and the additional activation if required for tunnelling to grain j. E_i denotes the charging energy of grain i which is the energy required to remove from or add a charge carrier (electron) to the grain. The increase of S_{ij} and E_{ij} in 10 hours milled sample is due to the wide range of size distribution. This will decrease the conductance according to equation 6.2. The dielectric permittivity and ac conductivity studies will throw more light on these findings.

The reports by Kulkarni et al suggests that if a magnetic ordering change is present in the samples, it can result in a decrease in activation energy [36]. Magnetisation measurements carried out on zinc ferrite samples indicate that (chapter 4) milling produces a magnetic ordering, which increases with milling. The change almost saturates with 5 hours of milling. This may be the reason for a continuous decrease of activation energy till 5 hours of milling, and the rise in activation energy for 10 hours milled sample. Some researchers have pointed out that when the voltage drop between neighbouring grains is much smaller than k_BT/e, charge carriers are thermally activated so as to tunnel [35]. Electrons tunnel between particles of approximately the same size. Large charging energy is required to tunnel to smaller particles while larger tunnel resistance is to be overcome when tunnelling to a larger particle. Hence the size of the particles must be uniform to favour tunnelling. Tunnelling probability of spin-polarized electrons and hence spin polarized electronic current is larger when the magnetisation of the particle is aligned [35]. This current can be said to be carrying the magnetisation

information in these materials. The current due to spin polarized tunnelling in an ideal grain interface can be expressed as

$$I_m = \eta\beta I_e/e \quad \ldots\ldots\ldots \quad (6.4)$$

This formula states that with each electron crossing the interface (I_e/e), one Bohr magneton β is associated and that there will be an imbalance in the spin population of the current to a degree of η ($|\eta| \leq 1$). The sign of η and spin polarized tunnelling current depends upon the spin imbalance due to the nonequilibrium magnetisation present in the material and grain interface effects [37].

6.3 Dielectric permittivity and ac conductivity studies on dry milled zinc ferrites

These samples were subjected to dielectric permittivity studies from which the dielectric permittivity, dielectric loss factor and ac conductivity values were calculated at different frequencies and temperatures. Moisture present in the air may enhance the dielectric permittivity since the resistivity diminishes with moisture presence, if the samples were not properly heat treated before the experiment is carried out [38]. Hence all the samples were properly dried in an oven before carrying out dielectric permittivity studies. Figure 6.3 represents the dielectric permittivity graphs of dry milled zinc ferrites at different temperatures and frequencies. By an analogy with the dispersion of light, the dependence of dielectric permittivity with frequency is known as dielectric dispersion [39]. At the lowest frequencies, significantly high dielectric permittivity values will arise from the dc conductivity of the medium, electrode polarization and interfacial polarization from the heterogeneous structure [40]. The dispersion in the high frequency region is solely explained by the Koops phenomenological theory (Maxwell-Wagner type) of well conducting grains separated by layers of lower conductivity [1-4,6-7,11-12,14,16,18,28-30,41-45].

The frequency dependence can be explained well by Rezlescu model according to which abnormal dielectric behaviour shown by the ferrite materials is due to the collective contribution of two types of carriers, p and n to the polarization [1,46]. The n type conduction is due to the electron exchange interaction $Fe^{2+} \leftrightarrows Fe^{3+}$ which results in a local displacement of the electrons in the direction of the applied electric field which determines the polarization. The origin of p type conduction arises from the occurrence of

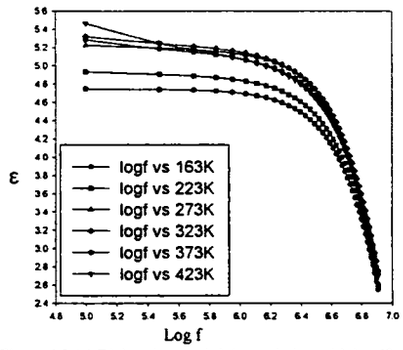

Figure 6.3 (a) Dielectric permittivity variation with log (frequency) for Unmilled $ZnFe_2O_4$ at different temperatures.

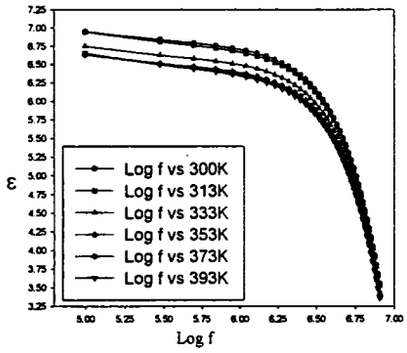

Figure 6.3 (b) Dielectric permittivity variation with log (frequency) for $ZnFe_2O_4$(5 minutes dry milled) at different temperatures.

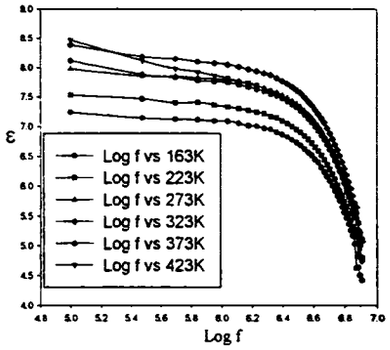

Figure 6.3 (c) Dielectric permittivity variation with log (frequency) for $ZnFe_2O_4$ (30 minutes dry milled) at differnet temperatures.

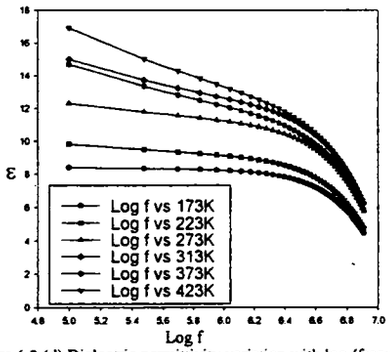

Figure 6.3 (d) Dielectric permittivity variation with log (frequency) for $ZnFe_2O_4$ (5 hours dry milled) at different temperatures.

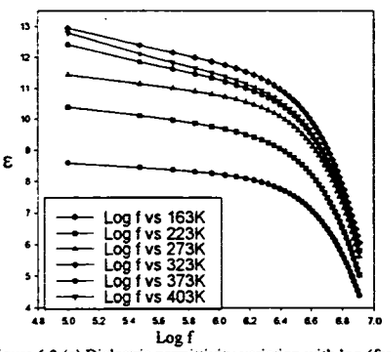

Figure 6.3 (e) Dielectric permittivity variation with log (frequency) for $ZnFe_2O_4$ (10 hours dry milled) at different temperatures.

Figure 6.3 Dielectric permittivity variation with logf at different temperatures for dry milled zinc ferrites.

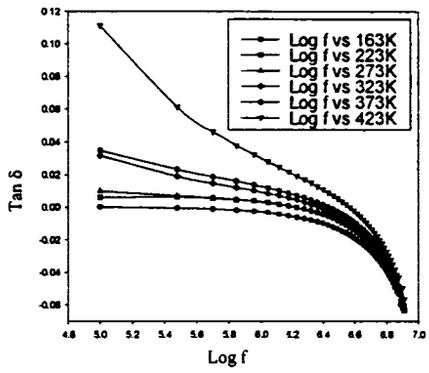

Figure 6.4 (a) Tan δ variation with log (frequency) for unmilled $ZnFe_2O_4$ at different temperatures.

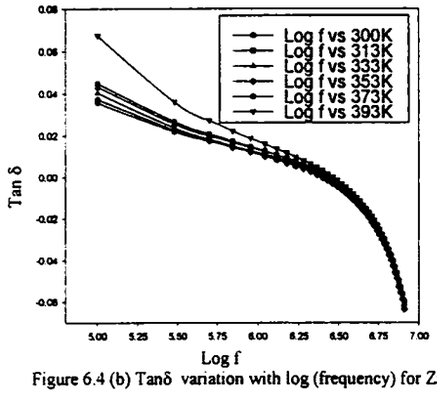

Figure 6.4 (b) Tanδ variation with log (frequency) for $ZnFe_2O_4$ (5 minutes dry milled) at different temperatures.

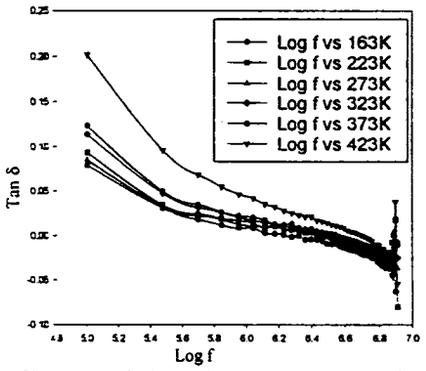

Figure 6.4 (c) Tanδ variation with log (frequency) for $ZnFe_2O_4$ (30 minutes dry milled) at different temperatures.

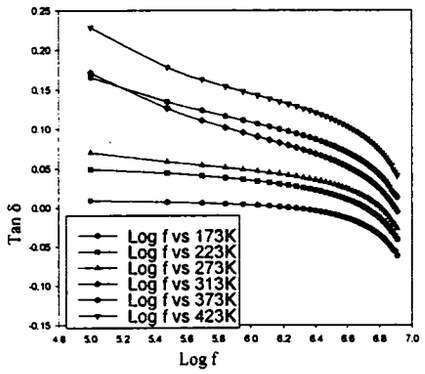

Figure 6.4 (d) Tan δ variation with log (frequency) for $ZnFe_2O_4$ (5 hours dry milled) at different temperatures.

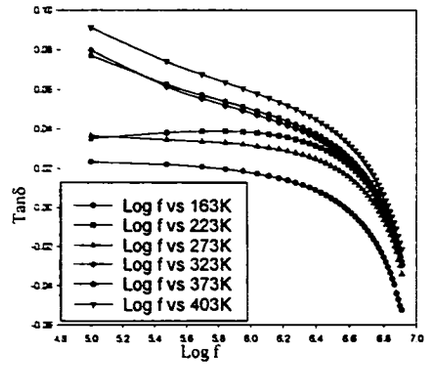

Figure 6.4 (e) Tan δ variation with log (frequency) for $ZnFe_2O_4$ (10 hours dry milled) at different temperatures.

Figure 6.4 Tanδ variation with logf at different temperatures for dry milled zinc ferrites.

anion vacancies due to the escape of oxygen ions from the spinel structure. Various researchers found out that $Fe^{2+} \leftrightarrows Fe^{3+}$ hopping is mainly responsible for conduction and suggested a decrease in dielectric permittivity with milling due to the lesser number of hoppings as a result of cation redistribution in nanoparticles. But our results are not in agreement with those observations. One of the reasons could be that lesser number of Fe^{2+} ions are present in the sample. Usually in ferrites the Fe^{2+} formation occurs at the time of high temperature sintering [6,18]. At higher sintering temperature, loss of zinc takes place due to volatilization [8]. This results in excess unsaturated oxygen ions, which then associates with surrounding Fe^{3+} ions reducing them to Fe^{2+}. This is less probable in our samples since our sintering temperature is much less ($<600^0$C) when compared to the solid state method of preparation. Our coprecipitated samples, smaller in size, also will decrease the chances of formation of Fe^{2-} since oxidation advances faster in smaller grains [6,8]. The enhancement of Fe^{3+} redistribution by milling again reduces the $Fe^{2+} \leftrightarrows Fe^{3+}$ hopping since less number of Fe^{3+} are available for electron exchange hopping.

The main contribution to the electrical conduction in coprecipitated sample followed by high energy ball milling could be the oxygen ion vacancies [15]. The mobility of this p type carrier is lower when compared with n type carriers and is more predominant at lower frequencies [2,17]. Hence as shown in figure, a sudden decrease in dielectric permittivity at higher frequency was observed which is sharp in milled samples where the p type carrier concentration is high due to more number of oxygen ion vacancies.

Since dc conductivity and dielectric permittivity decreases in 10 hours milled samples compared with 5 hours milled sample, its not the anion vacancy alone that influences the conduction. Since the lattice strain decreases and grain size decreases in 10 hours milled sample with respect to the 5 hours milled sample, conductivity is certainly influenced by these parameters as suggested by various researchers [32]. The prolonged milling although increases the grain size but size distribution increases. This will further reduce the electron tunnelling by $Fe^{2+} \leftrightarrows Fe^{3+}$, since electron tunnelling occurs only between particles of approximately same size. This is because large charging energy is

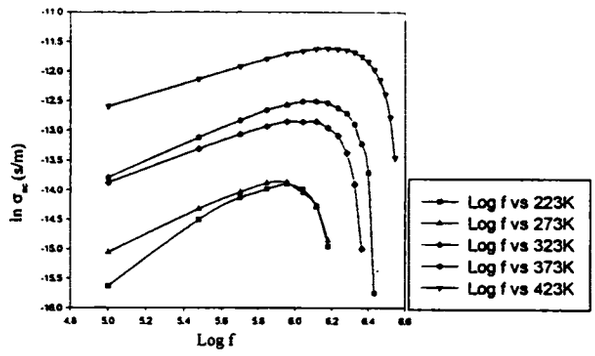

Figure 6.5 (a) ln σ_{ac} variation with log (frequency) for unmilled $ZnFe_2O_4$ at different temperatures.

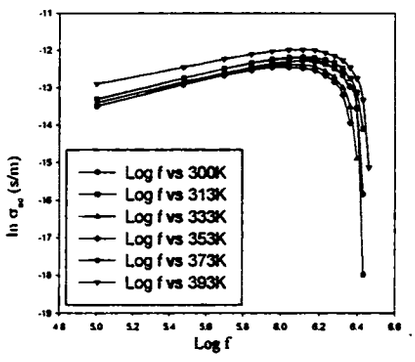

Figure 6.5 (b) ln σ_{ac} variation with log (frequency) for $ZnFe_2O_4$ (5 minutes dry milled) at different temperatures.

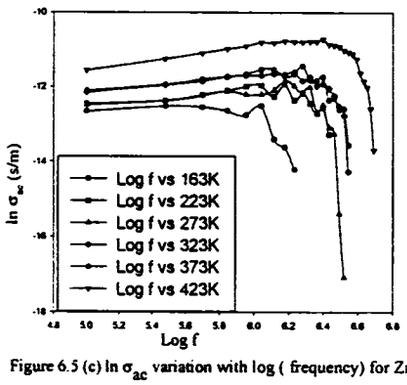

Figure 6.5 (c) ln σ_{ac} variation with log (frequency) for $ZnFe_2O_4$ (30 minutes dry milled) at different temperatures.

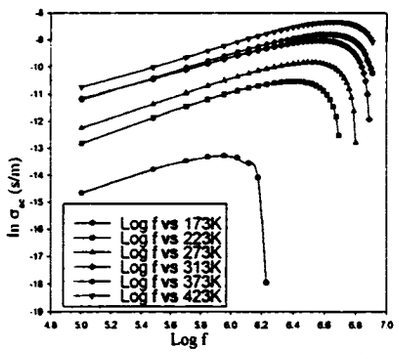

Figure 6.5 (d) ln σ_{ac} variation with log (frequency) for $ZnFe_2O_4$ (5 hours dry milled) at different temperatures.

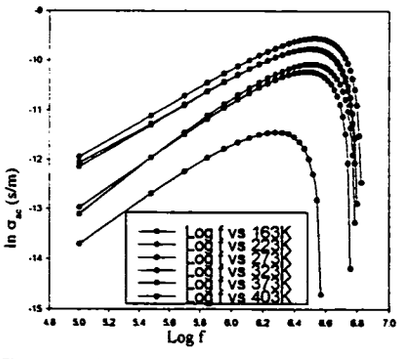

Figure 6.5 (e) ln σ_{ac} variation with log (frequency) for $ZnFe_2O_4$ (10 hours dry milled) at different temperatures.

Figure 6.5 ln σ_{ac} variation with logf at different temperatures for dry milled zinc ferrite.

required to tunnel to small particle and larger tunnel resistance has to be overcome while tunnelling to a larger particle. Thus the size distribution that exists in the samples oppose tunnelling [35]. The tunnelling distance and the charging energy between the grains do increase with prolonged milling and as a result, by equation (6.2) conductance gets decreased. One another reason for this decrease in conductivity and dielectric permittivity in 10 hours milled sample is due to the interaction of anion vacancies with ordered Fe^{3+} ions as a result of cation redistribution and α-Fe_2O_3 (which is antiferromagnetically ordered at room temperature) present, which stop the movement of trapped charges since holes are strongly coupled with both to the vibrational and magnetic degrees of freedom [47].

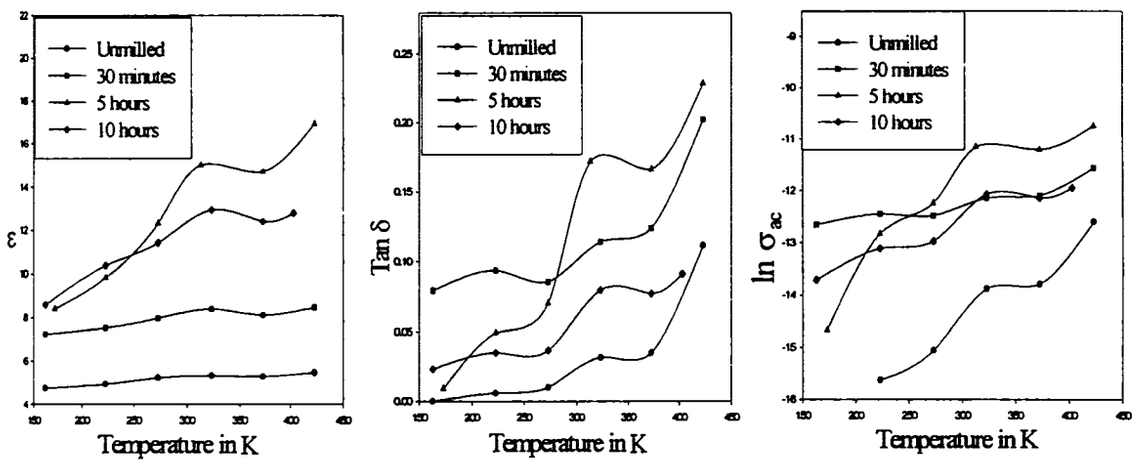

Figure 6.6 (a) Figure 6.6 (b) Figure 6.6 (c)

Figure 6.6. Dielctric permittivity [Figure 6.6(a)], dielectric loss factor [Figure 6.6(b)] and ac conductivity [Figure 6.6(c)] variation with temperature for dry milled zinc ferrite.

The temperature dependence of dielectric permittivity is shown in figure 6.6 (a). Ionic mechanism of polarization as well as drift mobility of charge carriers increases the dielectric permittivity when the temperature grows. In ionic dielectrics, when the temperature rises, the orientation of the dipoles is facilitated, and thus increases dielectric permittivity. As the temperature increases the chaotic thermal oscillations of molecules are intensified and the degree of orderliness of their orientation is diminished [39,48]. This causes the dielectric permittivity to pass through the maximum and then drop.

Similar results have been obtained for ultrafine zinc aluminate samples and they are discussed in chapter 8.

It may be noted here that magnetic ordering also undergo a change with temperature and this can also influence the conduction process. On increasing the temperature, electrical conductivity increases due to the increase in thermally activated drift mobility of charge carriers [1,11,12,14-15]. This increases the dielectric polarization causing an increase in dielectric permittivity. All the samples show a dielectric transition at around 320 K. This indicates a magnetic transition from superparamagnetic/partially ferrimagnetic to paramagnetic region [3]. The paramagnetic state represents a disordered state so that charge carriers need more energy to jump between adjacent sites [11]. Similar kind of transition with temperature is seen if the carriers are holes [47]. This once again confirms our conclusion that the predominant factor that influences the conduction process in nanocrystalline zinc ferrites is anion vacancies.

The amount of power losses in a dielectric under the action of the voltage applied is commonly known as dielectric loss [49]. This is a general term determining the loss of power in an electrical insulation both at a direct and an alternating voltage. Dielectric loss factor Tanδ in terms of real and imaginary parts of permittivity is given by

$$\text{Tan}\delta = \varepsilon''/\varepsilon' \quad \ldots\ldots\ldots \quad (6.5)$$

The dependence of loss factor on frequency is shown in figure 6.4 and it exhibits the same trend as that of dielectric permittivity. This finding is also in tune with Koops theory and follows the relation

$$\text{Tan}\delta = 4\pi\sigma_{ac}/\varepsilon\omega \quad \ldots\ldots\ldots \quad (6.6)$$

The temperature dependence of Tanδ shows similar behaviour as that of dielectric permittivity and can be explained by adopting the same approach by which dielectric permittivity is explained (figure 6.6(b)).

The frequency dependence of ac conductivity is shown in figure 6.5. The ac conductivity is found to be increasing with frequency, which is sharp for 5 hours and 10 hours, milled samples. At around 2 MHz, the ac conductivity falls for unmilled, 5 minutes milled and 30 minutes milled samples while for prolonged milled samples the onset is at a higher frequency. The decrease of ac conductivity after around 2 MHz is due to the fact that the grain boundaries through which the conduction takes place become

less active at higher frequencies to allow conduction [48]. The temperature dependence of ac conductivity resembles that of the dielectric permittivity and dielectric loss factor and is attributed to the thermally activated drift mobility of charge carriers and influence of the magnetic ordering on the electrical conduction (figure 6.6 (c)).

6.4 Dielectric permittivity and ac conductivity studies on wet milled zinc ferrites

Figure 6.7, figure 6.8 and figure 6.9 represents the dielectric permittivity, Tanδ and ac conductivity variation respectively with logf at different temperatures for wet milled zinc ferrites.

At low frequencies decrease of dielectric permittivity is sharp compared to the earlier trends observed for dry milled zinc ferrite samples. But there is no sharp decrease in dielectric permittivity at higher frequencies. This is an indication of the presence of lesser number of oxygen vacancies produced as a result of wet milling compared with dry milled samples. This is well established by examining the absolute dielectric permittivity values, which is not increased much in wet milled zinc ferrites (Ref table 6.2). Dielectric loss is greater when wet milling is employed and the ac conductivity values are almost comparable in both the cases.

Sample	Dielectric permittivity	
	Dry milling	Wet milling
Unmilled	5.47	7.24
30 minutes	8.39	8.52
5 hours	14.90	11.20

Table 6.2 Dielectric permittivity values at 100 kHz, at a temperature 300 K for milled zinc ferrites.

6.5 Conclusions

The dc conductivity and dielectric permittivity can be varied appreciably by high-energy ball milling in nanosized zinc ferrites produced by coprecipitation method. The dc conductivity and dielectric studies show a semiconducting behaviour and the main contribution towards conduction arise from large oxygen ion vacancies produced by milling. Dielectric results are in accordance with Koops phenomenological theory and

Rezlescu model. The lattice strain, grain size, size distribution and cation distribution do affect the dielectric behaviour. The partial redistribution of cations causes a ferrimagnetic ordering in milled samples. This partial ferrimagnetic ordering and the antiferromagnetic ordering due to the α-Fe_2O_3 becomes the reason for trapping of holes to reduce the conductivity in 10 hours milled sample. Temperature dependence of dielectric

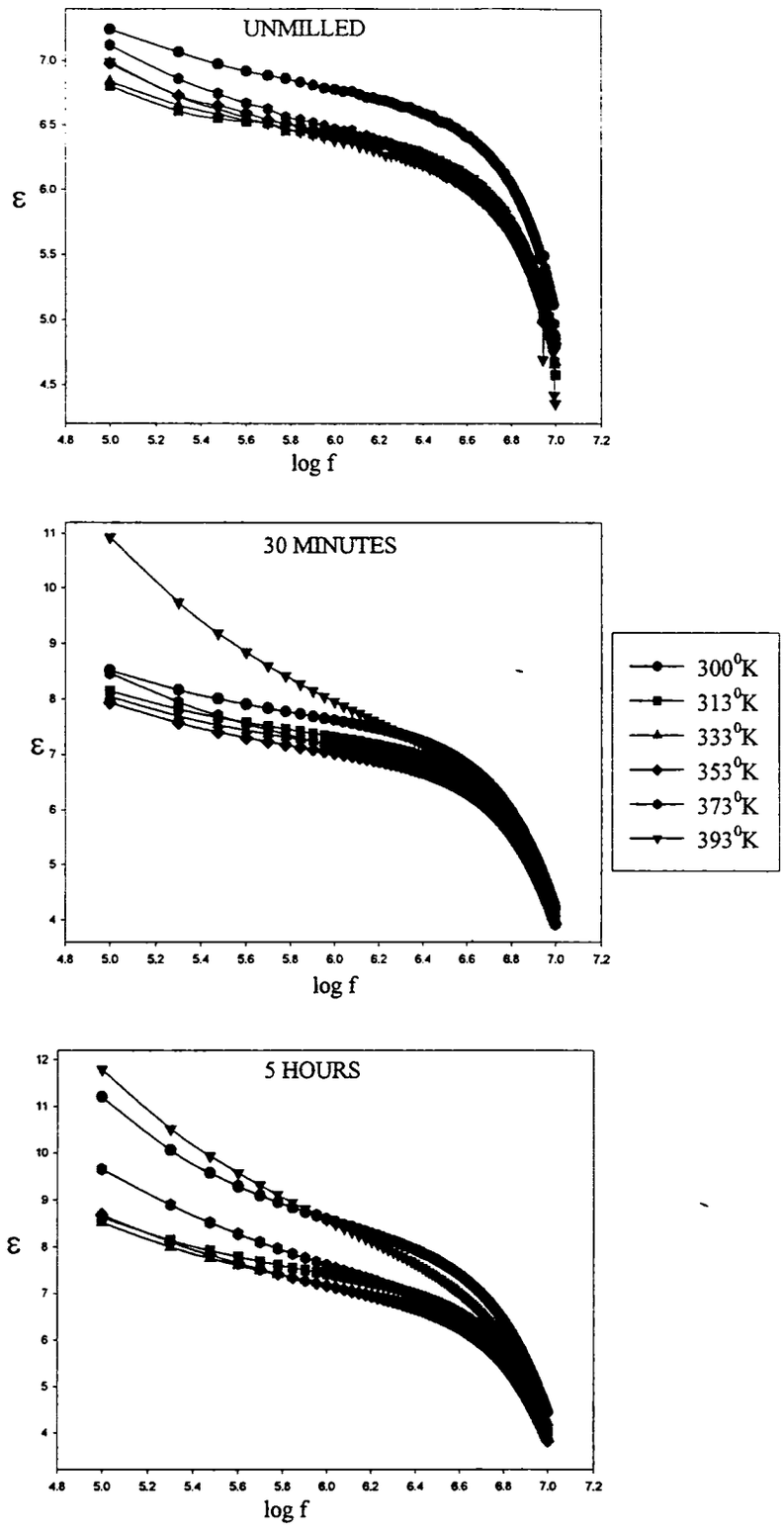

Figure 6.7 Dielectric permittivity variation with log (frequency) at different temperatures for wet milled zinc ferrites.

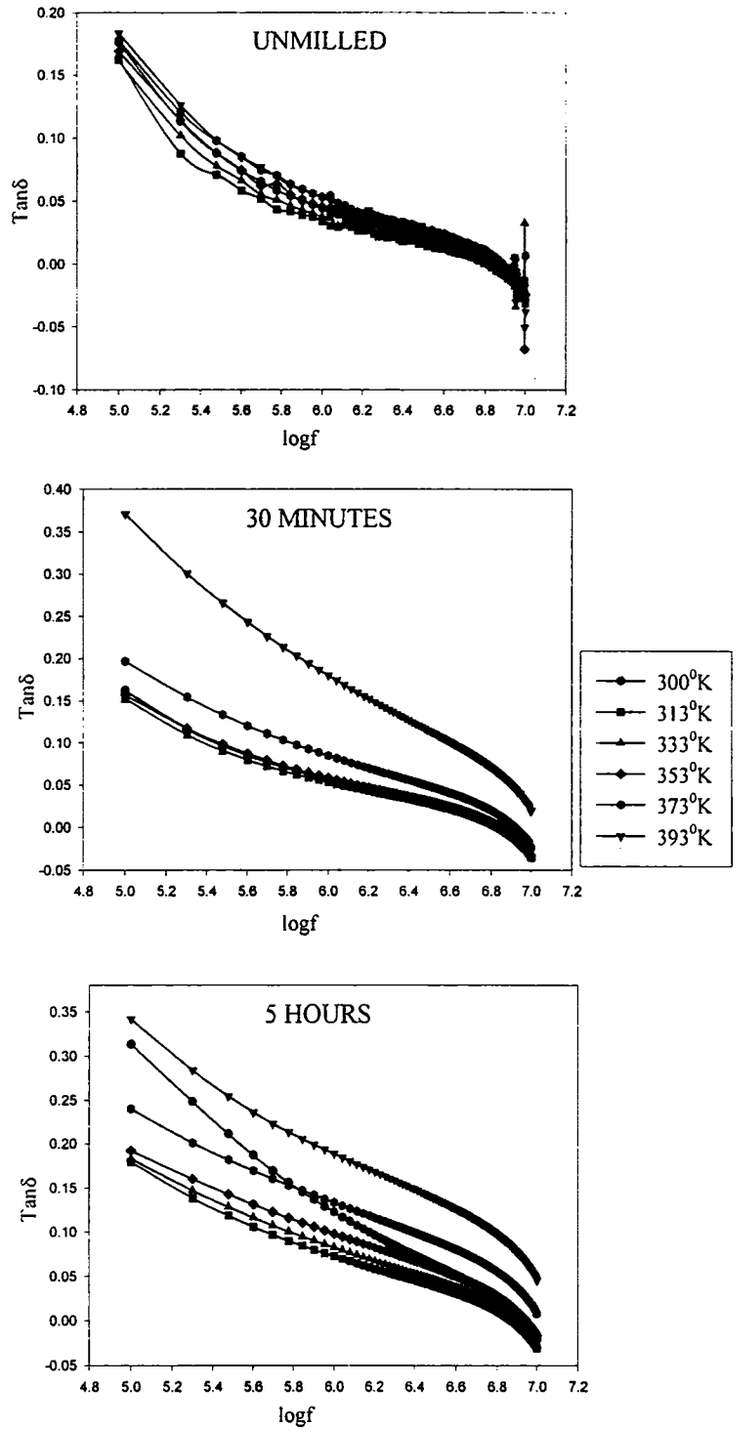

Figure 6.8 Tanδ variation with log (frequency) at different temperatures for wet milled zinc ferrites.

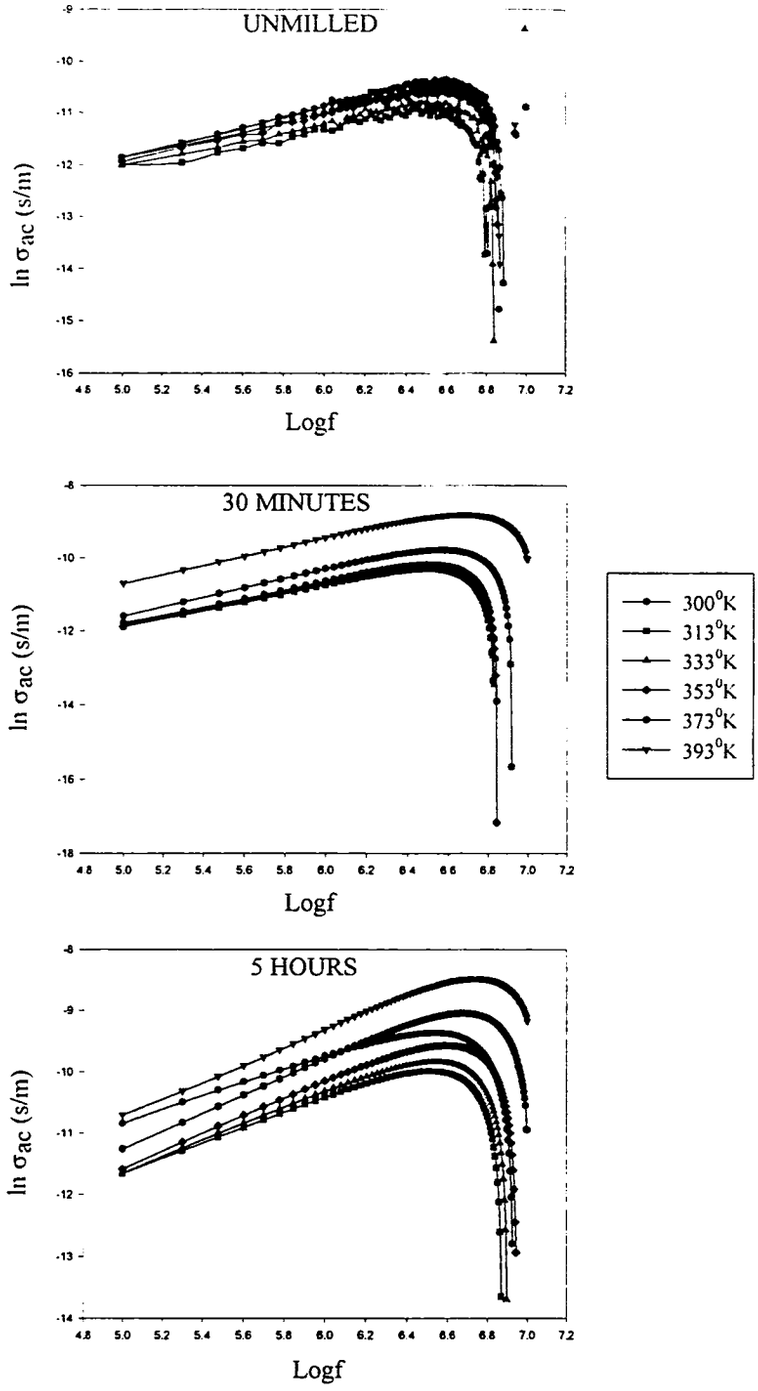

Figure 6.9 ln σ_{ac} variation with log (frequency) at different temperatures for wet milled zinc ferrites.

permittivity suggests that in ultrafine zinc ferrite, the majority charge carriers are the holes.

References:

1.Abdeen A M 1999 *J.Magn.Magn.Mater* **192** 121

2.Ismael H. El Nimr M K, Abou El Ata A M, El Hiti M A. Ahmed M A and Murakhowskii A A 1995 *J.Magn.Magn.Mater* **150** 403

3.Shaikh A M, Bellad S S and Chougule B K 1999 *J.Magn.Magn.Mater* **195** 384

4.Mohammed E M, Malini K A, Philip Kurian. Anantharaman M R 2002 *Materials Research Bulletin* **37** 753

5.Murthy V R K and Sobhandri J 1976 *Phys,stat.sol.(a)* **36** K133

6.Mangalaraja R V, Ananthakumar S, Manohar P and Gnanam F D 2002 *J.Magn.Magn.Mater* **253** 56

7.Mazen S A, Abdallah M H, Elghandoor M A and Hashem H A 1994 *Phys,stat.sol.(a)* **144** 461

8.Verma A, Goel T C, Mendiratta R G and Gupta R G 1999 *J.Magn.Magn.Mater* **192** 271

9.M A El Hiti 1996 *J.Phys.D.appl.Phys* **29** 501

10.B Viswanathan, V R K Murthy 1990 *Ferrite Materials, Science and Technology (Narosa Publishing House)* 26

11.Ahmed M A, El Hiti M a, El Nimr M K and Amer M A 1996 *J.Magn.Magn.Mater* **152** 391

12.Abdeen A M 1998 *J.Magn.Magn.Mater* **185** 199

13.Anantharaman M R, Jagatheesan S, Malini K A, Sindhu S, Narayanasamy A, Chinnasamy C N, Jacobs J P, Reijne S, Seshan K, Smits R H H and Brongersma H H 1998 *J.Magn.Magn.Mater* **189** 83

14.El Hiti M A 1996 *J.Magn.Magn.Mater* **164** 187

15.Ponpandian N and Narayanasamy A 2002 *J.Appl.Phys*. **92(5)** 2770

16.Koops C G 1951 *Phys.Rev* **83** 121

17.El Hiti M A, Ahmed M A, Mosaad M M and Attia S M 1995 *J.Magn.Magn.Mater* **150** 399

18.Chandra prakash and Baijal J S 1985 *J. less common metals* **107** 51

19.J G Na, M C Kim, T D Lee, S J Park, 1993 *IEEE Trans. Magn.* **29(6)** 3520

20.Zhenxing Yue, Ji Zhou, Longtu Li, Zhilun Gui, 2001 *J.Magn.Magn.Mater*. **233** 224

21.Pal M, Brahma P and Chakravorty D 1994 *J. Phys. Soc. Jap.* **63(9)** 3356

22.B V Bhise, M G Patil, M B Dongare, S R Sawant, S A Patil 1992 *Ind.J.Pure.Appl.Phys* **30** 385

23.D Ravinder and K Latha 1994 *J.Appl.Phys.* **75(10)** 6118

24.Navdeep k Gill, R K Puri, 1985 *J.Mat.Sci.Lett* **4** 396

25.B K Kuanr, G P Srivastava 1994 *J.Appl.Phys* **75(10)** 6115

26.S A Mazen, F Metawe, S F Mansour 1997 *J.Phys.D.Appl.Phys* **30** 1799

27.Pal M, Brahma P and Chakravorty D 1996 *J. Mag. Mag. Mater.***152** 370

28.Josyulu O S and Sobhanadri J 1980 *Phys.Status Solidi(a)* **59** 323

29.N saxena, B K Kuanr, Z H Zaidi, G P Srivastava 1991 *Phys.stat.sol(a)* **127** 231

30.Patil R.S., Kakatkar S.V, Maskar P.K. , Patil S.A and Sawant S.R, 1991 *Ind. J. Pure Appl. Phys.* **29** 589

31.R F Soohoo 1960 *Theory and application of ferrites, Prentice-hall Inc, New Jersey 24*

32.Manojkumar and Sekhon S S 2001 *J.Phys.D.Appl.Phys* **34** 2995

33.G F Goya and H R Rechenberg 1999 *J Magn.Magn.Mater.* **203** 141

34.Ping Sheng 1994 *Proceedings of the NATO Advanced study institute on Nanophase materials-syntheses, properties and applications, Kluwer academic publishers* 381

35.Xavier Battle and Amilcar Laborta 2002 *J.Phys.D.Appl.Phys* **35** R15

36.V R Kulkarni, M M Todkar, A S Vaigankar 1986 *Ind.J.Pure.appl.Phys* **24** 294

37.Hari Singh Nalwa 2000 *Nanostructured materials and technology, Academic press, california* 306

38.Tareev B 1979 *Physics of Dielectric Materials (Mir Publishers) Moscow* 60

39.Tareev B 1979 *Physics of Dielectric Materials (Mir Publishers) Moscow* 105

40.N E Hill, W E Vaughan, A H Price, M Davies, 1969 *Dielectric properties and molecular behaviour, Van-Nostrand reinhold company,London* 280

41.J.H.Nam, H.H.Jung, J.Y.Shin and J.H.Oh, 1995 *IEEE Trans. Magn.* **Vol. 31 No.6** 3985

42.Kuanr B K, Singh P K, Kishan P, Kumar N, Rao S L N, Prabhat K Singh, Srivastava G P 15 April 1988 *J.Appl.Phys.* **63(8)** 3780

43.J.Smit, and H.P.J. Wijn, 1959 *Ferrites, Philips Technical Library* 241

44.V P Miroshkin, YA I Panova, V V Passynkov 1981 *Phys.stat.Sol(a)* **66** 779

45.Jankowski Stanislaw 1988 *J.Am.Ceram.Soc.* **71(4)** C176

46.Ravinder D, Ramana Reddy A V and Rangamohan G 2002 *Materials Letters* **52** 259

47.Zheng X G, Sakurai Y, Okayama Y, Yang T Q, Zhang L Y, Yao X, Nonaka K and Xu C N 2002 *J.Appl.Phys* **92(5)** 2703

48.S Sindhu, M R Anantharaman, Bindu P Thampi, K a Malini, Philip Kurian 2002 *Bull.Mat.Sci* **25(7)** 599

49.Tareev B 1979 *Physics of Dielectric Materials (Mir Publishers) Moscow* 140

CHAPTER 7

EVALUATION OF STRUCTURAL PARAMETERS OF ZINC ALUMINATE - A NONMAGNETIC NORMAL SPINEL

7.1 Introduction

Zinc aluminate is a widely used catalyst for the dehydrogenation reaction [1-4]. Most of the earlier literature related to this material were in the micron regime. Moreover, this material resembles the crystal structure of zinc ferrite, whatever hypothesis is proposed for the cation redistribution or surface composition in the ultrafine regime should hold good for zinc aluminate too. As has been cited earlier in chapters 1 and 2, zinc aluminate/zinc ferrite crystallizes in the normal spinel structure in the coarser regime.

The preparation of zinc aluminate in the ultrafine regime has clearly been described in detail in chapter 2. In this chapter the structural properties of zinc aluminate has been dealt in detail. The effect of milling on the particle size and lattice parameter is dealt in detail. In later chapters the conductivity together with dielectric properties will be studied in detail. It is with this motive that these materials without any impurity is prepared and studied. The evaluation of structural parameter is important in the correlation of its structural properties with the electrical properties. The surface composition has been analysed by EDX with a view to correlating the observed conductivity of the milled samples with oxygen ion vacancies.

7.2 X-ray diffraction studies on dry milled zinc aluminates

Unmilled and dry milled zinc aluminates were subjected to X-ray diffraction studies and the XRD patterns are shown in figure 7.1. XRD pattern indicates monophasic zinc aluminate even after prolonged hours of milling. This is entirely different from the zinc ferrite results, where in zinc ferrite gets decomposed with milling. This confirms the high degree of stability of zinc aluminate against decomposition to its oxide constituents [5].

The XRD pattern exhibits broadening characteristic of fine particles [6]. Average size of the particle, which is calculated by Debye Scherrer formula, lie in the nanometer range (4-7nm) and found to be decreasing with milling time (figure 7.2). Thus high energy ball milling reduces particle size in the initial stage of milling. This

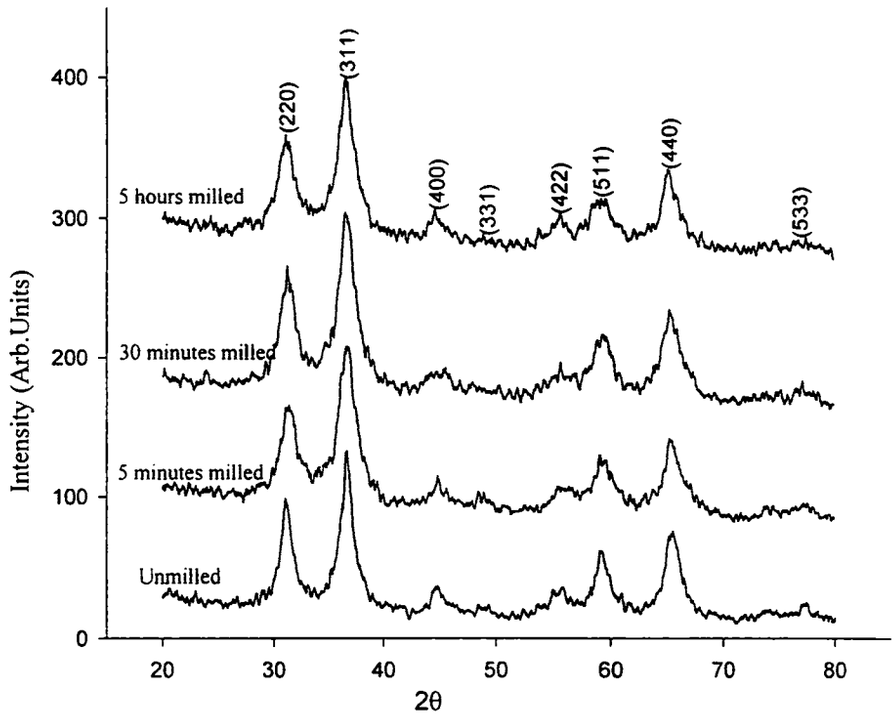

Figure 7.1 XRD patterns of unmilled and dry milled zinc aluminate.

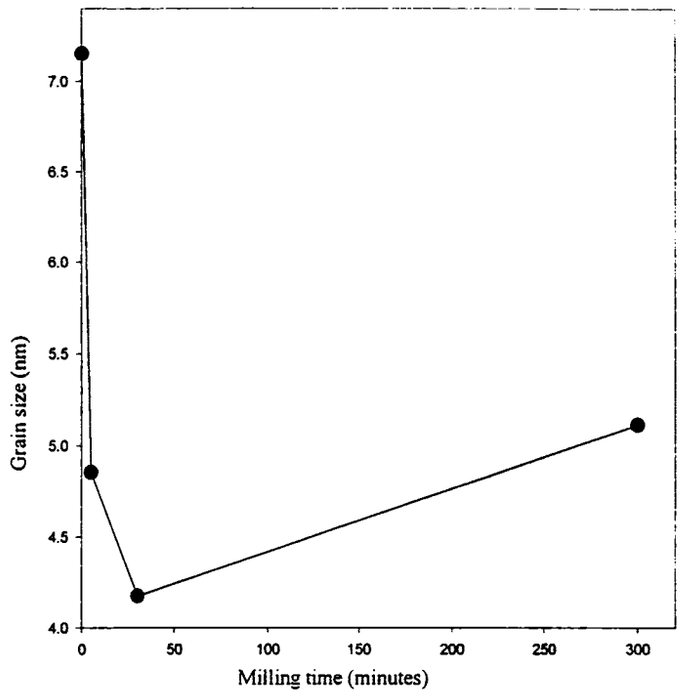

Figure 7.2 Particle size variation with milling time for dry milled zinc aluminate.

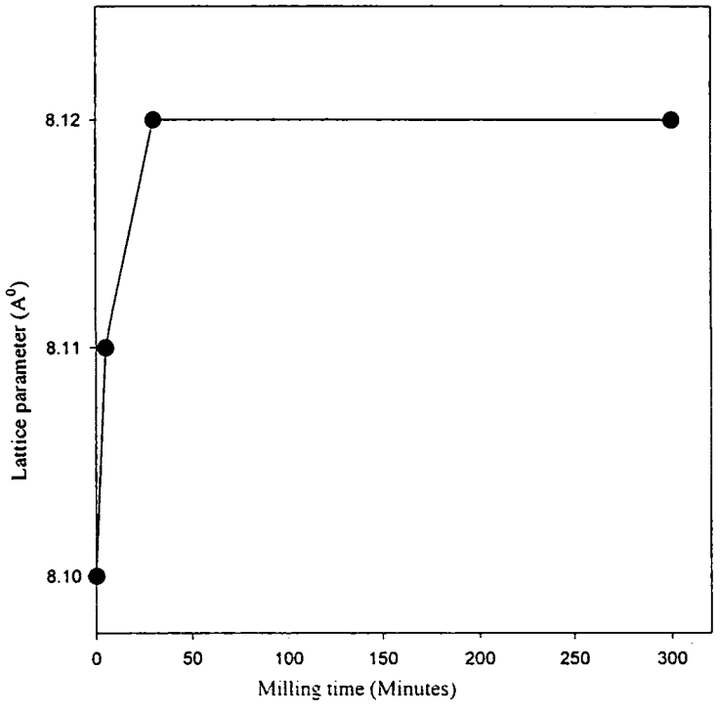

Figure 7.3 Lattice parameter variation with milling time for dry milled zinc aluminate.

reduction in particle size as the milling time increases may be due to the fact that the kinetic energy generated by the series of collisions among balls is transferred to the system but there is no sudden decrease as in the case of particles prepared by the solid state reactions. This is because the starting powder (coprecipitated) itself is nanometer sized. Also there are reports that within 24 minutes of milling, size reduction may attain its maximum [7]. The reason for not obtaining a great reduction in size with prolonged milling is due to the high local temperature and pressure generated during the combustion as a result of the high energy ball milling [8]. The difficulty in maintaining the very high stress during milling (discussed in section 2.2) is one of the reasons for slowing down the reduction of grain size.

Assuming cubic crystal symmetry for these materials, lattice parameter was calculated and the variation of lattice parameter with milling time is plotted and is shown in figure 7.3. Lattice parameter is found to be increasing marginally with milling. An attempt was made to calculate the strain developed in the lattice by the method described in chapter 3 and because of the non-linear nature of the graphs, this was in vain (figure 7.4). This peculiar behaviour could be due to the highly ultrafine nature of the material.

7.3 EDX studies on dry milled zinc aluminates

Energy dispersion X-ray intensities were converted to the relative concentrations and are tabulated in table 7.1. The experiment is carried out over different areas and almost the same composition matching with the theoretical values is observed for dry milled and unmilled zinc aluminates indicating good chemical homogeneity in these samples.

7.4 X-ray diffraction studies on wet milled zinc aluminates

Unmilled and wet milled zinc aluminates were subjected to X-ray diffraction studies and the XRD patterns are shown in figure 7.5. XRD pattern indicates monophasic characteristic even after hours of milling. This result is also entirely different from that of zinc ferrite results, where zinc ferrite gets decomposed with milling. This is indicative of good thermal stability of zinc aluminate against decomposition to the component oxides and is in conformity with that of the reported results by various researchers [5].

The broad shape of the diffraction peaks indicates the formation of fine particle structure with small crystallite size distribution by the effect of high energy ball milling [6]. Average size of the particle, which is calculated by Debye Scherrer

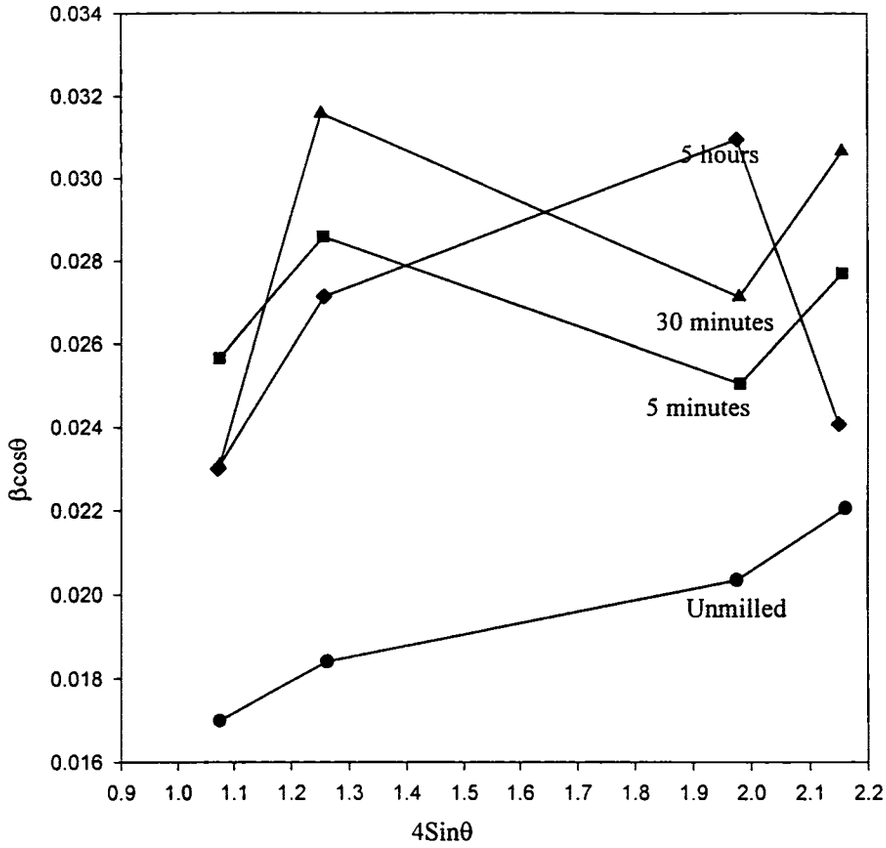

Figure 7.4 4Sinθ Vs βCosθ curves for unmilled and dry milled zinc aluminates.

Sample	Zn Atom.%	Al Atom.%	O Atom.%
Unmilled	15.277	32.004	52.72
5 minutes dry milled	18.618	30.887	50.495
30 minutes dry milled	17.962	28.998	53.040
5 hours dry milled	16.714	25.208	58.078
Theoretical composition	14.286	28.571	57.143

Table 7.1 EDX results on dry milled zinc aluminates suggesting high quality homogeneity in these materials.

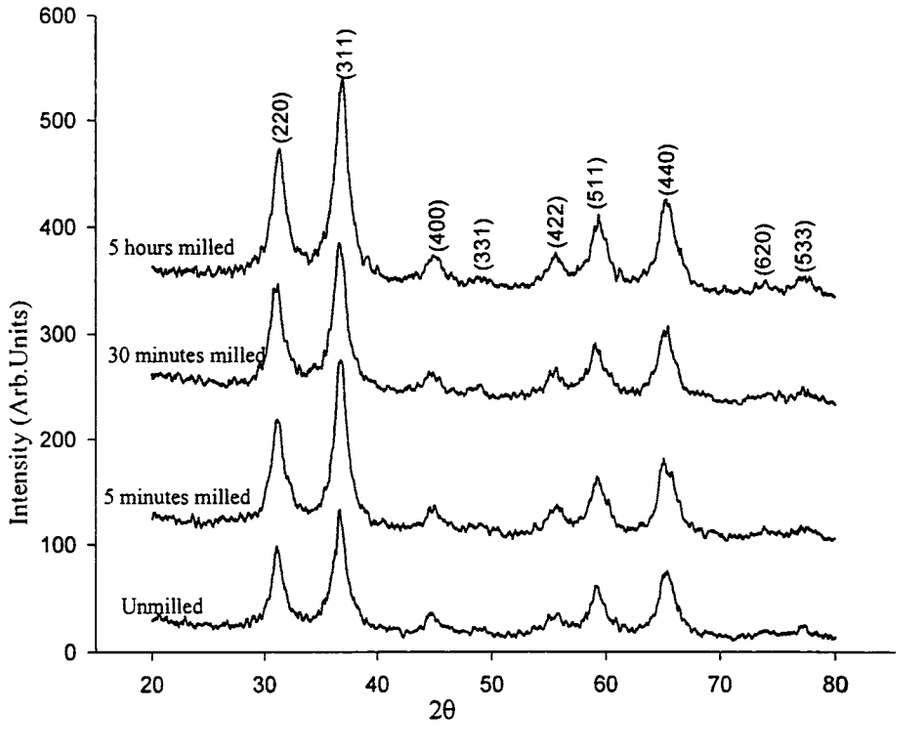

Figure 7.5 XRD patterns of unmilled and wet milled zinc aluminate.

formula, were in the nanometer range (6-7 nm) and found to be decreasing with milling time and stabilises with 30 minutes milling (figure 7.6). Thus the high energy ball milling reduces the particle size in the initial stage of milling. This reduction in particle size as the milling time increases may be due to the fact that the kinetic energy generated by the series of collisions among balls is transferred to the system. But only a marginal decrease in size is achieved in the wet milled case. This may be due to the fact that in wet milling, kinetic energy transfer is not direct but through the medium which slows down reduction of grain size. The lack of sudden decrease as in the case of particles prepared by the solid state reaction method is because the starting powder (coprecipitated) itself is of nanometer sized. Also there are reports that within 24 minutes of milling, size reduction may attain its maximum [7]. The reason for not obtaining a great reduction in size with prolonged milling is due to the high local temperature and pressure generated during the combustion as a result of the high energy ball milling [8]. Also the difficulty in maintaining the very high stress during milling (discussed in section 2.2) slows down reduction of grain size.

Assuming cubic symmetry for these materials, lattice parameter was calculated and the variation of lattice parameter with milling time is evaluated and depicted in figure 7.7. No significant change in lattice parameter is observed with milling. An attempt to calculate the strain developed in the lattice by the method described in chapter 3 was made but found to be difficult to extract any value from the plots [figure 7.8].

7.5 EDX studies on wet milled zinc aluminates

Energy dispersion X-ray intensities were converted to the relative concentrations and tabulated in table 7.2. The experiment is carried out over different areas and almost the same composition matching with the theoretical values is observed for wet milled and unmilled zinc aluminates suggesting a high quality chemical homogeneity in these samples.

7.6 Conclusions

Unmilled and milled samples, in wet and dry conditions are found to be monophasic. Particle size estimation indicates that nanometer sized zinc aluminate particles are crystallized. Without any detectable traces of impurities like ZnO, zinc aluminate appears to be thermally stable with respect to zinc ferrite. Lattice parameter does not vary significantly with milling time. EDX studies matched well with the theoretical elemental composition of these materials.

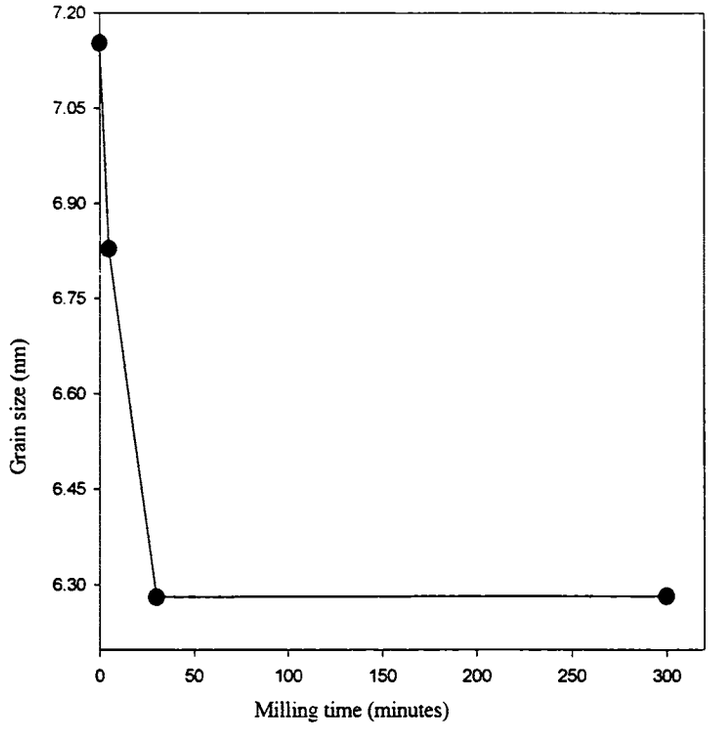

Figure 7.6 Particle size variation with milling time for wet milled zinc aluminate.

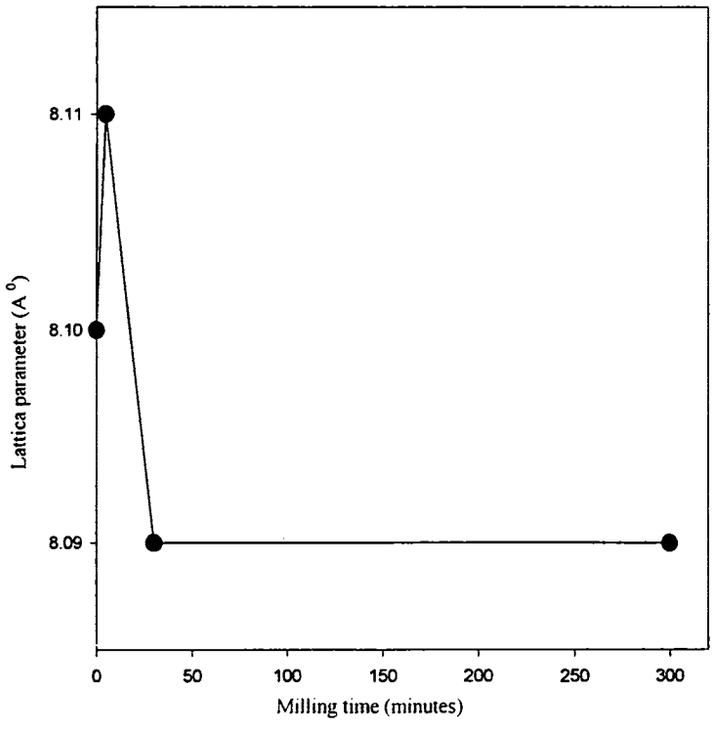

Figure 7.7 Lattice parameter variation with milling for wet milled zinc aluminate.

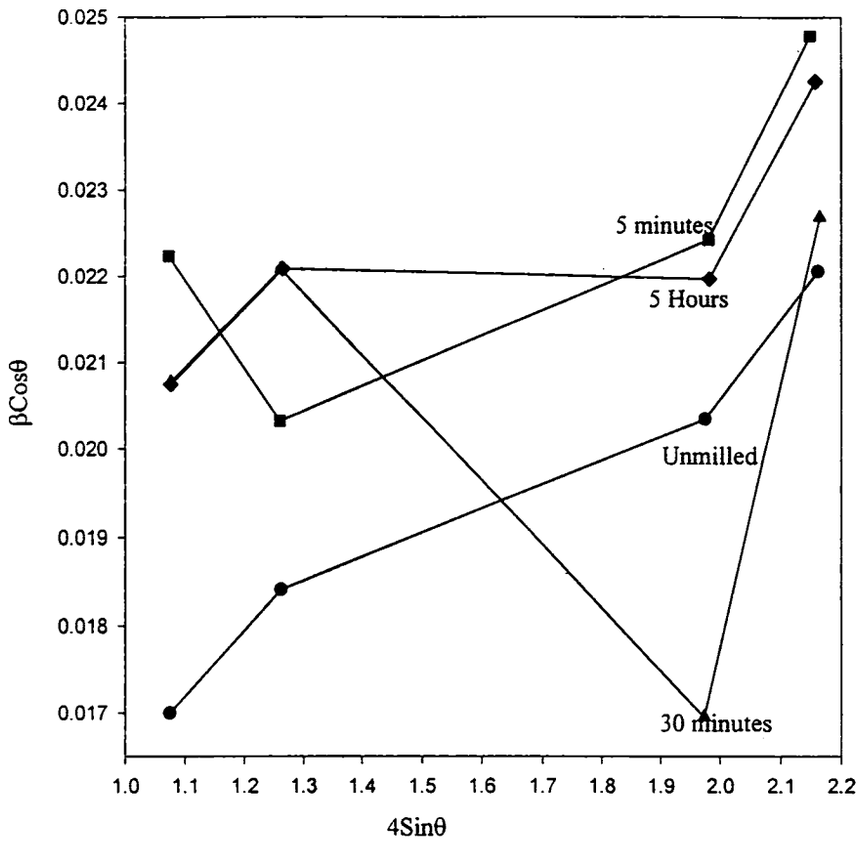

Figure 7.8 4Sinθ Vs βCosθ curves of unmilled and wet milled zinc aluminate.

Sample	Zn Atom.%	Al Atom.%	O Atom.%
Unmilled	15.277	32.004	52.72
5 minutes wet milled	14.645	31.859	53.496
30 minutes wet milled	16.582	36.15	47.268
5 hours wet milled	15.917	32.685	51.398
Theoretical composition	14.286	28.571	57.143

Table 7.2. EDX results on wet milled zinc aluminates suggesting high quality homogeneity in these materials

References:

1.Alexandra Navrotsky, 1986 *Am.Minerl.* **71** 1160

2.Hugh S$_T$. C. O'Nell and Alexandra Navrotsky, 1983 *Am.Mineral.* **68** 181

3.S Mathur, M. Hass, N. Lecerf, M. Veith, H. Shen, S. Hufner, R.Haherkorn, H.P. Beck and M. Jillavi 2001 *J.Am.Ceram.Soc.* **84(9)** 1921

4.Sergio Lucchesi, Umberto Russo, Antonio Della Giusta 1991 *Eur. J.Mineral.* **11** 501

5.Ravindra Pandey, Julian D Gale, Suresh K Sampath and Jose M Recio 1999 *J.Am.Ceram.Soc.* **82(12)**

6.Arcos D, Valenzuela R, Vazquez M and Vallet-Regi M 1998 *J.solid state Chem* **141** 10

7.Sepelak V, Tkacova K, Boldyrev V V, Wibmann S and Becker K D 1997 *Physica B* **234-236** 617

8.Young –Soon Kwon, Konstantin B.Gerasimov and Sok-keel Yoon 2002 *J. Alloys and compounds* **346** 276

CHAPTER 8

DC CONDUCTIVITY AND DIELECTRIC PERMITTIVITY STUDIES ON ULTRAFINE ZINC ALUMINATE

8.1 Introduction

Zinc aluminate represents a nonmagnetic system, which is isostructural with zinc ferrite, is a widely used catalyst. It has been found that the electrical conduction mechanism in zinc ferrite has been influenced by a variety of factors like oxygen ion vacancies, spin polarized tunnelling and intergranular tunnelling. A similar investigation on zinc aluminate by employing dc conductivity measurements together with dielectric permittivity measurements will generate a wealth of information. This will aid in understanding the conduction process taking place in ultrafine zinc aluminate particles and help in formulating a mechanism for conduction. Thus the conduction process in a magnetic and a nonmagnetic system can be compared and correlated.

8.2 DC conductivity studies on dry milled zinc aluminates

The dc conductivity studies were carried out in dry milled zinc aluminates in the voltage range 12-25 by using a computer controlled keithley 236 source/measure unit. The details of these experiments are cited in chapter 2. The V-I graphs are shown in figure 8.1 and it exhibits an ohmic behaviour for all samples. From the X-ray diffraction studies, it is clear that these are ultrafine particles in the range 4-7nm. Usually fine particles have inhomogeneous grain structure of different grain sizes. Conduction in these inhomogeneous grain structured materials are aided by the tunnelling of charge carriers between the grains [1].

The effect of temperature on the dc electrical conductivity (σ_{dc}) for all samples is illustrated in figure 8.2. Electrical conductivity increases with temperature and this can be attributed to the increase in drift mobility of electric charge carriers that are thermally activated upon an increase in temperature [2-6]. This behaviour is common in semiconducting materials, and obeys the Arrhenius relation

$$\sigma T = \sigma_0 \, Exp \, (-E_a/kT) \quad \ldots\ldots\ldots\ldots \quad (8.1)$$

Where E_a is the activation energy for conduction and k the Boltzmann constant.

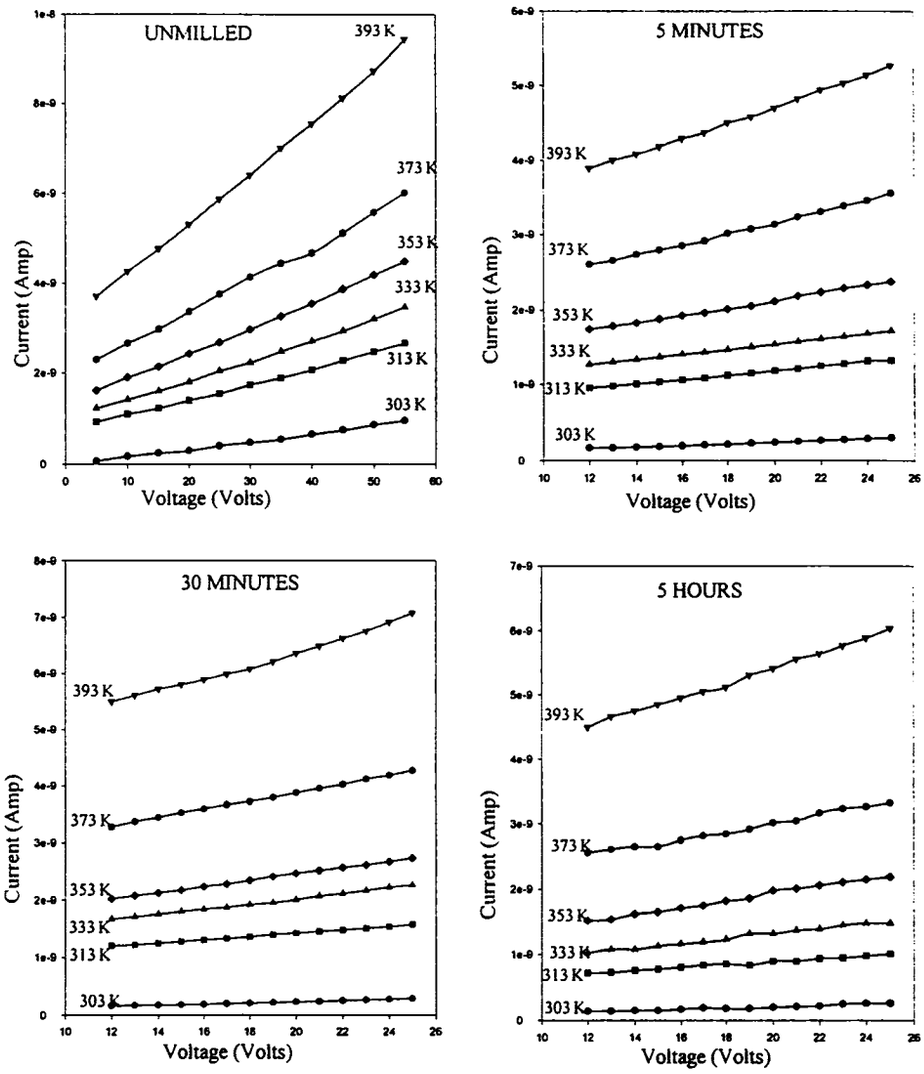

Figure 8.1 V-I graphs of zinc aluminate unmilled and dry milled at different temperatures.

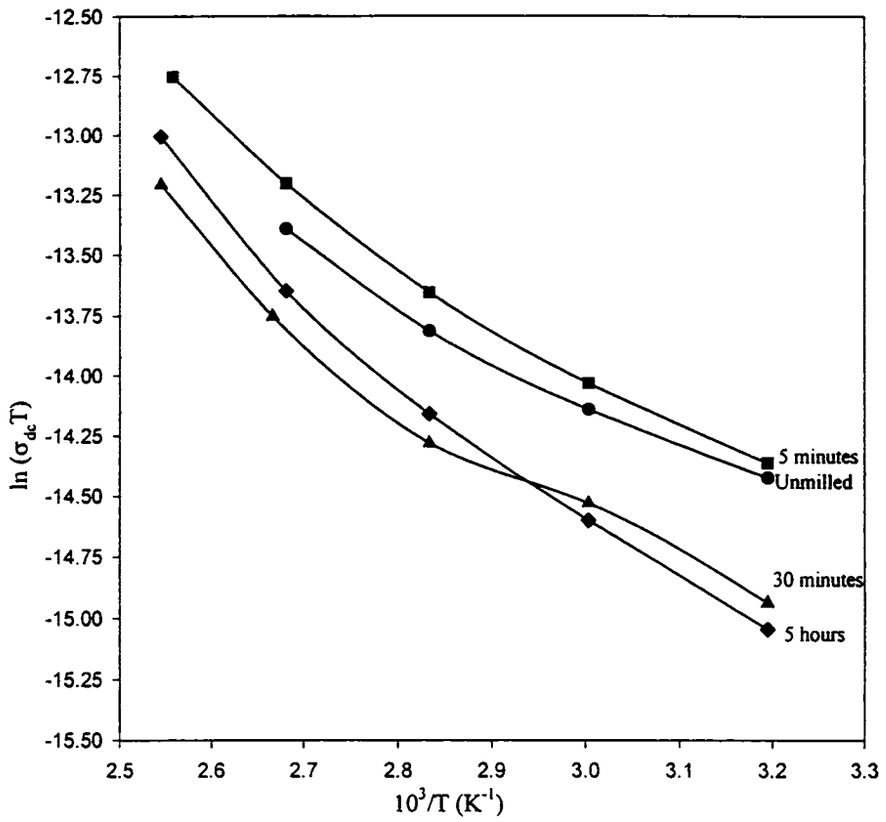

Figure 8.2 ln (σ_{dc}T) Vs 10^3/T graphs for zinc aluminate, dry milled for different times.

Sample	Unmilled	5 minutes	30 minutes	5 hours
Activation energy (eV)	0.2026	0.2162	0.2205	0.2652

Table 8.1. Activation energy for conduction calculated from dc conductivity experiments for dry milled zinc aluminate.

Activation energy for conduction for all samples were calculated by plotting $\ln(\sigma_{dc}T)$ Vs $10^3/T$ curves and they are shown in figure 8.2 and are summarized in table 8.1. No appreciable change in activation energy with milling is observed in these materials. A small increase in activation energy with milling may be due to the increase in inhomogenity produced by milling, which reduces conduction. Conductivity is less pronounced when compared to milled zinc ferrite samples (ref. chapter 6), which is probably due to the absence of Fe^{2+}/Fe^{3+} ions and non-existence of a magnetic ordering. Hence the conduction in zinc aluminate system is solely because of oxygen ion vacancies. Equation (4.2) is applicable here too, which suggests a possible reduction in conduction with milling due to the increase in size distribution of the grains. Equation (4.2) is given by,

$$G_{ij} = G_0 \exp(-2\chi S_{ij} - E_{ij}/kT)$$

Zinc ferrite, is less stable, in terms of decomposition and production of oxygen vacancies and the oxygen ion vacancies generated during the initial phase of milling is primarily responsible for the conduction process. However, in zinc aluminates, as evidenced from EDX results, there is no reduction of oxygen, and hence lesser number of oxygen ion vacancies. Hence it is reasonable to assume that the grain structure plays an important role in the conduction process [6-7]. It may be noted here that zinc aluminate are finer and has a heterogeneous grain structure. These aspects account for large tunnelling distance (S_{ij}) and charging energy (E_{ij}) [8].

8.3 DC conductivity studies on wet milled zinc aluminates

The dc conductivity studies were carried out in wet milled zinc aluminates in the voltage range 12-25. The V-I graphs shown in figure 8.3 exhibits an ohmic behaviour for all samples. There is no marked difference in dc conductivity values between the wet and dry milled zinc aluminates. Conductivity exhibited by wet milled samples is only marginally less with respect to the dry milled samples. Figure 8.4 illustrates the effect of the temperature on the dc electrical conductivity (σ_{dc}) for wet milled zinc aluminates and table 8.2 summarizes the activation energy for conduction evaluated from the graphs in figure 8.4. It is known that porosity, dc conductivity and dielectric permittivity are interrelated. The evaluation of dielectric permittivity and ac conductivity is bound to provide invaluable information as regard the mechanism of conduction. These measurements are carried out to fulfill this motive.

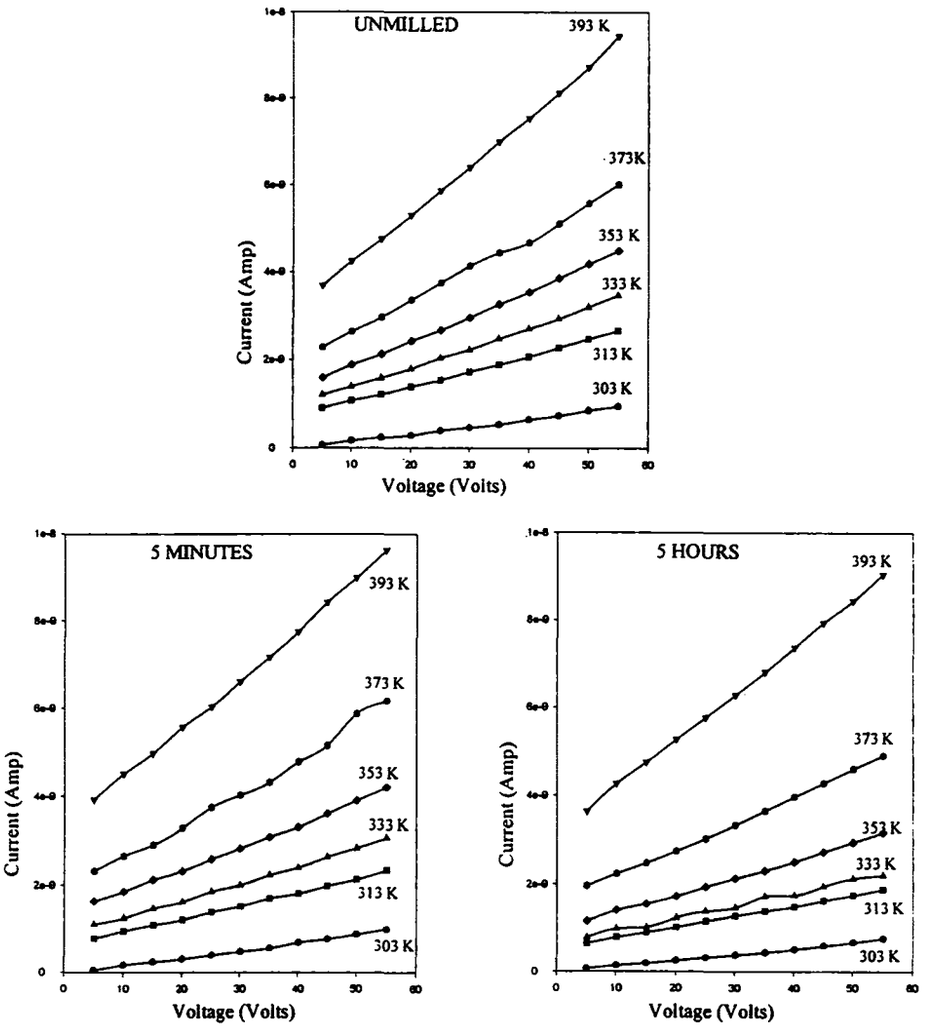

Figure 8.3 V-I graphs of zinc aluminate unmilled and wet milled at different temperatures.

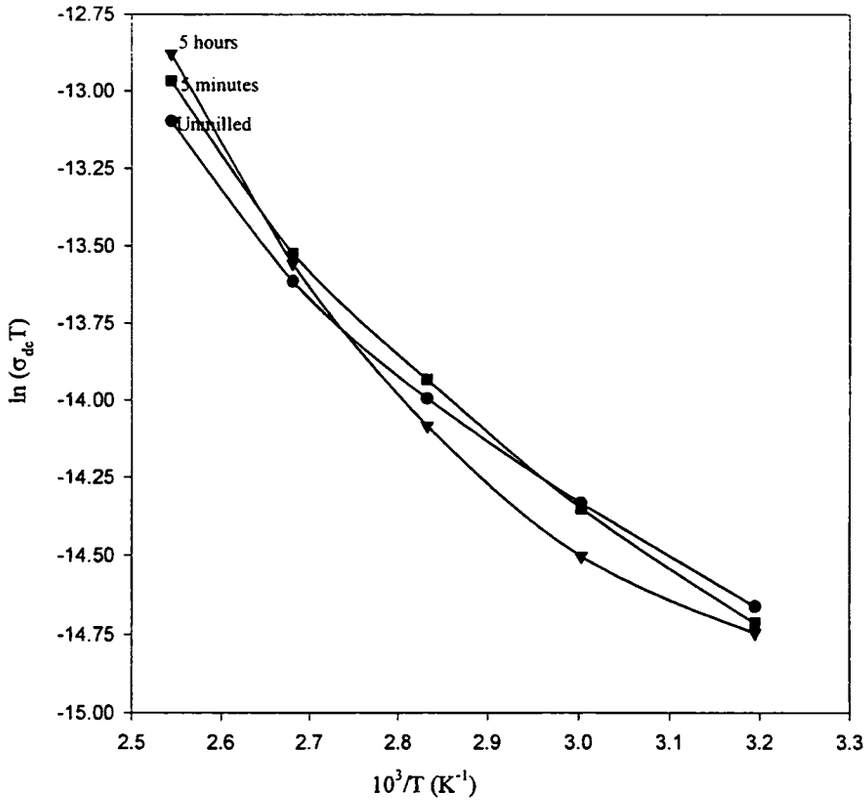

Figure 8.4 ln (σ_{dc}T) Vs 10^3/T graphs for zinc aluminates wet milled for different milling times.

Sample	Unmilled	5 minutes	5 hours
Activation energy (eV)	0.2026	0.2278	0.2449

Table 8.2 Activation energy for conduction calculated from dc conductivity experiments for wet milled zinc aluminate.

8.4 Dielectric permittivity and ac conductivity studies on dry milled zinc aluminates

Dielectric permittivity, dielectric loss factor (Tanδ) and ac conductivity were evaluated for dry milled zinc aluminate in the frequency range 100kHz-8MHz. The temperature dependence is also studied for these samples in the temperature range 163 K to 393 K. Moisture influences the dielectric results and hence special care was taken to heat treat the samples before being subjected to dielectric permittivity measurements.

Figure 8.5 represents the dielectric permittivity dispersion graphs of dry milled zinc aluminates at different temperatures. This dispersion can be explained by Koops phenomenological theory of well conducting grains separated by layers of lower conductivity [2-4,9-23]. From figure (6.3) and (8.3), it can be noticed that the decrease in dielectric permittivity is sharper in the case of zinc aluminate systems which is an indication of the contribution of hole carriers in the conduction process. The hole carriers are generated by the oxygen ion vacancies which are generated during coprecipitation and increased by ball milling. The absolute value of dielectric permittivity is very less (between 1.5 and 5.5) with respect to zinc ferrite. In zinc aluminates only oxygen ion vacancies contributes to the conduction and polarisation while in zinc ferrites the effect of Fe^{2+}/Fe^{3+} hopping and magnetic ordering do influence the conduction and polarisation.

Figure 8.6 represents the dielectric loss factor (Tanδ) variation with frequency at different temperatures for unmilled and dry milled zinc aluminate samples. The low values are encouraging from the application point of view. The decreasing trend is in accordance with the Koops phenomenological theory.

Figure 8.7 represents the frequency dependence of ac conductivity on dry milled zinc aluminates. In contrast, in the case of zinc ferrites (ref. figure 6.5), it is observed that the onset of transition starts at a lower frequency in zinc aluminates. This is because the presence of oxygen vacancies create hole carriers and hence in the conduction process occuring in zinc aluminate system, the holes cannot follow the applied electric field at high frequencies [9,24].

Figure 8.8 represents the temperature dependence of dielectric permittivity. A broad transition at around 310 K is observed for all samples. The broad transition is specific to ultrafine particles. Ionic mechanism of polarization as well as drift mobility

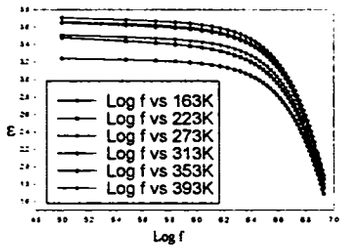

Figure 8.5(a) Dielectric permittivity dispersion curves at different temperatures for unmilled $ZnAl_2O_4$.

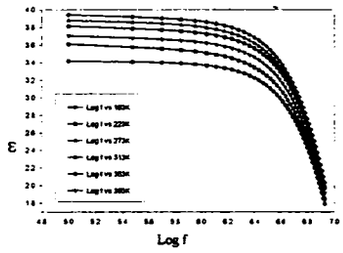

Figure 8.5(b) Dielectric permittivity dispersion curves at different temperatures for 5 minutes dry milled $ZnAl_2O_4$.

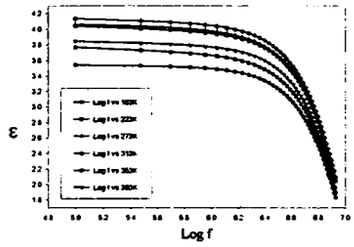

Figure 8.5(c) Dielectric permittivity dispersion curves at different temperatures for 30 minutes dry milled $ZnAl_2O_4$.

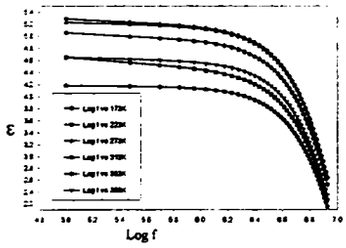

Figure 8.5(d) Dielectric permittivity dispersion curves at different temperatures for 5 hours dry milled $ZnAl_2O_4$.

Figure 8.5 Dielectric permittivity dispersion curves at different temperatures for dry milled $ZnAl_2O_4$.

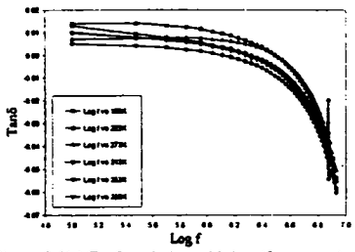

Figure 8.6(a) Tanδ variation with log (frequency) at different temperatures for unmilled $ZnAl_2O_4$.

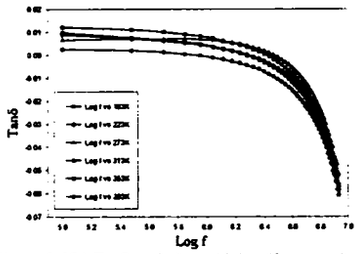

Figure 8.6(b) Tanδ variation with log (frequency) at different temperatures for 5 minutes milled $ZnAl_2O_4$.

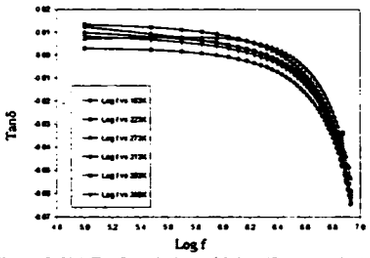

Figure 8.6(c) Tanδ variation with log (frequency) at different temperatures for 30 minutes milled $ZnAl_2O_4$.

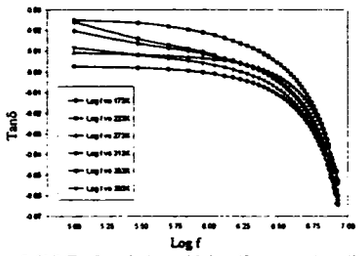

Figure 8.6(d) Tanδ variation with log (frequency) at different temperatures for 5 hours milled $ZnAl_2O_4$.

Figure 8.6 Tanδ variation with log (frequency) at different temperatures for dry milled $ZnAl_2O_4$.

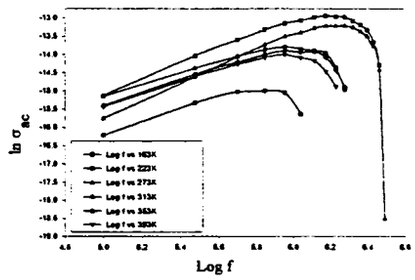

Figure 8.7(a) ln σ_{ac} variation with log (frequency) at different temperatures for unmilled $ZnAl_2O_4$.

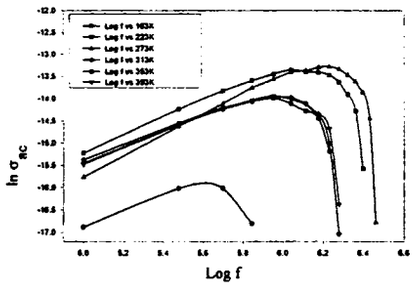

Figure 8.7(b) ln σ_{ac}variation with log (frequency) at different temperatures for 5 minutes milled $ZnAl_2O_4$.

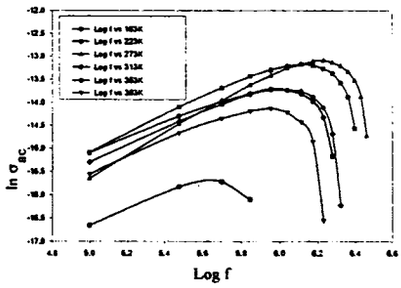

Figure 8.7(c) ln σ_{ac}variation with log (frequency) at differen temperatures for 30 minutes milled $ZnAl_2O_4$.

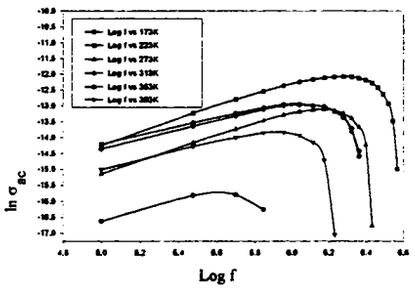

Figure 8.7(d) ln σ_{ac}variation with log (frequency) at different temperatures for 5 hours milled $ZnAl_2O_4$.

Figure 8.7 ln σ_{ac}variation with log (frequency) at different temperatures for dry milled $ZnAl_2O_4$.

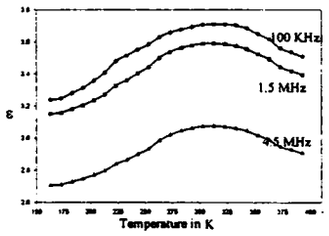

Figure 8.8(a) Dielectric permittivity variation with temperature for unmilled $ZnAl_2O_4$ at different frequencies.

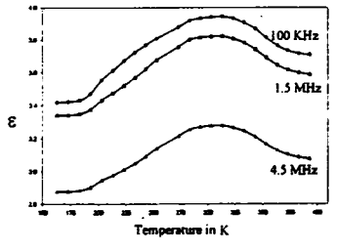

Figure 8.8(b) Dielectric permittivity variation with temperature for 5 minutes milled $ZnAl_2O_4$ at different frequencies.

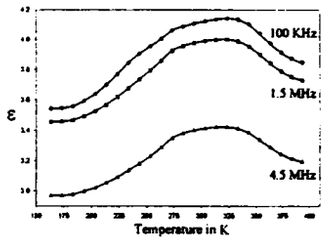

Figure 8.8(c) Dielectric permittivity variation with temperature for 30 minutes milled $ZnAl_2O_4$ at different frequencies.

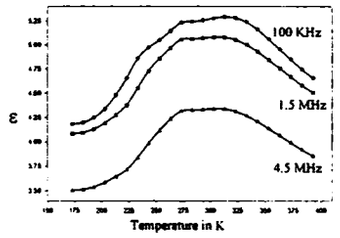

Figure 8.8(d) Dielectric permittivity variation with temperature for 5 hours milled $ZnAl_2O_4$ at different frequencies.

Figure 8.8 Dielectric permittivity variation with temperature for dry milled $ZnAl_2O_4$ at different frequencies.

of charge carriers increases the dielectric permittivity when the temperature increases. In ionic dielectrics, when the temperature rises, the orientation of the dipoles is facilitated, and thus increases permittivity. As the temperature increases, the chaotic thermal oscillations of molecules are intensified and the degree of orderliness of their orientation is diminished [25-26]. This causes the dielectric permittivity to pass through a maximum and then drops.

8.5 Dielectric permittivity and ac conductivity studies on wet milled zinc aluminates

Wet milled zinc aluminates were subjected to dielectric permittivity measurements. Figure 8.9 shows the dielectric dispersion curves at different temperatures. A small increase in dielectric permittivity with milling is observed which is less when compared to dry milled samples. This is due to the reduced number of charge carriers produced during wet milling. Table 8.3 represents the dielectric permittivity values for dry milled and wet milled zinc aluminates at 100 kHz near room temperature.

Sample	Dielectric permittivity	
	Dry milling	Wet milling
Unmilled	3.71	3.71
30 minutes	4.12	4.05
5 hours	5.28	4.24

Table 8.3 Dielectric permittivity values at 100 kHz, at a temperature 300 K for milled zinc aluminates.

Tanδ (figure 8.10) and ac conductivity (figure 8.11) shows the same trend as that of dry milled samples. Figure 8.12 shows the temperature dependence of dielectric permittivity, which also shows a broad transition as in the case of dry milled zinc aluminates.

8.6 Conclusions

The high energy ball milling does not influence dc conductivity and dielectric properties of zinc aluminates. This establishes the relative stability of these materials against decomposition and against vacancy production. Dielectric transition with temperature is due to the chaotic thermal oscillation of the molecules. Wet and dry

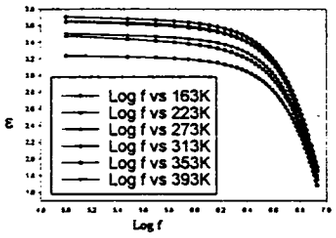

Figure 8.9(a) Dielectric permittivity dispersion curves at different temperatures for unmilled $ZnAl_2O_4$.

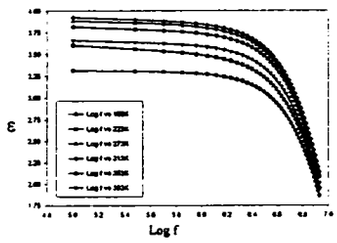

Figure 8.9(b) Dielectric permittivity dispersion curves at different temperatures for 5 minutes milled $ZnAl_2O_4$.

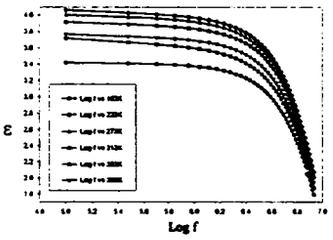

Figure 8.9(c) Dielectric permittivity dispersion curves at different temperatures for 30 minutes milled $ZnAl_2O_4$.

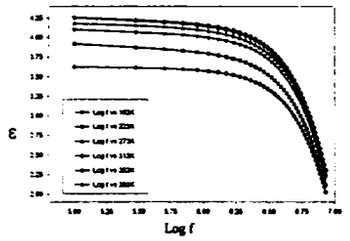

Figure 8.9(d) Dielectric permittivity dispersion curves at different temperatures for 5 hours milled $ZnAl_2O_4$.

Figure 8.9 Dielectric permittivity dispersion curves at different temperatures for wet milled $ZnAl_2O_4$.

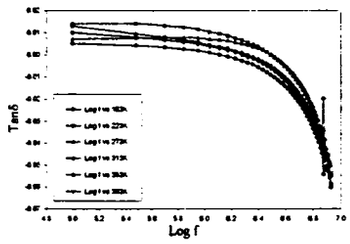

Figure 8.10(a) Tanδ variation with log (frequency) at different temperatures for unmilled $ZnAl_2O_4$.

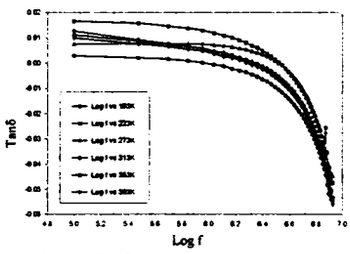

Figure 8.10(b) Tanδ variation with log (frequency) at different temperatures for 5 minutes milled $ZnAl_2O_4$.

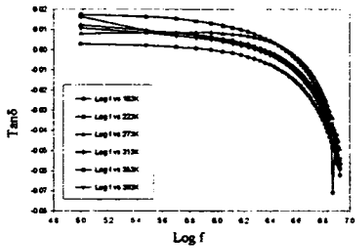

Figure 8.10(c) Tanδ variation with log (frequency) at different temperatures for 30 minutes milled $ZnAl_2O_4$.

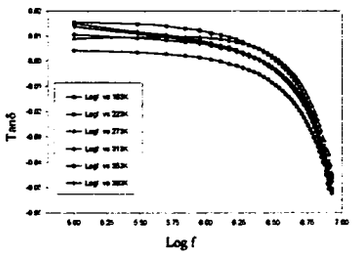

Figure 8.10(d) Tanδ variation with log (frequency) at different temperatures for 5 hours milled $ZnAl_2O_4$.

Figure 8.10 Tanδ variation with log (frequency) at different temperatures for wet milled $ZnAl_2O_4$.

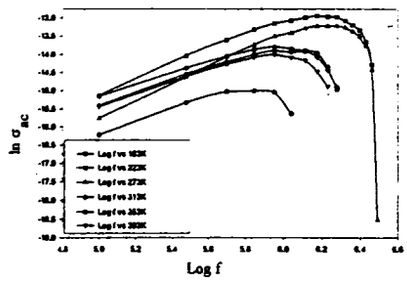

Figure 8.11(a) ln σ_{ac} variation with log (frequency) at different temperatures for unmilled $ZnAl_2O_4$.

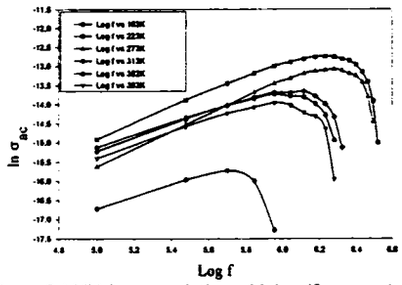

Figure 8.11(b) ln σ_{ac} variation with log (frequency) at different temperatures for 5 minutes milled $ZnAl_2O_4$.

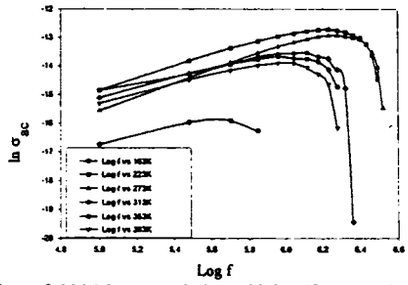

Figure 8.11(c) ln σ_{ac} variation with log (frequency) at different temperatures for 30 minutes milled $ZnAl_2O_4$.

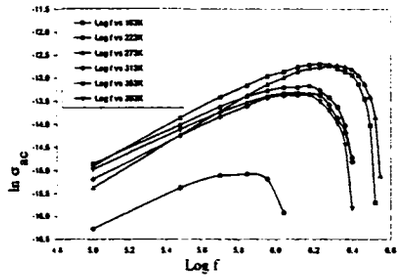

Figure 8.11(d) ln σ_{ac} variation with log (frequency) at different temperatures for 5 hours milled $ZnAl_2O_4$.

Figure 8.11 ln σ_{ac} variation with log (frequency) at different temperatures for wet milled $ZnAl_2O_4$.

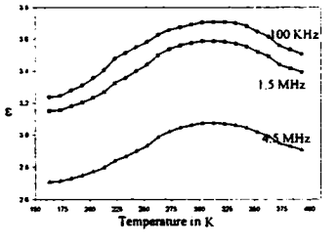

Figure 8.12(a) Dielectric permittivity variation with temperature for unmilled $ZnAl_2O_4$ at different frequencies.

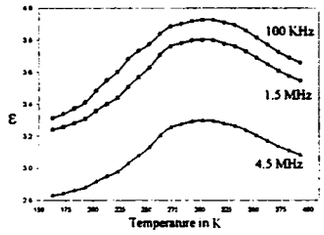

Figure 8.12(b) Dielectric permittivity variation with temperature for 5 minutes milled $ZnAl_2O_4$ at different frequencies.

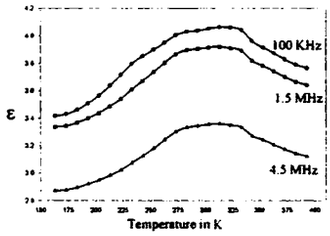

Figure 8.12(c) Dielectric permittivity variation with temperature for 30 minutes milled $ZnAl_2O_4$ at different frequencies.

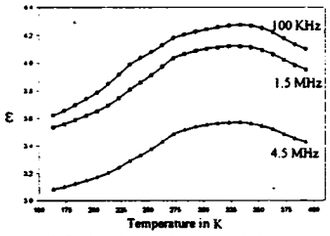

Figure 8.12(d) Dielectric permittivity variation with temperature for 5 hours milled $ZnAl_2O_4$ at different frequencies.

Figure 8.12 Dielectric permittivity variation with temperature for wet milled $ZnAl_2O_4$ at different frequencies.

milling shows almost the same results. Oxygen ion vacancies (holes) are the probable charge carrier in zinc aluminate.

References:

1.Xavier Battle and Amilcar Laborta 2002 *J.Phys.D.Appl.Phys* **35** R15

2.Abdeen A M 1999 *J.Magn.Magn.Mater* **192** 121

3.Ahmed M A, El Hiti M a, El Nimr M K and Amer M A 1996 *J.Magn.Magn.Mater* **152** 391

4.Abdeen A M 1998 *J.Magn.Magn.Mater* **185** 199

5.El Hiti M A 1996 *J.Magn.Magn.Mater* **164** 187

6.Ponpandian N and Narayanasamy A 2002 *J.Appl.Phys.* **92(5)** 2770

7.G F Goya and H R Rechenberg 1999 *J Magn.Magn.Mater.* **203** 141

8.Ping Sheng 1994 *Proceedings of the NATO Advanced study institute on Nanophase materials-syntheses, properties and applications, Kluwer academic publishers* 381

9.Ismael H, El Nimr M K, Abou El Ata A M, El Hiti M A, Ahmed M A and Murakhowskii A A 1995 *J.Magn.Magn.Mater* **150** 403

10.Shaikh A M, Bellad S S and Chougule B K 1999 *J.Magn.Magn.Mater* **195** 384

11.Mohammed E M, Malini K A, Philip Kurian, Anantharaman M R 2002 *Materials Research Bulletin* **37** 753

12.Mangalaraja R V, Ananthakumar S, Manohar P and Gnanam F D 2002 *J.Magn.Magn.Mater* **253** 56

13.Mazen S A, Abdallah M H, Elghandoor M A and Hashem H A 1994 *Phys,stat.sol.(a)* **144** 461

14.Koops C G 1951 *Phys.Rev* **83** 121

15.Chandra prakash and Baijal J S 1985 *J. less common metals* **107** 51

16.Josyulu O S and Sobhanadri J 1980 *Phys.Status Solidi(a)* **59** 323

17.N saxena, B K Kuanr, Z H Zaidi, G P Srivastava 1991 *Phys.stat.sol(a)* **127** 231

18.Patil R.S., Kakatkar S.V, Maskar P.K. , Patil S.A and Sawant S.R, 1991 *Ind. J. Pure Appl. Phys.* **29** 589

19.Jankowski Stanislaw 1988 *J.Am.Ceram.Soc.* **71(4)** C176

20.J.H.Nam, H.H.Jung, J.Y.Shin and J.H.Oh, 1995 *IEEE Trans. Magn.* **Vol. 31 No.6** 3985

21.Kuanr B K, Singh P K, Kishan P, Kumar N, Rao S L N, Prabhat K Singh, Srivastava G P 15 April 1988 *J.Appl.Phys.* **63(8)** 3780

22.J.Smit, and H.P.J. Wijn, 1959 *Ferrites, Philips Technical Library* 241

23.V P Miroshkin, YA I Panova, V V Passynkov 1981 *Phys.stat.Sol(a)* **66** 779

24.El Hiti M A, Ahmed M A, Mosaad M M and Attia S M 1995 *J.Magn.Magn.Mater* **150** 399

25.Tareev B 1979 *Physics of Dielectric Materials (Mir Publishers) Moscow* 105

26.S Sindhu, M R Anantharaman, Bindhu P Thampi, K a Malini, Philip Kurian 2002 *Bull.Mat.Sci* **25**(7) 599

CHAPTER 9
CONCLUSIONS

Fine particles of inorganic materials are ideal templates for studying various phenomenon occuring at the nanolevel. This includes quantum magnetisation, quantum tunnelling, superparamagnetism, spin glass behaviour and the like. This is abundantly true for inorganic magnetic materials. Huge prospects of exploiting this phenomenon commercially for various applications in the form of new and improved gadgets and also as potential replacement for the obsolete is surely one of the motivation for delving into the physics of these materials at the nanolevel. This will help scientists to tailor materials for various applications. This thesis also should be considered as an attempt to look into the properties at the interface and to study the interfacial phenomenon resulting out of cation migration to sites of different coordinations. This thesis delved into the anomalous properties exhibited by zinc ferrite in the ultrafine domain. An attempt was also made to study zinc aluminate in the fine particle regime. This is because zinc aluminate represents a nonmagnetic normal spinel system and a widely studied material for catalytic applications.

Various methods of preparation/synthesis are available for preparing fine particles. The notable among them are the low temperature coprecipitation methods, sol gel, reaction milling, reverse micelle etc. It must be noted here that solid state/ceramic techniques results in coarser particles and the preparation are energy intensive. Alternate techniques for the preparation of zinc aluminate and zinc ferrite were adopted here. The method of coprecipitation of zinc aluminate and zinc ferrite from its constituent nitrates were employed for the preparation of these materials.

The preparative conditions have been optimized and standardized. It is to be remembered that most of the synthesis routes are sample specific and pH conditions and temperature are very critical. It has been found that an optimum pH of 12 and a temperature 373 K are ideal for the coprecipitation of the samples.

It was possible to synthesize phase pure materials. The particle size as well as structural parameters of these materials are evaluated by XRD. Further ball milling (HEBM) and simultaneous (ex situ) estimation of particle size by XRD indicate that

the technique of HEBM has been able to reduce the particle size substantially. Fine particles of zinc aluminate in the range 4-7nm could be synthesized.

Normally XRD is employed as an alternate tool to gauge the grain size which is governed by the relation $0.9\lambda/\beta\cos\theta$. However this is not often without errors. It is well known that factors like thermal effects, strain, instrumental effects can contribute to the broadening of XRD peaks. A simple technique for the evaluation of strain was employed and the contribution of strain towards the broadening of XRD peaks is separated from grain size effects. The evaluation of grain size after eliminating the contribution of strain is in conformity with that of the particle size estimated from transmission electron micrographs for zinc ferrite. The particles are spherical in shape and they lie in the range 10-16nm. The evaluation of strain for the ball milled samples of zinc ferrite indicates that ball milling introduces strain and thought to be responsible for lattice contraction which was found in the case of dry milling.

The distribution of particles of size was confirmed by TEM studies in dry milled specimens. It was observed that prolonged milling does not yield a further reduction in size due to the high local temperature and pressure produced during the milling.

A comparison of structural parameters of zinc ferrites and zinc aluminates reveal that zinc aluminate is a relatively stable compound and ball milling does not induce any decomposition. On the other hand, zinc ferrite upon ball milling decomposes to α-Fe_2O_3 and ZnO, though, the amount of ZnO and α-Fe_2O_3 is minute. The method of coprecipitation ensures complete homogeneity of zinc aluminate samples as evidenced from EDX results. Further reduction of particle size by HEBM does not decompose zinc aluminate to ZnO and Al_2O_3. On comparison with zinc ferrite, very small particles of zinc aluminate in the range 4-7nm could be synthesized by coprecipitation and subsequent ball milling.

The ensurance of complete homogeneity and structurally pure zinc aluminate augurs well when zinc aluminate is thought of as a catalyst. The employment of wet milling or dry milling does not produce noticeable changes as far as structural properties and homogeneity of zinc aluminate samples are concerned.

Magnetic properties of ultrafine zinc ferrite has been at the centerstage for almost a decade because of the anomaly exhibited by these materials in the

nanoregime. This material has been a breeding ground for testing various hypotheses of many researchers. Opinions are divided and findings on the electrical and magnetic properties of ultrafine zinc ferrite by various researchers are also at variance. If cation redistribution of Zn^{2+}/Fe^{3+} ions is thought of as a probable reason for the observed magnetisation of zinc ferrite at room temperature, then questions like – where do they get energy from for migration?, what are the contribution of lattice/madelung energy and site preference energy in facilitating a redistribution and an inversion?, do preparative techniques have any bearing on this?- are also important questions to be answered.

The magnetisation studies carried out on ultrafine zinc ferrite reveals that zinc ferrite exhibits a net magnetisation at room temperature and saturation magnetisation M_s increases with increase in fineness. Both dry and wet milling methods were adopted to prepare zinc ferrite and in both cases it has been found that the saturation magnetisation increases with milling time.

One of the reasons for the anomaly exhibited by zinc ferrite samples could be cation redistribution and subsequent emergence of ferrimagnetic ordering in these systems and bond breakage at the surface and emergence of surface spin disorder. Since the sample does not saturate even at a moderate field of 10 kOe, the presumption that zinc ferrite in the ultrafine regime exhibit FM ordering remains largely speculative. This means that the magnetic constituents of zinc ferrite could comprise of a purely ferrimagnetic component, a superparamagnetic component and possibly a spin glass like entity. Identification and establishment of the constituents for sure needs sophisticated thermomagnetisation measurements and evaluation of ac magnetic susceptibility over a wide range of temperatures. ZFC-FC measurements are known techniques to extract information about superparamagnetic nature of these fine particles. This technique has an inherent drawback in that, as it is not possible to derive the exact signature of these magnetisation constituents vis-à-vis superparamagnetism or spin glass.

AC magnetic susceptibility also gives information on the transitions. However they are also not accurate. For the first time, third order susceptibility measurements were carried out on ultrafine zinc ferrite samples to distinguish between superparamagnetic and spin glass behaviours. ZFC-FC measurements on wet and dry

milled samples bring forth two clear cut patterns. Wet milled samples do not produce any transition in the measurement range of experiments while dry milled samples display clear signs of either superparamagnetic or spin glass transitions. From ZFC-FC measurements, it has been found out that the transition temperatures (T_B/T_G) shifts towards room temperature with increase of fineness in particles. This is an important finding as far as applications are concerned. If zinc ferrite can be prepared in the thin film form with appropriate composition, this narrow transition being in a metastable state can be easily switched by an energetic beam of laser. This could be a potential material for magneto optical applications. ZFC-FC measurements only indicate the transition temperature and could be because of superparmagnetism or spin glass.

Further, evaluation of third order susceptibility reveals that 10 hours milled zinc ferrite samples are predominantly superparamagnetic in nature. These conclusions have been drawn based on a model proposed by Sherrington-Kirkpatrikc and the Bethe approximation and they were applied to the zinc ferrite systems. However definitive evidence for superparamagnetic characteristics was not forthcoming for the unmilled samples. The theoretically fit Langevin function tallies well with that of the experimental values, which again confirm the presence of a superparamagnetic component in fine particle zinc ferrite.

Mössbauer spectroscopy has been considered to be a complementary tool to vibrating sample magnetometry and ac magnetisation studies to explore the various interactions taking place in magnetic systems. Investigations carried out using Mössbauer spectroscopy on selected samples of milled and unmilled zinc ferrites at room temperature and low temperatures reveal that the spectrum consists of tell tale signatures of a typical ferrimagnetic ordering together with signs of a superparamagnetic component. Conclusive evidence was extracted from the spectrum suggesting a strong ferrimagnetic ordering in the samples. This was evidenced from the six finger pattern exhibited by the spectrum. The emergence of a doublet along with a sextet reveals the presence of a superparamagnetic component. An isomer shift of around 0.34-0.37 mm/s observed in the sextet is an evidence for the presence of Fe^{3+} ions only and no signs of Fe^{2+} ions are there in the spectrum. The hyperfine field does not change with milling indicating enhanced ferrimagnetic ordering. All these

findings supports and complement the conclusion drawn from vibrating sample magnetometry/ac magnetic susceptibility measurements. Thus it can be concluded that in ultrafine particles, the increased ferrimagnetic ordering displayed by the particles with increase in fineness is due to the cation redistribution. It is also possible that a large fraction of Fe^{3+} ions are situated at the surface leading to surface discontinuity.

The process of electrical conduction in ferrites have been thought to be a hopping mechanism where charge carriers hop between dissimilar valence states of cations present. When it comes to the question of ultrafine particles, the phenomenon of conduction is aided by the quantum mechanical processes namely spin polarized tunnelling and intergranular tunnelling. A detailed investigation on the electrical properties of ultrafine zinc ferrites establishes the fact that the conduction process in ultrafine zinc ferrites are not due to hopping but, due to the presence of oxygen ion vacancies produced during milling. The observed dc conductivity in milled samples could not be fitted satisfactorily to a model proposed by Rezlescu. The dielectric permittivity studies conducted on milled zinc ferrite samples suggest that milling increases the dielectric permittivity. The dielectric permittivity results are in accordance with the Koops phenomenological theory.

These studies also reveal that dielectric properties can be varied appreciably by high-energy ball milling in nanosized zinc ferrites produced by coprecipitation method. A semiconducting behaviour was observed in these materials with the oxygen vacancies acting as the main charge carrier for conduction, which was produced at the time of coprecipitation and milling. The magnetic ordering due to the cation redistribution and presence of α-Fe_2O_3 do affect the electrical transport properties. Temperature dependence of dielectric permittivity confirms the belief that holes are the majority charge carriers in the transport process.

Milling does not produce noticeable affects on the dc conductivity and dielectric permittivity of zinc aluminates. However, the mechanism of conduction in zinc aluminate is because of the presence of oxygen ion vacancies or intergranular tunnelling. This is in contrast to the conduction process taking place in zinc ferrite, which is influenced by a host of factors like, small amount of Fe^{2+}/Fe^{3+}, oxygen ion vacancies, spin polarized tunnelling and presence of α-Fe_2O_3. Through this

investigation, a model based on cation redistribution and subsequent bond breakage at the surface, which results in superexchange path breaking is thought to be responsible for the ferrimagnetic ordering and the presence of superparamagnetism in ultrafine zinc ferrites. Further investigations by employing neutron scattering experiments together with ESCA is necessary to validate the exact nature of magnetic ordering. Neutron scattering experiments will clearly reveal the bulk magnetic structure. However, the presence of surface spins and the possible presence of spin glass clusters needs to be investigated separately, possibly by employing synchrotron radiation. These experiments could not be carried out because of time constraints. Further, scope exists to carry out similar investigations on normal spinels like $CdFe_2O_4$ in order to check this hypothesis. Results on the studies of inverse spinels will be useful to discuss the various aspects of this hypothesis.

It will be a good futuristic proposition to prepare thin films of zinc ferrite by sputtering or pulsed laser deposition (PLD) techniques and study the surface properties of these materials with a view to exploiting the potential of these materials as probable magneto optical storage devices or as magneto optical sensors. Fine particles of ferrites are precursors to the synthesis of rheological fluids. Ferrofluids are important commercially for various applications. If ferrofluids based on $ZnFe_2O_4$ can be synthesized by the modification of coprecipitation adopted here, it is bound to exhibit interesting and useful properties. This can be exploited for commercial use.

From the fundamental point of view, a detailed investigation on the surface properties together with magnetic measurements will reveal a lot of physics at the interfaces, which is essentially of quantum magnetic in origin. Evidence for spin polarized tunnelling and intergranular tunnelling in zinc ferrites also is an indication that they could be exhibiting giant magnetoresistance (GMR) or colossal magnetoresistance (CMR) at a particular finite particle size. So scope exists to prepare ultrafine zinc ferrite and to carry out study on the magneto transport properties and explore the possibilities of GMR and CMR sensors based on zinc ferrites.

A thorough study using dc conductivity measurements on normal spinel systems like $MgAl_2O_4$ or systems resembling $ZnAl_2O_4$ could bring forth lot of useful characteristics suited for catalytic reactions. The hypothesis of cation redistribution

and emergence of surface spins with increase of fineness could be tested. However, ample scope exists to carry out further studies on the finite size effects on the 3d transition elements like Nickel, Cobalt and Iron and also on normal spinels in the nanoregime. Thus through this study, it was possible to successfully investigate the finite size effects on the structural, electrical and magnetic properties of normal spinels in the ultrafine regime.

Annexure – I

Rietveld analysis of ultra fine zinc aluminates and zinc ferrites

Zinc aluminates and zinc ferrites represent a class of materials which are generally known by the name spinels. They resemble the crystal structure of the naturally occurring mineral $MgAl_2O_4$ and all materials exhibiting this structure are called spinels. Spinels can be further classified into normal spinels, inverse spinels or random spinels. The general formula can be written as AB_2O_4 where A is a divalent ion in the tetrahedral site and B is a trivalent cation which is situated on the octahedral site. The randomness or inversion is generally determined by the nature of the cation, cationic radius, their site preference energy etc.

Under normal circumstances zinc ferrites and zinc aluminates represent a typical normal spinel where zinc cations have an exclusive tetrahedral site preference because of its favourable site preference energy. If the particle size of these materials is in the micron regime zinc cations occupy tetrahedral sites exclusively and these materials in the micron regime exhibit no inversion and are normal spinels. However, in the nanoregime, because of size effects, zinc ferrites exhibit anomaly and these size effects are manifested in the form of ferrimagnetic properties instead of antiferromagnetic properties. There have been reports aplenty on this anomaly and the investigation into these anomalies is one of the focal theme of this investigation too (thesis).

Here zinc ferrite represents a magnetic system while zinc aluminate belongs to a non magnetic system. X-ray powder diffraction is an effective tool to identify the phases and is very often successful. However with the advent of fast computers and other refining techniques like Rietveld analysis, identification of phases and detection of impurities has become very easy. An ordinary PC with P-IV configuration is more than sufficient for carrying out this task.

The effect of milling on various properties of zinc aluminate and zinc ferrites formed part of this thesis.

Fresh samples of zinc ferrites and zinc aluminates were prepared by cold precipitation techniques as already described in the experimental section of this thesis. The purity of these samples was ensured by subjecting these samples to X-ray diffraction analysis. Initial x-ray diffraction analysis indicates that these materials are phase pure and the method of preparation is consistent and impurity free. Zinc aluminate and zinc ferrites could be prepared any number of times. However, a complete analysis using Rietveld analysis gives an insight into the occurrence of ferrimagnetism in nano zinc ferrites and if the origin of the ferrimagnetism is due to cation redistribution, zinc has to occupy the octahedral site (B) which is contrary to the earlier school of thought.

If Zinc chooses to migrate the octahedral sites, while all other parameters remaining the same, it would be worthwhile to inspect the occurrence of a similar cation redistribution in a non magnetic system like zinc aluminate. If cation redistribution occurs in systems like zinc aluminate it will have wider ramification in the area of catalysis because zinc aluminate is a commonly used catalyst for many reactions. This is one of the motives in employing Rietveld refinement on these samples.

The raw X-ray diffraction data were employed for the Rietveld analysis of X-ray diffraction data for zinc ferrite pure, zinc ferrite (milled) and zinc aluminate samples prepared by cold coprecipitation technique. A brief discussion about the Rietveld analysis is given below for completion and continuity, especially, about the program and other details.

Rietveld refinement of X-ray powder diffraction data opens a new avenue and it enables to gather accurate information on the crystal structure. It also helps to identify trace impurities and aid to pinpoint rearrangement of cation between the octahedral and tetrahedral sites.

The program FULLPROF was employed for the analysis

The program FULLPROF has been mainly developed for Rietveld analysis of X-ray powder diffraction data collected at constant or variable step in scattering angle 2θ. The program is also used as a Profile Matching tool, without any prior knowledge of the crystal structure. Single Crystal refinements can also be performed alone or in

combination with powder data. This program can also be utilized for the analysis of neutron diffraction data and also for the analysis time of flight (TOF) neutron scattering. The first versions of the program FullProf were based on the code of the DBW program, which, in turn, is also a major modification of the original Rietveld-Hewat program. The program FullProf was developed starting with the code DBW3.2S (Versions 8711 and 8804), but is has been so modified and only the name of some basic subroutines and variables owe their existence to the original version.

Some of the most important features of FULLPROF are that this can be employed for analyzing the following data.

- X-ray diffraction data: laboratory and synchrotron sources.
- One or two wavelengths (eventually with different profile parameters).
- Background: fixed, refinable, adaptable, or with Fourier filtering.
- Choice of peak shape for each phase: Gaussian, Lorentzian, modified Lorentzians, pseudo-Voigt, Pearson-VII, Thompson-Cox-Hastings (TCH) pseudo-Voigt, numerical, split pseudo-Voigt, convolution of a double exponential with a TCH pseudo-Voigt for TOF.
- Absorption correction for a different geometry. Micro-absorption correction for Bragg-Brentano set-up.
- Choice between three weighting schemes: standard least squares, maximum likelihood and unit weights.
- Magnetic structure refinement (crystallographic and spherical representation of the magnetic moments). Two methods: describing the magnetic structure in the magnetic unit cell of making use of the propagation vectors using the crystallographic cell. This second method is necessary for incommensurate magnetic structures.
- Profile Matching. The full profile can be adjusted without prior knowledge of the structure (needs only good starting cell and profile parameters).
- Quantitative analysis without the need of structure factor calculations.
- Montecarlo/Simulated Annealing algorithms have been introduced to search the starting parameters of a structural problem using integrated intensity data.

In FULLPROF the control of the refined parameters is achieved by using codewords. These are the numbers C_x that are entered for each refined parameter. A zero codeword means that the parameter is not being refined. For each refined parameter, the codeword is formed as:

$$C_x = sign(a)(10p + |a|)$$

where p specifies the ordinal number of the parameter .

We started the refinement procedure by modifying a PCR file for another sample to suit our purpose, since this is one of the best methods for creating a new PCR file. The structure parameters such as lattice parameter is modified so as to match the new material. The scale factor is adjusted to reproduce fairly matching intensity for the generated pattern. Using FullProf program, the refinement of the first sample {$ZnAl_2O_4$] was started using the model taken from PCR file for another ferrite, in which the space group is Fd3m; its origin is at 4 3m at -1/8, -1/8, -1/8 from the centre 3m, and the oxygen anions occupy position 32b, while the tetrahedral and octahedral sites occupy the positions 8f and 16c, respectively.

The experimental profile was fitted by modified THOMPSON COXHASTING PESUDO-VOIGT function, recommended by the international union of Crystallography. In the first step of the refinement the global parameters (2θ, zero, instrumental profile, profile asymmetry, background, specimen displacement) were refined. This refinement yielded a pattern which nearly matches with the experimental profile. However the patterns are slightly shifted to the higher angle sides indicating the need for introducing further parameters into the refinement. In the next step, the structure parameters (atomic coordinates, specimen profile breadth parameter, lattice parameter, preferred orientation and site occupancy) were refined in the sequence mode which yielded a pattern that resembled much like the observed profile. The site occupancy in the two positions (octahedral and tetrahedral sites) were constrained in order to keep the sum of the same cations in the two sites is always in its stoichiometric value. However, the agreement from theoretical and experimental profiles are not exact and hence more parameters are included in the refinement. In the last cycle, when the discrepancy factor Rwp (R-weight

patterns) has reached its minimum value, all the parameters (global and structural) were refined simultaneously until a good goodness of fit is attained.

The use of Rietveld analysis for in depth description of mechanically induced disordering [ball milled] needs a cautious selection of the sample. The sample microstructure before milling will be modified by the stress induced during milling. Milling induced morphological changes are rather broad and usually results in multiple phases. Sample selection was thus based on a compromise between two requirements: first, the mechanically induced disorder should manifest itself by qualitative changes in the magnetic properties, and second, the refinement of the resulting structure using Rietveld analysis should give informations regarding the morphological changes in the material with ball milling., that is the refined structure parameters should be physically acceptable and must correspond to the values estimated by other means there by providing ample proof for the structure and magnetic property changes in the material.. These requirements are met by a sample milled in a planetary ball mill for different times. The samples are extracted at different intervals and subjected to x ray diffraction and the resulting patterns were analysed using Rietveld method.

Good understanding about the properties of Zinc Ferrite requires detailed knowledge of its crystallographic structure and associated parameters. Many parameters contribute to the integrated x ray intensity of a sample subjected to x-ray diifraction viz, the distribution of the magnetically active iron cations at the crystallographic sites, the mean square displacement of the atoms from their average positions or temperature coefficients, and the mean structural coherence length. The distribution of cations over the tetrahedral and octahedral sites determines the magnetic properties which control the magnetization properties, the mean square displacement of the atoms governs the sign and magnitude of the exchange interactions between the magnetic moments of Fe & Zn cations, and the structural coherence length governs the magnetic coherence length known as the magnetic domain size. Such comprehensive information can only be derived from Rietveld refinement of x ray diffraction data of the samples. The refined pattern for, pristine zinc aluminate, pristine zinc ferrite and ball milled zinc ferrite are shown in fig1: fig.2 and fig.3 respectively.

We find that the atomic arrangement of $ZnFe_2O_4$ may be well described in terms of a spinel-type structure, with the Fe^{3+} and Zn^{2+} cations dispersed over the tetrahedral and octahedral sites close to random. The spinel-type arrangement inherently contains a considerable local randomness. In the course of the analysis, the two types of cations (Zn^{2+} and Fe^{3+}) were allowed to occupy either of the two distinct crystallographic positions [A] and [B] in the spinel lattice. The occupancy factors of the cation positions were constrained so as to preserve the stoichiometric composition of the material.

A single-phase model based on the spinel-type structure reproduces the experimental data for the crystalline ferrite very well. A closer examination of the results, however, shows that the Rietveld analysis yielded negative mean-square (m.s.) atomic displacements ('thermal factors'). Such unrealistic displacement parameters are known to result from Rietveld analyses of powder diffraction patterns of materials with considerable inherent disorder.

The cation distribution in the spinel structure of the nanocrystalline ferrite is close to random. Obviously the distribution of cations in ferrites engineered at nanoscales could be different from that in their bulk crystalline counterparts. The XRD patterns of the samples $ZnFe_2O_4$, represents the single phase spinel structure. The second important result obtained by Rietveld analysis is that mechanical activation leads to the contraction of the ferrite crystal lattice characterized by the decrease of the a value from 0.8443 nm (for the as-prepared sample) to 0.8424 nm [milled sample].

On applying the full pattern fitting of Rietveld method using FULLPROF program, exact coordinates of atoms, unit cell dimensions, atom occupation factors, interatomic distances as well asymmetry have been determined.

Conventionally it is well known that Zn^{2+} have a strong A-site preference. Only Fe3+ is believed to be distributed randomly between the two sites in such a way governed by the presence of different concentrations of Zn^{2+}. However Rietveld refinement on Zn Ferrite prepared with a definite stoichiometry reveals site interchange of Fe^{3+} ion and a

reciprocal interchange also hold since the stoichiometry is constant. Also the pattern corresponding to pure zinc ferrite and the absence of other phases rules out the possibility of γ-Fe_2O_3 formation. Hence one can infer with confidence that the magnetization enhancement in zinc ferrite is primarily due to inversion of cations and not from the formation of other magnetically active components. The preferential site occupancy of Zn^{2+} and the concepts of electronic structure of the lattice ions are used to explain these. The 4s & 4p or 5s & 5p electrons of Zn^{+} are able to form covalent bond with the 2p electron of oxygen ion. Usually large divalent cations, like Zn, tend to occupy the tetrahedral site as this is favoured by polarization effects of the oxygen atoms intermediate between A and B sites. This results in the re-expansion of tetrahedral sites by an equal displacement of 4 oxygen ions outwards along the diagonal of the cube. At the same time the oxygen ions connected with the octahedral sites move in such a way as to shrink the size of the octahedral site by the same amount as the tetrahedral site expands. This behaviour is reflected in the enlargement of the bond length of the tetrahedral polyhedron.

An inversion of about 9% has been found in the case of pure zinc ferrite. This is consistent with the magnetic properties exhibited by ultra fine zinc ferrite. Refinement carried out in zinc aluminate (Fig.1) indicates that there is no evidence for inversion and the normal spinel nature of zinc aluminate is retained. Refinement conducted on milled zinc aluminate also point to the fact that milled samples do not undergo any inversion or disassociation. This observation is consistent with the results obtained by X-ray diffraction analysis. Rietveld refinement carried out on ball milled zinc ferrite samples show that there occurrs disassociation of $ZnFe_2O_4$ while the inversion percentage has reduced. A representative fit is shown in Fig.3. In short, Rietveld refinement carried out on pristine zinc ferrites, pristine zinc aluminate and ball milled samples led to the following conclusions.

a) Pure zinc ferrite in the nanoregime exhibit ferrimagnetism at room temperature and the origin of magnetism or exchange interaction is due to the cation redistribution. Zinc instead of occupying tetrahedral site exclusively migrates to octahedral site pushing some of the Fe ions to the A sites resulting in an A-B interaction leading to ferrimagnetism.

b) Pure and milled zinc aluminate in the ultra fine regime does not undergo any inversion whatsoever and retains the normal spinel nature of a classical spinel represented by $MgAl_2O_4$.

c) Ball milled zinc ferrite samples also undergo inversion but at the same time disassociates to α -Fe_2O_3 and ZnO.

However, fineness induces more inversion and increase in magnetisation value.

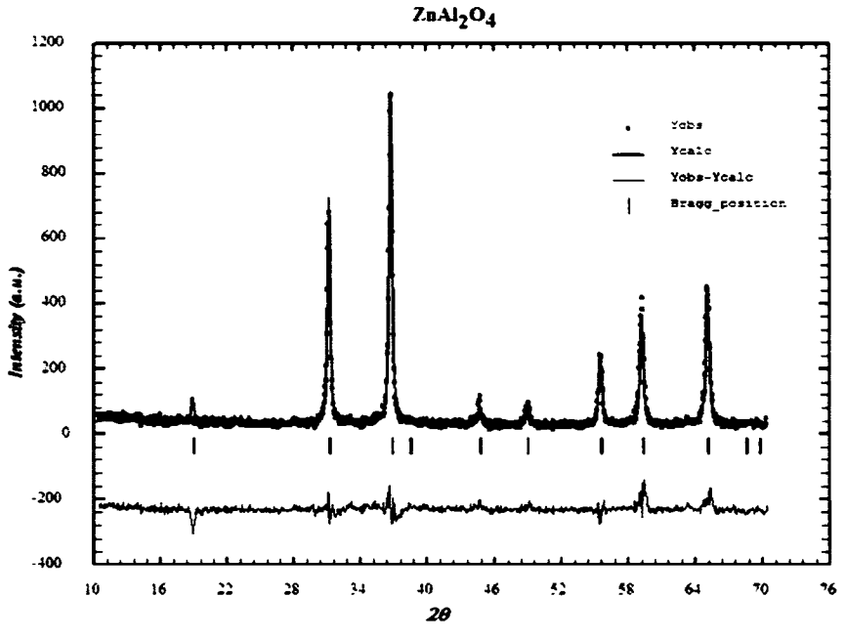

Fig.1 Rietveld fitted data for pristine zinc aluminate

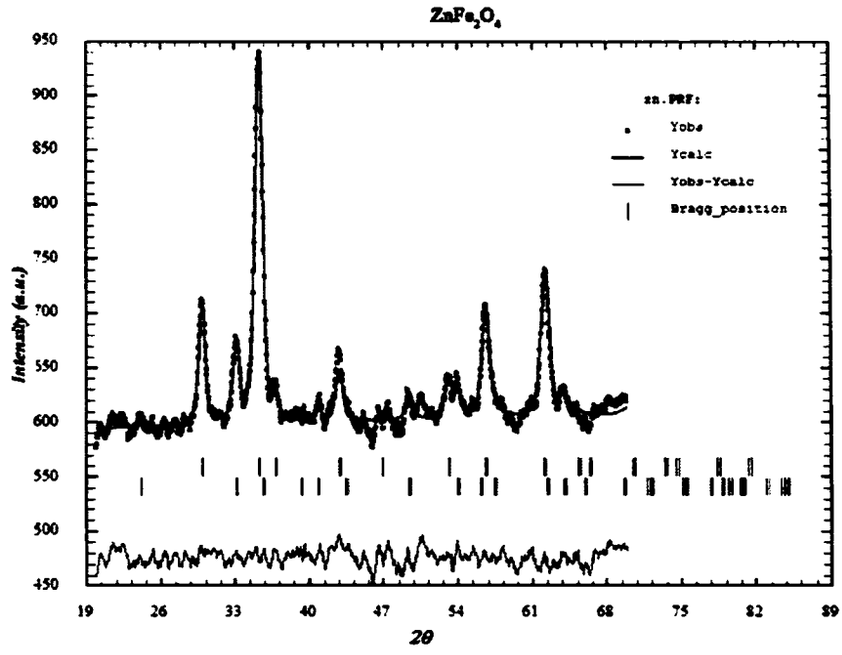

Fig.2: Rietveld Fitted Data For Pristine Zinc Ferrite

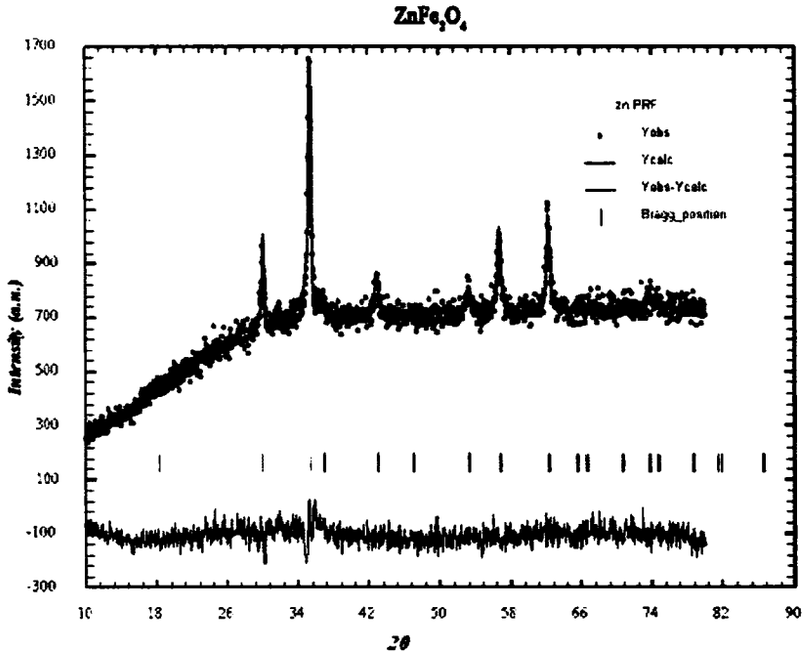

Fig.3: Rietveld Fitted Data for Ball Milled Zinc Ferrite

References

1. On the magnetic properties of ultrafine zinc particles. ***M R Anantharaman***, S.Jagatheesan, K.A.Malini, S.Sindhu, A.Narayanasamy, C.N.Chinnasamy, J.D.Jacobs, S.Reijne, K.Seshan, R.H.H.Smits, H.H.Brongersma Journal of Magnetism and Magnetic Materials, 189, 83 (1998).
2. Effect of mechanical milling on the structural, magnetic and dielectric properties of coprecipitated ultrafine Zinc ferrrites S. D. Shenoy, P. A. Joy, ***M R Anantharaman*** Journal of Magnetism and Magnetic Materials, 269 (2004) 217-226
3. Mechanically Induced structural disordering in spinel ferrites ,Vladmir Sepelak,and Klara Tkaeova, Acta Montanistica Slovaca Roèník 2 (1997), 3, 266-272
4. Application of Rietveld Method to the StructuralCharacteristics of Substituted Copper FerriteCompound,I.S. Ahmed Farag, M. A. Ahmed, S. M. Hammad, A. M. Moustafa, Cryst. Res. Technol. ,36,(2001), 1 85–92
5. Cation Distribution In Synthetic Zinc Ferrite ($Zn_{0.97}Fe_{2.02}O_4$) From In Situ High-Temperatureneutron Powder Diffraction Alessandro Pavese, Davide Levy, and Andreas Hoser ,American Mineralogist, 85, (2000), 1497–1502
6. X-ray Diffraction, A Practical Approach,C.Suryanarayana and M Grant Norton, Plenum Press, New York, London,1998
7. International Tables for X-ray Crystallography Volume-1,Symmetry Groups ,Norman F.M .Henry and Kathleen Lonsdale ,The International Union of Crystallography,The Kynoch Press,Birmingham,England,1965.
8. An Introduction to the program FULLPROF 2000,(Version July2001), Juan Rodríguez-Carvajal,Laboratoire Léon Brillouin (CEA-CNRS),CEA/Saclay, 91191 Gif sur Yvette Cedex, FRANCE .